CHAOTIC DYNAMICS

an introduction

G. L. BAKER AND J. P. GOLLUB

BAKER AND GOLLUB CHAOTIC DYNAMICS

CHAOTIC DYNAMICS

an introduction

G. L. BAKER AND J. P. GOLLUB

BAKER AND GOLLUB CHAOTIC DYNAMICS

Contents

CHAPTER ONE

Introduction

The irregular and unpredictable time evolution of many nonlinear systems has been dubbed 'chaos.' It occurs in mechanical oscillators such as pendula or vibrating objects, in rotating or heated fluids, in laser cavities, and in some chemical reactions. Its central characteristic is that the system does not repeat its past behavior (even approximately). Periodic and chaotic behavior are contrasted in Figure 1.1. Yet, despite their lack of regularity, chaotic dynamical systems follow deterministic equations such as those derived from Newton's second law.

The unique character of chaotic dynamics may be seen most clearly by imagining the system to be started twice, but from slightly different initial conditions. We can think of this small initial difference as resulting from measurement error, for example. For nonchaotic systems this uncertainty leads only to an error in prediction that grows *linearly* with time. For chaotic systems, on the other hand, the error grows *exponentially* in time, so that the state of the system is essentially unknown after a very short time. This phenomenon, which occurs only when the governing equations are nonlinear, is known as *sensitivity to initial conditions*. Henri Poincaré (1854–1912), a prominent mathematician and theoretical astronomer who studied dynamical systems, was the first to recognize this phenomenon. He described it as follows: '. . . it may happen that small differences in the initial conditions produce very great ones in the final phenomena. A small error in the former will produce an enormous error in the latter. Prediction becomes impossible, and we have the fortuitous phenomenon' (Poincaré, 1913).

If prediction becomes impossible, it is evident that a chaotic system

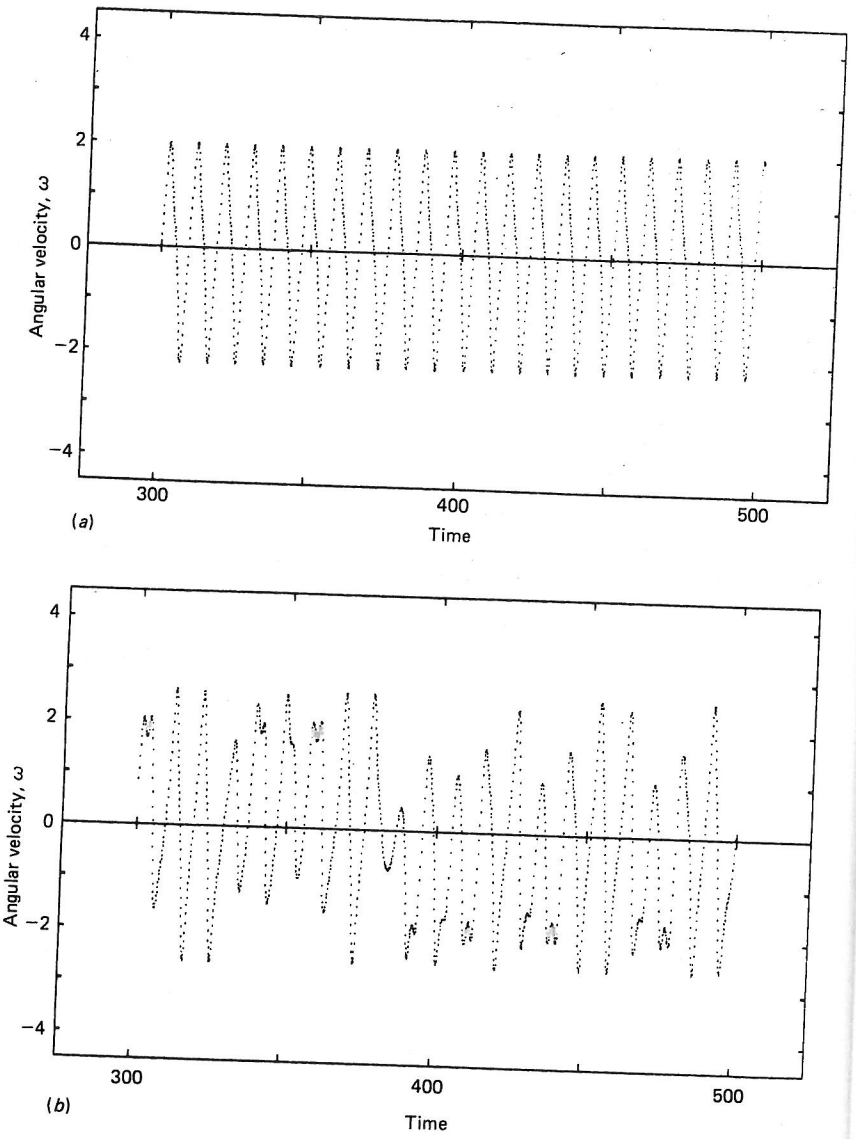

Fig. 1.1 The damped, driven pendulum can exhibit both periodic and chaotic motions. Here, the angular velocity is shown as a function of time for the two cases.

can resemble a stochastic system (a system subject to random external forces). However the source of the irregularity is quite different. For chaos, the irregularity is part of the intrinsic dynamics of the system, not unpredictable outside influences.

Chaotic motion is not a rare phenomenon. Consider a dynamical system described by a set of first order differential equations. Several

necessary conditions for chaotic motion are that (*a*) the system has at least three independent dynamical variables, and (*b*) the equations of motion contain a nonlinear term, that couples several of the variables. The equations can often be expressed in the form:

$$\begin{aligned} dx_1/dt &= F_1(x_1, x_2, \cdots, x_n) \\ dx_2/dt &= F_2(x_1, x_2, \cdots, x_n) \\ &\vdots \\ dx_n/dt &= F_n(x_1, x_2, \cdots, x_n) \end{aligned}$$

where n must be at least 3. Two examples of appropriate nonlinear equations are:

$$\begin{aligned} dx_1/dt &= \alpha x_1 + \beta x_2 + \gamma x_1 x_2 + \cdots + \delta x_n \\ dx_1/dt &= \alpha x_1 + \beta x_2 + \gamma \sin x_2 + \cdots + \delta x_n \end{aligned}$$

where α, β, γ, δ are constants. In each case the nonlinear term couples both x_1 and x_2. Systems such as these are often chaotic for some choices of the constants.

The fact that only three variables are required for chaos was surprising when first discovered. We shall see that three-space is sufficient to allow for (*a*) divergence of trajectories, (*b*) confinement of the motion to a finite region of the phase space of the dynamical variables, and (*c*) uniqueness of the trajectory. The nonlinearity condition is perhaps less surprising. Solutions to linear differential equations can always be expressed as a linear superposition of periodic functions, once initial transients have decayed. The effect of a nonlinear term is often to render a periodic solution unstable for certain parameter choices. While these conditions do not guarantee chaos, they do make its existence possible.

The nonlinearity condition has probably been responsible for the late historical development of the study of chaotic systems. Despite the fact that chaotic systems are deterministic and are described by many of the long-known classical equations of physics, the development of the subject itself is more recent. This circumstance may arise from the fact that, with the exception of some first order equations, nonlinear differential equations are either difficult or impossible to solve analytically. Although it is sometimes possible to use linearized approximations, the solution of nonlinear differential equations generally requires numerical methods whose practical implementation demands the use of a digital computer. The first numerical

study to detect chaos in a nonlinear dynamical system was that of Lorenz's model of convective fluid flow (Lorenz, 1963). Similarly, the majority of the diagrams in this book are based upon the use of numerical methods on a personal computer to solve nonlinear equations.

From these general comments on chaotic systems, we turn to the physical system that is the focus of this work – the damped, driven pendulum. The choice of the pendulum as a model system has strong historical precedent in physics. Galileo postulated the constancy of period for small amplitude oscillations of the pendulum from observations of swaying lamps in the cathedral at Pisa, in 1581 (Robinson, 1921). He took up the problem of the relationship between the period and pendulum length in his famous *Dialogue on the Two Principal World Systems* in 1632, and in 1637 he suggested that the square of the period was proportional to the length of the pendulum for small oscillation amplitudes (Dugas, 1958). The pendulum also served as a primary timing mechanism for clocks and as a method of measuring variations in the earth's gravitational field. As a pedagogical device the pendulum has long been a standard mechanical example in introductory physics and classical mechanics courses. Now, 400 years after Galileo's initial work, the pendulum has again become an object of research as a chaotic system. The references scattered throughout this work attest to its popularity.

The damped, sinusoidally driven pendulum of mass m (or weight W) and length l is described by the following equation of motion:

$$ml\frac{d^2\theta}{dt^2}+\gamma\frac{d\theta}{dt}+W\sin\theta=A\cos(\omega_D t).$$

This equation expresses Newton's second law with the various terms on the left representing acceleration, damping, and gravitation. The angular velocity of the forcing, ω_D, may be different from the natural frequency of the pendulum. In order to minimize the number of adjustable parameters the equation may be rewritten in dimensionless form as:

$$d^2\theta/dt^2+(1/q)d\theta/dt+\sin\theta=g\cos(\omega_D t)$$

where q is the damping or quality parameter, g is the forcing amplitude, not to be confused with the gravitational acceleration, and ω_D is the drive frequency. The low-amplitude natural angular frequency of the pendulum is unity, and time is regarded as dimen-

sionless. (This particular notation follows that used by Gwinn and Westervelt. See for example, Gwinn and Westervelt (1986).) This equation satisfies the necessary conditions for chaos when it is written as a set of first order equations:

$$d\omega/dt = -(1/q)\omega - \sin\theta + g\cos\phi$$
$$d\theta/dt = \omega$$
$$d\phi/dt = \omega_D.$$

The variable ϕ is introduced as the phase of the drive term. The necessary three variables (ω,θ,ϕ) are evident, and the $\sin\theta$ and $g\cos\phi$ terms are clearly nonlinear. Whether the motion is chaotic depends upon the values of the parameters g, ω_D, and q. For some values the pendulum locks onto the driving force, oscillating in a periodic motion whose frequency is the driving frequency, possibly with some harmonics or subharmonics. But for other choices of the parameters the pendulum motion is chaotic. One may view the chaos as resulting from a subtle interplay between the tendency of the pendulum to oscillate at its 'natural' frequency and the action of the forcing term. The transitions between nonchaotic and chaotic states, due to changes in the parameters, occur in several ways and depend delicately upon the values of the parameters.

A variety of analytic and computational tools may be used in the study of chaotic systems. In Chapter 2 several of these are discussed. The pendulum's phase space and its properties are described, together with the conceptual device known as the Poincaré section. Then, since Fourier spectra are an indicator of chaotic motion, some elements of Fourier analysis are outlined. Chapter 3 is a description of the application of these and other techniques to the pendulum.

The driven pendulum would seem to be one of the simplest physical systems. Yet its behavior is rich and complex. The study of its motion can be facilitated by simple mathematical models formulated as difference equations, that provide a discrete *mapping* of the system from one state to another. Mappings have the advantage of being conceptually simple and numerically efficient, and they may be used as paradigms for various aspects of the pendulum motion. Chapter 4 contains discussions of three such maps, the logistic map, the circle map, and the horseshoe map. We use them to provide insight into the behavior of the pendulum.

Chapter 5 is concerned with the geometric structure of the *attractor* that describes the chaotic pendulum. The attractor, and its Poincaré section, are *fractal* structures with noninteger dimensionality. Various approaches to the calculation of fractal dimension are described. Another geometric feature is the exponential divergence of the chaotic trajectories on the attractor. The rate of this divergence is characterized by Lyapunov exponents. The calculation of these exponents and their relation to (*a*) the fractal dimension, (*b*) the dissipative nature of the pendulum, and (*c*) the duration of predictable behavior are also discussed.

Finally, in Chapter 6 a few general comments are made on the relationship of chaotic behavior to other areas of physics. While chaotic behavior occurs broadly, three areas are given brief descriptions: fluid dynamics, chemical reactions, and lasers. The relation of chaos to quantum mechanics and the connection of chaos with irreversibility are also discussed briefly.

Two appendices present numerical aspects of this book. Appendix A is a description of the Runge–Kutta algorithm used to solve the pendulum differential equation. Appendix B provides brief descriptions and listings of the computer programs used throughout the text, and in the computer exercises given at the end of several of the chapters. The listings utilize the language True BASIC™ but they are adaptable to any compiled BASIC or other high level language. (Interpreted BASIC, which is typically delivered with current microcomputers, is too slow for most of these simulations. The exceptions are the mappings in Chapter 4.)

CHAPTER TWO

Some helpful tools

In this chapter we discuss three mathematical constructs that are generally useful in the study of dynamical systems: phase space, the Poincaré section, and power spectra. Phase space is the mathematical space of the dynamical variables of a system. The Poincaré section is a 'snapshot' of the motion in the phase space, taken at regular time intervals. The power spectrum is computed using Fourier analysis to display the frequency composition of the time variation of the dynamical variables.

Phase space

The phase space of a dynamical system is a mathematical space with orthogonal coordinate directions representing each of the variables needed to specify the instantaneous state of the system. For example, the state of a particle moving in one dimension is specified by its position (x) and velocity (v); hence its phase space is a plane. On the other hand, a particle moving in three dimensions would have a six-dimensional phase space with three position and three velocity directions. A phase space may be constructed in several different ways. For example, momenta can be used instead of velocities.

Let us focus the discussion on the pendulum and begin with the familiar simple pendulum in the small amplitude approximation where the restoring term, $\sin\theta$, is taken as θ. (Recall that the equations are written in dimensionless form for simplicity, with time measured in units of the inverse of the natural frequency.) The

equation of motion is

$$d^2\theta/dt^2 + \theta = 0.$$

With the addition of the angular velocity variable, $\omega \equiv d\theta/dt$, this linear, second order equation can be reduced to two first order equations:

$$d\omega/dt = -\theta$$

and

$$d\theta/dt = \omega.$$

In this way each dynamical variable has its own first order differential equation. Without loss of generality, the initial conditions can be chosen so that the solution becomes

$$\theta = a_i \cos t \text{ and } \omega = a_i \sin t$$

where $\{a_i\}$ represents the possible amplitudes of the motion. This solution set gives the parametric curves for ω and θ, and one can eliminate the time parameter to give a two-dimensional representation for differing values of a_i. This diagram, shown in Figure 2.1, is

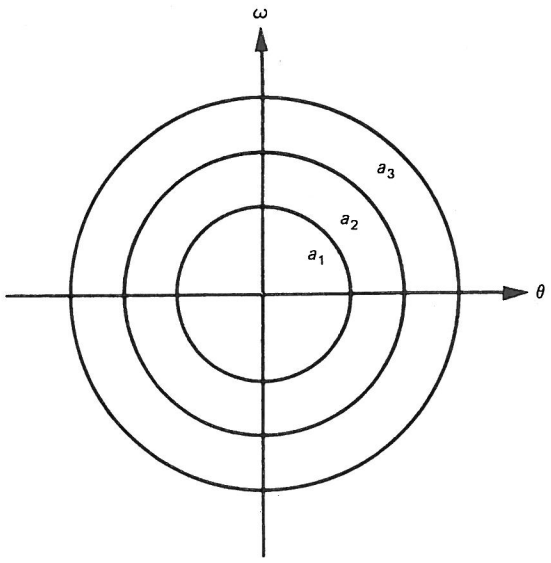

Fig. 2.1 Phase diagram of the linear pendulum. The angular velocity, ω, and the angular displacement, θ, are the coordinate axes.

the appropriate *phase space diagram* (in this case a phase plane diagram). Each value of a_i yields a closed orbit of fixed energy. The energy increases with the square of the radius a_i. The orbit is usually called a *phase trajectory*.

An important feature of the trajectory is that two trajectories corresponding to similar energies will pass very close to each other, but the orbits will not cross each other. This *noncrossing* property derives from the fact that past and future states of a deterministic mechanical system are uniquely prescribed by the system state at a given time. A crossing of trajectories at time t would introduce ambiguity into past and future states, thereby rendering the system indeterminate. Such indeterminacy would contradict the assumed uniqueness of the trajectory. Figure 2.2 shows the indeterminacy of trajectories emanating from a hypothetical crossing.

Another important feature of the phase space of *conservative* (constant energy) systems is the *preservation of areas*. This means that all the points found in a given area of phase space at one time move in such a way that at a later time the area occupied by these points remains the same. This feature is illustrated in Figure 2.3 and in Examples 2.1 and 2.2.

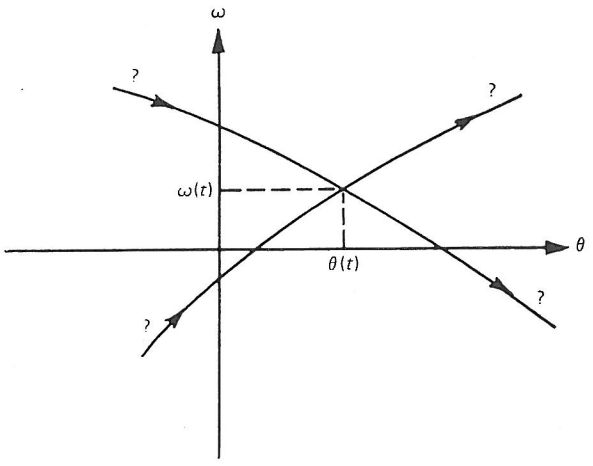

Fig. 2.2 The noncrossing property of phase trajectories. Crossing of trajectories violates uniqueness of trajectories in a deterministic dynamical system.

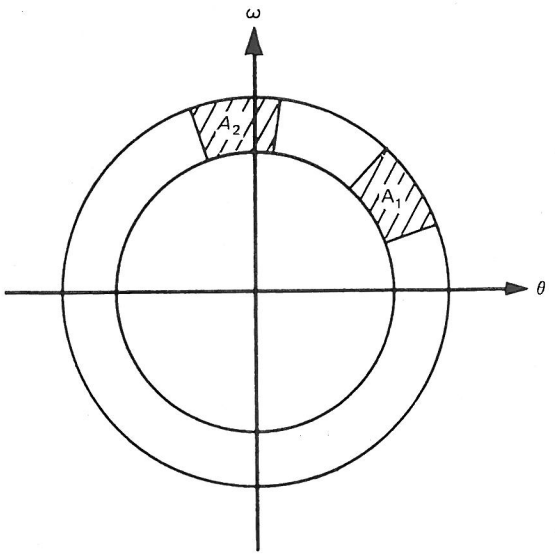

Fig. 2.3 Preservation of phase space area.

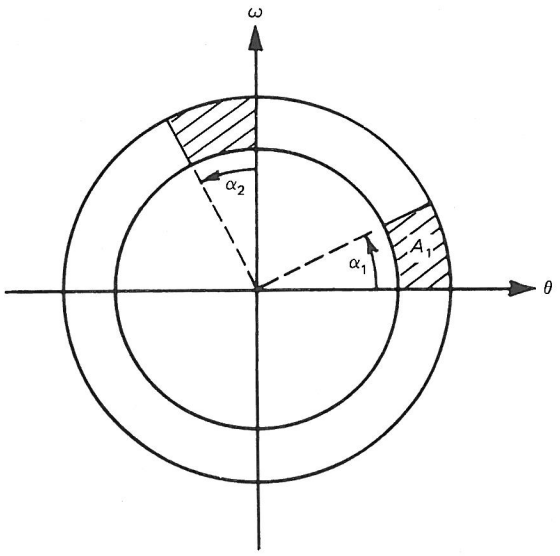

Fig. 2.4 Evolution of the linear oscillator described in Example 2.1.

Example 2.1. For the linear oscillator $d^2\theta/dt^2+\theta=0$ consider the evolution of the area A_1 as shown in Figure 2.4 during one quarter of the period. Since the system is energy conserving, A_1 should remain constant. Because of the circular symmetry, preservation of the area

can be shown by proving that every point in A_1 rotates (at a constant radius) through the same angle in the quarter period. The energy conserving feature ensures that each point rotates at a constant radius because the energy of the oscillator is proportional to the square of the radius. For the rotation angle we note that since $\theta = a\cos t$ and $\omega = a\sin t$, the polar angle of a given point is

$$\alpha(t) = \tan^{-1}(\tan t) = t.$$

Therefore at $t = t_0 + \pi/2$, $\alpha(t_0 + \pi/2) = t_0 + \pi/2$. But since $\alpha(t)$ was arbitrary, all points rotate by $\pi/2$ in one quarter period, and the area is preserved.

Example 2.2. As another example of area preservation consider the very simple motion of a constant velocity rotor. The two first order equations become

$$d\omega/dt = 0$$

and

$$d\theta/dt = \omega_0.$$

The corresponding phase trajectories are just horizontal lines with differing angular velocities, ω_{0i}, as shown in Figure 2.5. The linear dependence of θ on ω_{0i} ensures that an initial rectangle of points transforms to a parallelogram with a constant base and height, thereby maintaining the original area.

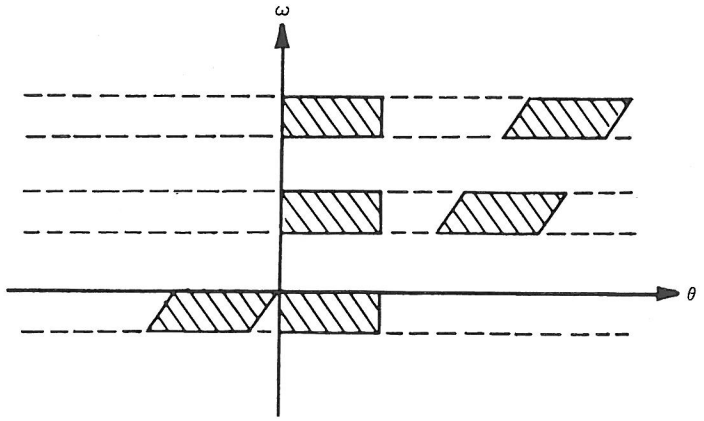

Fig. 2.5 Phase space diagram of a constant velocity rotor.

Example 2.2 also raises the question of boundaries on the phase plane coordinates. In contrast to the linearized pendulum whose finite motion allowed both θ and ω to be bounded conveniently in phase space, the angular coordinate θ for the rotor can increase (positively or negatively) without bound. Yet physically θ is periodic. Therefore the phase diagram is also made periodic by imposing *periodic boundary conditions* on θ as illustrated in Figure 2.6. The θ axis can be limited to $[-\pi,\pi]$, and the two edges of this domain are regarded as identical. As the rotor goes around in the positive θ direction, its phase representation disappears off the right edge of the phase diagram and immediately reappears on the left side. Similar periodic boundary conditions can also be usefully applied to the forced pendulum whose motion passes through the vertical direction.

The property of area preservation, or volume preservation in a higher dimensional space, is a general feature of conservative systems. This property leads to a classification of dynamical systems into two categories – *conservative* or *dissipative* – depending upon whether the phase volumes stay constant or contract, respectively. For example, the linearized undamped pendulum conserves energy, and its trajectories preserve phase area. On the other hand, the trajectories of the linearized damped pendulum,

$$d^2\theta/dt^2 + d\theta/dt + \theta = 0,$$

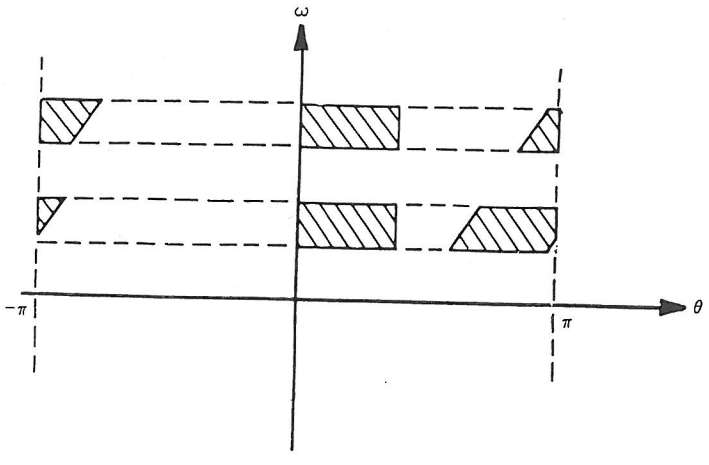

Fig. 2.6 Phase space diagram of the rotor with periodic boundary conditions. Phase points moving to the right disappear at $\theta=\pi$ and then reappear at $\theta=-\pi$.

decay to a single point: $\omega = 0 = \theta$. This area contraction is illustrated in Figure 2.7. Such a point is called an *attractor*, because a finite set of initial coordinates (θ,ω) converge to it. Obviously phase area is *not* preserved and the system is said to be dissipative.

Using these phase space characteristics we can develop a method for determining from the equations of motion whether a system is conservative or dissipative. The development of the method is easiest to understand in three space dimensions; thus we assume phase coordinates x_1,x_2,x_3, as in Figure 2.8. The equations of motion of the system can be written in terms of the phase 'velocity' components,

$$\begin{aligned} dx_1/dt &= F_1(x_1,x_2,x_3), \\ dx_2/dt &= F_2(x_1,x_2,x_3), \\ dx_3/dt &= F_3(x_1,x_2,x_3). \end{aligned}$$

$\nabla \cdot F = 0 \Rightarrow$ conservative
phase space volume constant

Now consider a volume region V with surface S, and assume a net flow of points from V. For a small region ΔS, the flow (or flux) from the region is the component of the velocity vector $\mathbf{v}$ perpendicular to the surface, multiplied by the element of surface area, ΔS. Since the velocity vector $\mathbf{v} = (dx_1/dt, dx_2/dt, dx_3/dt)$, is specified by the above set of differential equations, then the flux out of the small region is $\mathbf{F} \cdot \mathbf{n}\Delta S$. The net flux out of the entire surface is

$$\text{Flux} = \int_S (\mathbf{F} \cdot \mathbf{n}) dS,$$

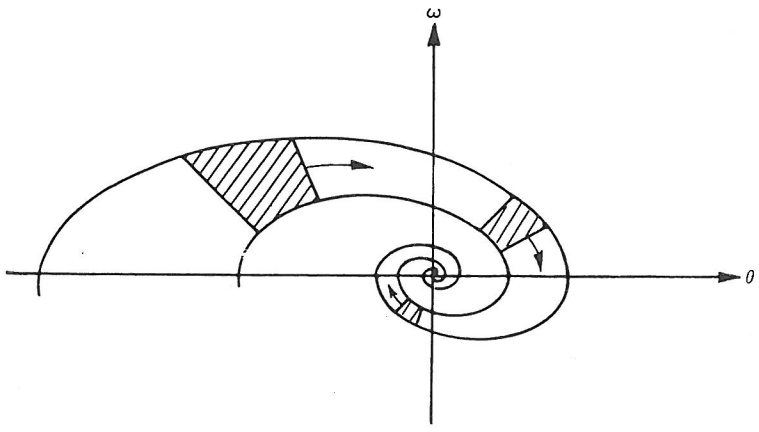

Fig. 2.7 Phase space diagram of the dissipative linear pendulum. Phase area is not preserved.

where **n** is the unit normal vector to the surface, S. Since the flux is the 'velocity' of the phase points from the volume V, then in time δt the indicated volume will change by an amount equal to

$$\delta t \times \text{Flux} = \delta t \int_S (\mathbf{F} \cdot \mathbf{n}) \mathrm{d}S.$$

Therefore phase area is preserved or not preserved, depending on the flux integral being zero or negative, respectively. But even this integral will generally be difficult to evaluate, and therefore we simplify the calculation further by using the *divergence theorem* from vector calculus:

$$\int_S (\mathbf{F} \cdot \mathbf{n}) \mathrm{d}S = \int_V (\nabla \cdot \mathbf{F}) \mathrm{d}V.$$

(See, for example, Thomas and Finney (1979).)

This theorem converts an integral of a vector field such as **F**, on a closed surface S, into an integration of the divergence of **F** over the enclosed volume. Furthermore, the preservation of phase volume should be independent of the particular volume chosen, and it is

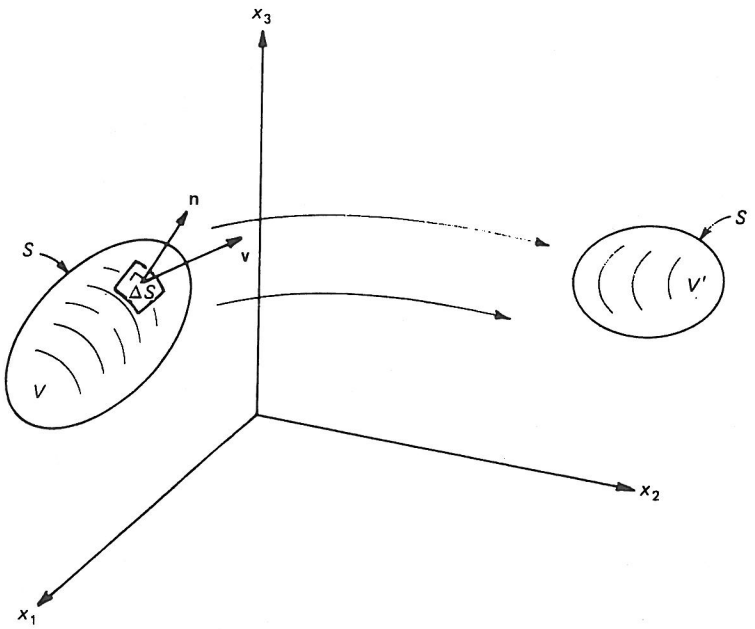

Fig. 2.8 Evolution of a volume in three-dimensional phase space.

therefore sufficient to examine $\nabla \cdot \mathbf{F}$ alone. If this quantity is zero, the system is termed *conservative*, whereas if the divergence of phase velocity is negative the system is *dissipative.* The kinematic properties of the flux in phase space for a conservative system are analogous to the flow of an incompressible fluid in hydrodynamics. (The term *Hamiltonian* is sometimes used in connection with phase volume preserving systems. Many dynamical systems obey Hamilton's equations of motion and such systems are called *Hamiltonian* systems. These systems preserve volume in phase space, according to Liouville's theorem, and therefore Hamiltonian systems are a subset of the set of conservative systems. See Helleman (1983).)

Liouville's Theorm

Example 2.3. Let us write both of our example pendula in the phase velocity form and determine their phase space preservation characteristics by this method.

(i) $d^2\theta/dt^2 + \theta = 0$ (undamped) becomes

$d\theta/dt = \omega$ and $d\omega/dt = -\theta$.

Therefore $\mathbf{F} = (\omega, -\theta)$ and $\nabla \cdot \mathbf{F} = \partial\omega/\partial\theta + \partial(-\theta)/\partial\omega = 0$, indicating that phase area is preserved.

(ii) $d^2\theta/dt^2 + d\theta/dt + \theta = 0$ (damped) becomes

$d\theta/dt = \omega$ and $d\omega/dt = -\omega - \theta$.

Therefore $\mathbf{F} = (\omega, -\omega - \theta)$ and $\nabla \cdot \mathbf{F} = \partial\omega/\partial\theta + \partial(-\omega-\theta)/\partial\omega = -1$, indicating that phase area diminishes in time and the system is, as expected, dissipative.

These two examples show how easily the divergence criterion may be applied. For the driven pendulum the equation:

$$d^2\theta/dt^2 + (d\theta/dt)/q + \sin\theta = g\cos(\omega_D t)$$

is converted to a set of first order equations:

$$\frac{\omega}{\omega_0} t = \frac{2}{3} t$$

$$t = \omega_0[s^{-1}]\, t'[s]$$

$$d\omega/dt = -\omega/q - \sin\theta + g\cos\phi,$$
$$d\theta/dt = \omega,$$
$$d\phi/dt = \omega_D.$$

$\phi = \omega_0 t + \phi_0$

Then the right sides form the components of the three-dimensional

vector **F**. It is left as an exercise for the reader to show that $\nabla \cdot \mathbf{F} = -1/q$ and that, therefore, the system is dissipative.

We have looked at phase diagrams for the damped and undamped linearized pendula. Let us now introduce the full nonlinear restoring torque, $\sin\theta$. Figure 2.9 shows the phase plane for the undamped pendulum:

$$d^2\theta/dt^2 + \sin\theta = 0.$$

For small values of $d\theta/dt$ and θ, the diagram appears similar to that of the pendulum in the linear approximation, but as θ approaches $\pm\pi$ – a pendulum swing that would go all around the circle – the picture changes. At $(\pm\pi,0)$ the slope develops a discontinuity. The largest of the closed trajectories bounds the region where the motion is oscillatory (or vibrational). On the open trajectory of higher angular velocity, the pendulum goes completely around the circle, and its motion is a rotation modulated by oscillation. The average angular velocity becomes nonzero. (One might compare this to a direct current electrical signal modulated by an alternating current signal.) The corresponding time series of these motions are shown in Figure 2.10.

Consider now the addition of a damping term so the equation becomes

$$d^2\theta/dt^2 + d\theta/dt + \sin\theta = 0.$$

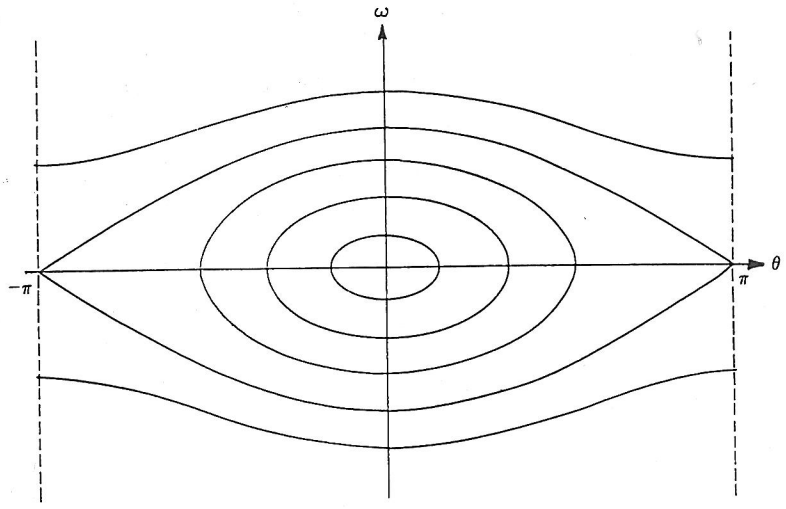

Fig. 2.9 Phase diagram of the nonlinear pendulum. The restoring force term contains $\sin\theta$.

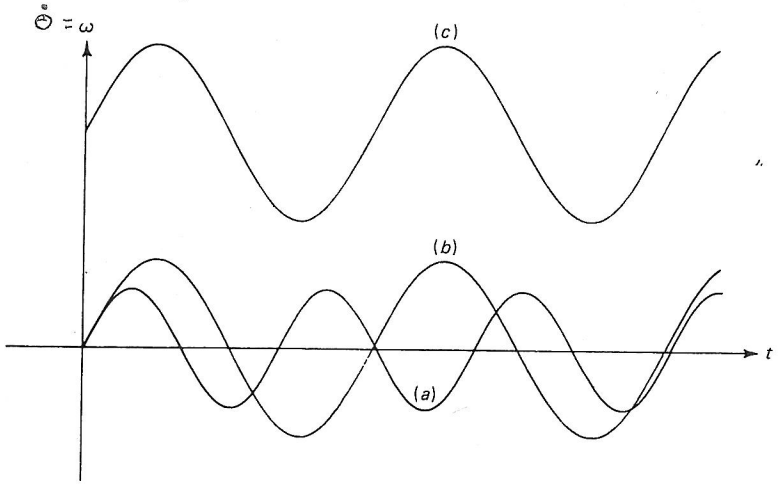

Fig. 2.10 Angular velocity time series. In contrast to the linearized pendulum, the period of the motion for the nonlinear pendulum increases with increasing amplitude. Curves (*a*) and (*b*) show oscillatory motions of differing amplitudes. Curve (*c*) shows the pendulum with sufficient energy to exhibit both rotary and oscillatory motions.

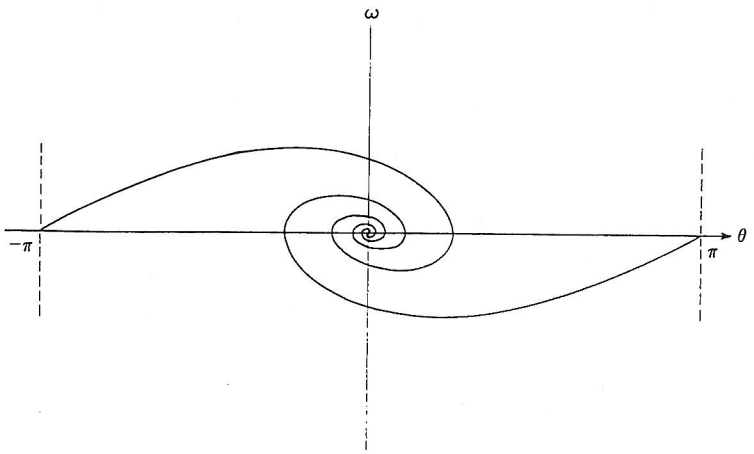

Fig. 2.11 Pair of phase space trajectories for the damped pendulum.

Typical trajectories are shown in Figure 2.11. As indicated previously, the damping term results in an attractor at the origin where $\sin\theta \approx \theta$. Now, however, further attractors are added at $\theta = \pm n\pi$, $\omega = 0$. This can be seen by setting the phase velocity equal to zero and solving for the stationary values of θ and ω; that is,

$$d\theta/dt = \omega = 0$$
$$d\omega/dt = -\omega - \sin\theta = 0.$$

While these attractors are points where the phase velocity goes to zero, questions arise as to the stability of these points. Will the

trajectories tend to go back to these critical points if slightly perturbed? Will the stability depend upon the direction of the perturbation? These questions can be answered by looking carefully at the critical points. A useful technique for examining dynamical behavior near critical points involves the assumption that the system will not deviate substantially from linear behavior *near the critical points*. Then each of the nonlinear terms in the differential equations is given a linear approximation near the critical points. This method was developed by Poincaré in 1914 (Hayashi, 1964).

For the case of the damped pendulum,

$$d\theta/dt = \omega$$
$$d\omega/dt = -\omega - \sin\theta,$$

it is easy to see (Problem 6) that near $\theta = \pm n\pi$, where n is even, the linear approximation is

$$d\theta/dt = \omega$$
$$d\omega/dt = -\omega - (\theta - n\pi),$$

and when n is odd the linear approximation becomes

$$d\theta/dt = \omega$$
$$d\omega/dt = -\omega + (\theta - n\pi).$$

In each case θ is transformed to a value centered at the critical point such that $\theta \to \Delta\theta = \theta - n\pi$ and therefore the linearized phase plane equations are

n=even; $d\Delta\theta/dt = \omega$, $d\omega/dt = -\omega - \Delta\theta$ $\qquad$ n=odd; $d\Delta\theta/dt = \omega$, $d\omega/dt = -\omega + \Delta\theta$.

Following the usual method for solving sets of first order linear differential equations, trial solutions of the form $\Delta\theta = Ae^{\lambda t}$ and $\omega = Be^{\lambda t}$ may be substituted into the equations; this yields two pairs of homogeneous algebraic equations. The condition for a nontrivial solution is the vanishing of the determinant of the coefficients of A and B. This condition produces quadratic characteristic equations in λ for each case:

$\lambda^2 + \lambda + 1 = 0$: n=even $\qquad$ $\lambda^2 + \lambda - 1 = 0$: n=odd

For the n=even case, the λ values are complex conjugates with negative real parts. This implies that both $\Delta\theta$ and ω will spiral inward toward the equilibrium point attractor, which is called a *focus*. This

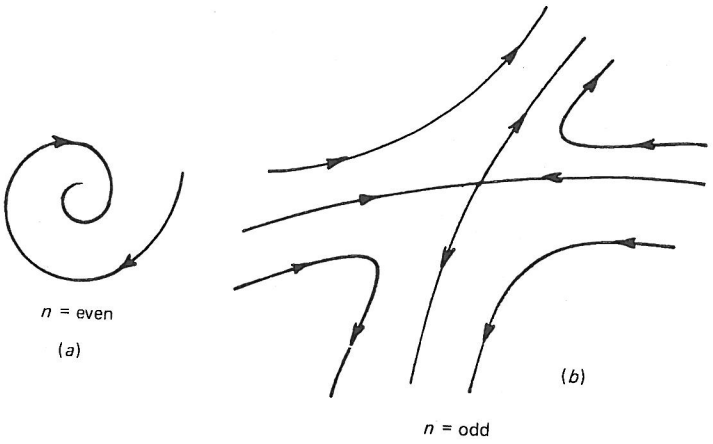

Fig. 2.12 Critical points in phase space: (*a*) focal point (*b*) saddle point. In (*b*) the trajectories going to the saddle point are stable whereas the trajectories coming from the saddle point are unstable.

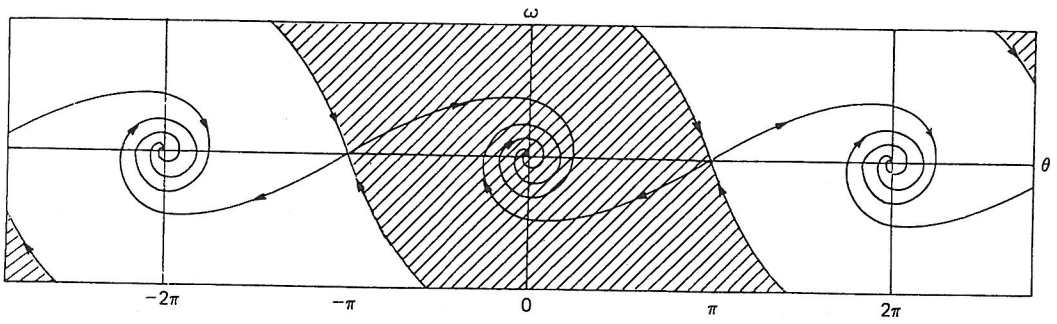

Fig. 2.13 Phase space diagram of the damped pendulum. Alternate shaded and unshaded regions are basins of attraction. All points within a particular basin are attracted to the focal point within the basin.

case is shown in Figure 2.12(*a*). On the other hand, the $n=$odd condition produces two real values of λ, one positive and one negative. In this case the stable phase trajectories move toward the critical point in one direction (negative exponent), but the unstable trajectories move away from it in another direction (positive exponent). This kind of critical point is called a *saddle point* and is shown in Figure 2.12(*b*). The respective directions are obtained by determining the A and B coefficients appropriate to each λ value. Note how the unstable trajectory directions correspond to the only possible directions for the pendulum, located momentarily at the saddle point. The details of the solution are left as an exercise (Problem 7). Putting all this information together, the phase diagram for the damped pendulum can be drawn as in Figure 2.13.

This phase diagram suggests yet another property of trajectories in phase space. As drawn in Figure 2.13, the phase space is divided into alternating regions as indicated by the shading. Inside each region all the trajectories will eventually spiral to the enclosed focal point. Each region is the set of all initial conditions (ω,θ) of trajectories that will eventually converge on a specific attractor – in this case a focal point. Such regions are called *basins of attraction*. Furthermore, each of the diagonal curves (Figure 2.13) dividing one basin from another is called a *separatrix*. The arrows on the separatrix (and elsewhere) indicate the flow of the trajectories, toward and away from the saddle points. We will see (Chapter 3) that one characteristic of chaos is the partial dissolution of the separatrix as the basins start to merge.

While most of the discussion so far has focused on the phase *plane*, it is important to realize that the phase space construction need not be confined to two dimensions. A previously introduced equation set,

$$dx_1/dt = F_1(x_1,x_2,x_3),$$
$$dx_2/dt = F_2(x_1,x_2,x_3),$$
$$dx_3/dt = F_3(x_1,x_2,x_3),$$

would define a three-dimensional phase space. We may use this set of equations to illustrate some further properties of phase space. We have already described the divergence method for determining if the above system is conservative. Further, it is evident that the equations are not explicitly time-dependent. The equation set is then called *autonomous* and describes a time-independent flow in phase space, similar to a set of stream lines in a fluid. In fact, the vector **F** is called a *flow*. Autonomous systems also obey the noncrossing property described earlier. However, a projection of a higher dimensional space onto a plane might show apparent crossings which do not represent actual interactions.

The autonomous property is sufficiently useful that it is often desirable to convert a time variable to some other variable in order to make a nonautonomous system into an autonomous system. For example, the variable ϕ is introduced in the driven pendulum equations as $d\phi/dt = \omega_D$ so that the system's dynamical variables become θ, ω, and ϕ. This is convenient since the explicit time dependence enters as a *periodic* term, $g\cos(\omega_D t)$, and therefore ϕ can be a periodic variable. Then in a three-dimensional phase space, both θ and ϕ can be given periodic boundary conditions such as $\theta \in [-\pi,\pi]$

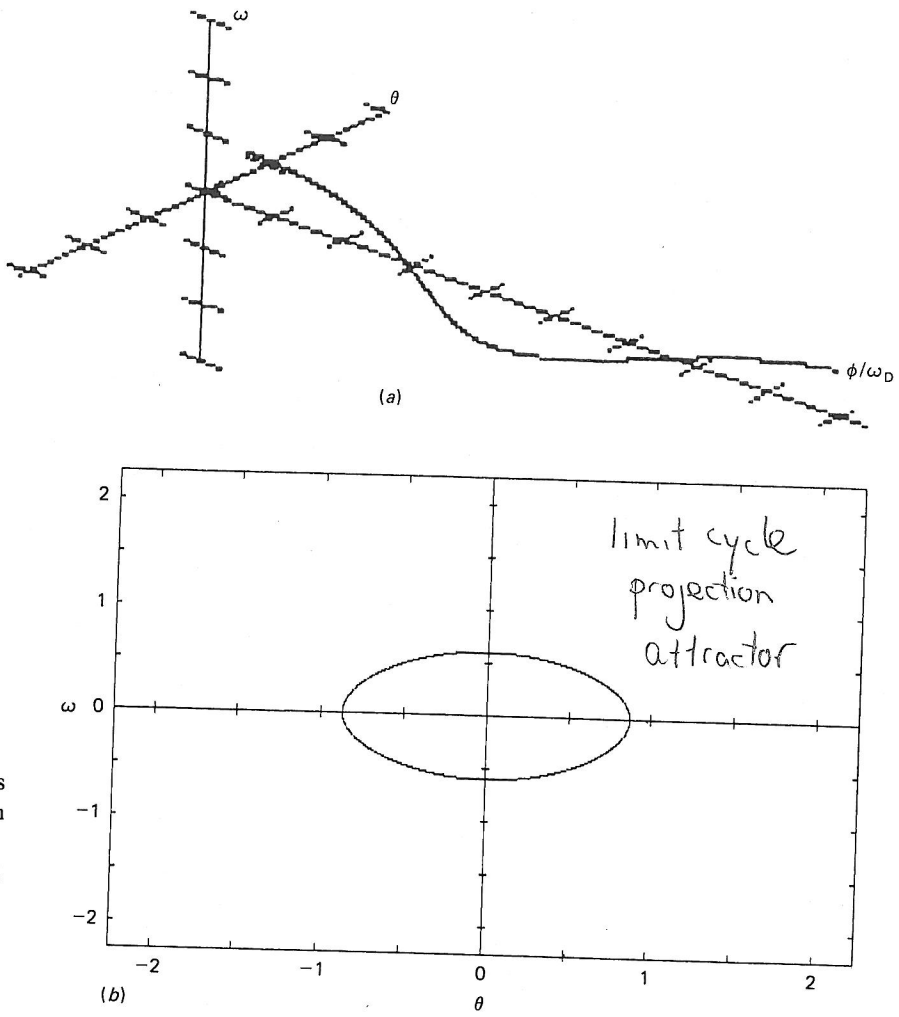

Fig. 2.14 Phase diagrams for the moderately-driven pendulum, $g=0.5$: (*a*) three-dimensions, and (*b*) two-dimensions ($q=2$).

and $\phi\in[0,2\pi]$. In Figures 2.14(*a*) and (*b*), a moderately-driven pendulum system is illustrated in both three- and two-dimensional phase spaces. The two-dimensional diagram is a projection of the three-dimensional diagram. These diagrams show the state of the pendulum after the initial transient effects have disappeared and after the system has evolved to a steady state. The resulting closed orbit is an *attractor* in the same sense as the point is an attractor for the dissipative, nondriven pendulum. This attractor is obviously one-dimensional and is called a *limit cycle.*

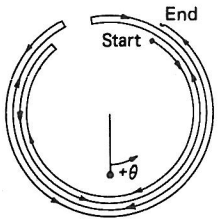

(a)

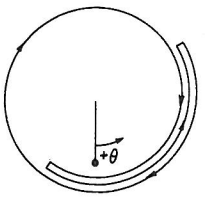

(b)

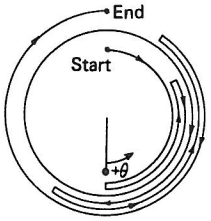

(c)

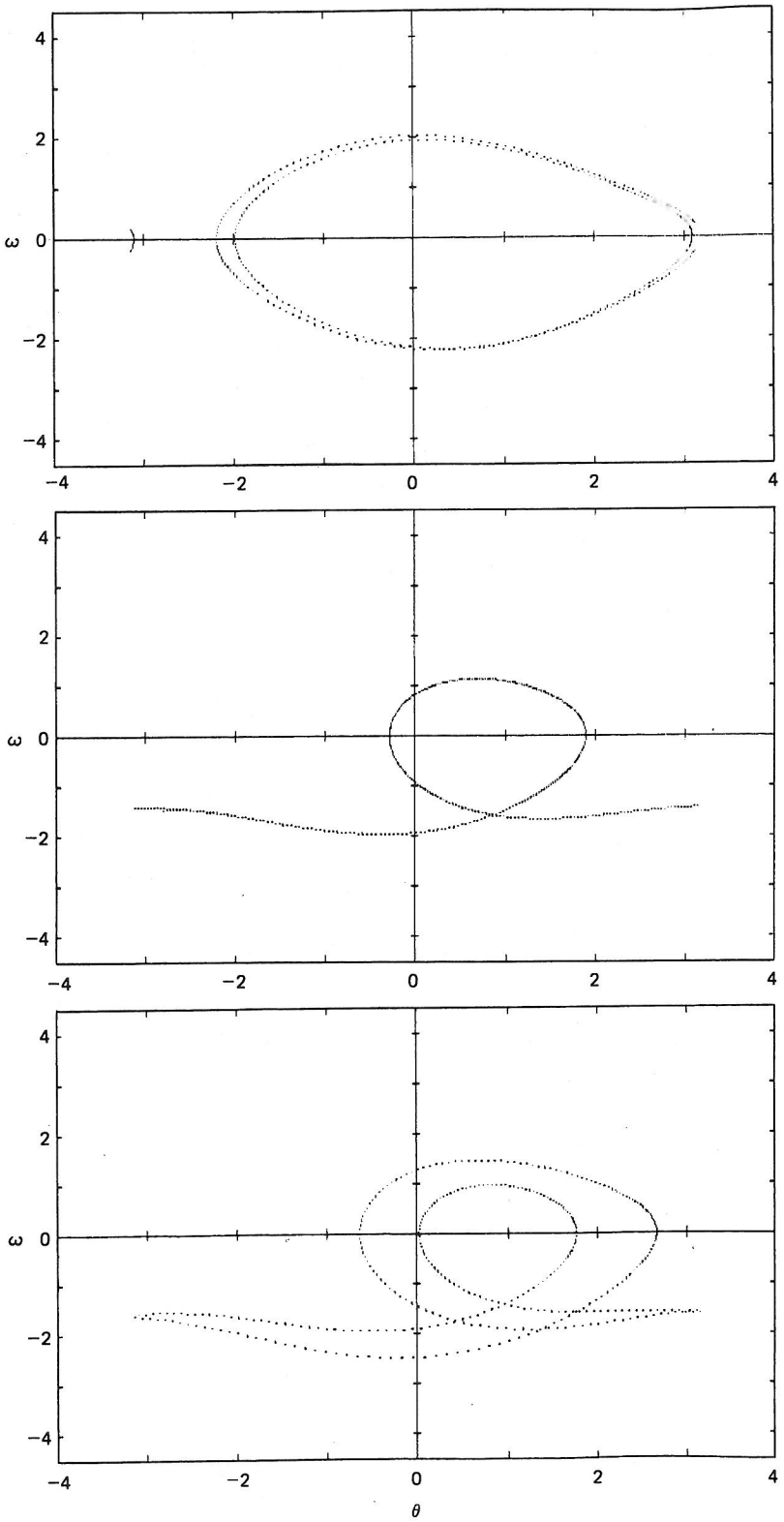

Fig. 2.15 Steady state phase diagram and sketch of the corresponding pendulum motion for different drive amplitudes. All motions are periodic and one complete cycle is shown in each case. The direction of the arrow depends on the initial conditions. (*a*) $g=1.07$; (*b*) $g=1.35$; (*c*) $g=1.45$. ($q=2$).

The motion of the pendulum illustrated in Figure 2.14 is a simple oscillation. As the drive amplitude increases, more complex motions occur, both periodic and chaotic. Some examples of more complex periodic motions are illustrated in Figure 2.15, for various drive amplitudes (g). The path in real space and the corresponding phase plane diagram are shown in each case. The orbits involve a superposition of oscillation and complete rotation.

Poincaré section

A Poincaré section is a device invented by Henri Poincaré as a means of simplifying phase space diagrams of complicated systems. It is constructed by viewing the phase space diagram stroboscopically in such a way that the motion is observed periodically. For the driven pendulum, the strobe period is the period of the forcing.

In order to make this idea more concrete let us refer to the moderately driven pendulum whose attractor was shown in Figure 2.14(*a*). The Poincaré method consists of cutting or sectioning the spiral attractor at regular intervals and looking at these sections along the ϕ axis through the (θ,ω) plane. If this sectioning is done at intervals corresponding to the forcing motion, then the stroboscopic pictures all show one point. The motion always comes back to the same (θ,ω) coordinates as ϕ is increased by 2π. Figure 2.16 illustrates the result.

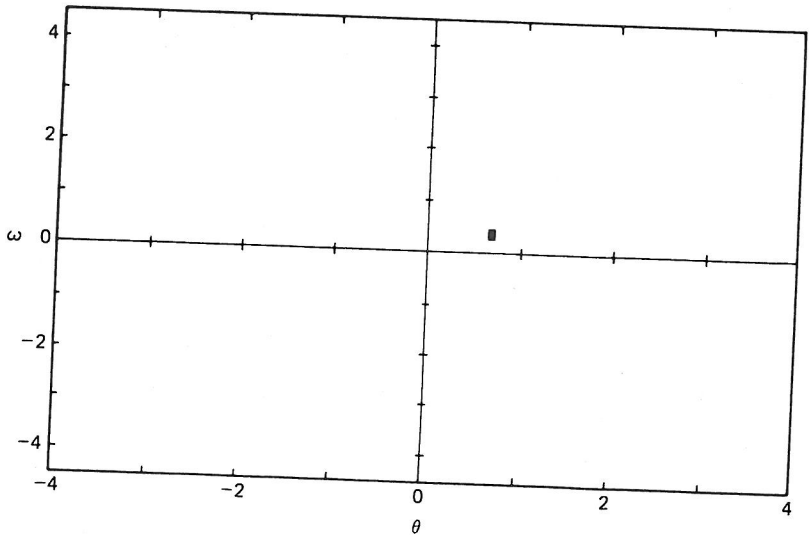

Fig. 2.16 Poincaré section of the linearized pendulum ($g=0.5$, $q=2$, $\phi=0$).

This strobe diagram is called a *Poincaré section* as the graph is 'cut' periodically.

The Poincaré section can provide information about the ratio of the strobe frequency, ω_S, to the natural frequency of the dynamical motion, ω_0. For example, if a motion whose natural frequency was equal to 1 were strobed at a frequency equal to 2, the Poincaré section would have two points. In general, if the natural frequency of the motion, ω_0, is equal to $(p/q)\omega_S$ where p/q is rational, then there are q points, and the order of their appearance is such that, as a given point appears on the circle, the next $[q-(p+1)]$ positions are skipped. All of the q points, however, are eventually filled in. Figure 2.17 illustrates the situation where, for example, when $\omega_0=\frac{4}{5}\omega_S$, there are five points and $5-(4+1)=0$ positions are skipped as the points go counterclockwise around the circle. These strobe points provide the coordinate values for θ and ω on the Poincaré plot, and the numbering of the points represents their order of appearance.

If the pendulum goes all the way around, then ω has a direct current component as well, and the pattern of dots is not centered on the origin. Since the mixture of rotation and oscillation may lead to a nonzero average displacement $\langle\theta\rangle$, the offset will generally be asymmetric. Furthermore, if the relation between the strobe frequency and the pendulum frequency is irrational (incommensurate), then the strobe points will never quite repeat and the points will gradually fill in a circle on the Poincaré section. Finally, if the system becomes dissipative – in the pendulum case by the addition of a damping term – then the points on the Poincaré section will move toward the appropriate attractor. These ideas are illustrated in Figure 2.18.

For a dynamical system with a periodic forcing term, the Poincaré section provides a simplification of the phase diagram while retaining the essential features of the dynamics. Therefore it is ideally suited to the driven pendulum. In Figure 2.19, some of the periodic motions illustrated by phase diagrams in Figure 2.15 are shown as Poincaré sections. For the periodic motions, the appearance of these sections is quite simple. But in Chapter 3, where the chaotic behavior of the pendulum is described, the simplification of phase space provided by the Poincaré section is shown to be very important for an understanding of the physics. One useful tool for the study of chaos is the observation of the distribution of points on a computer-generated Poincaré section.

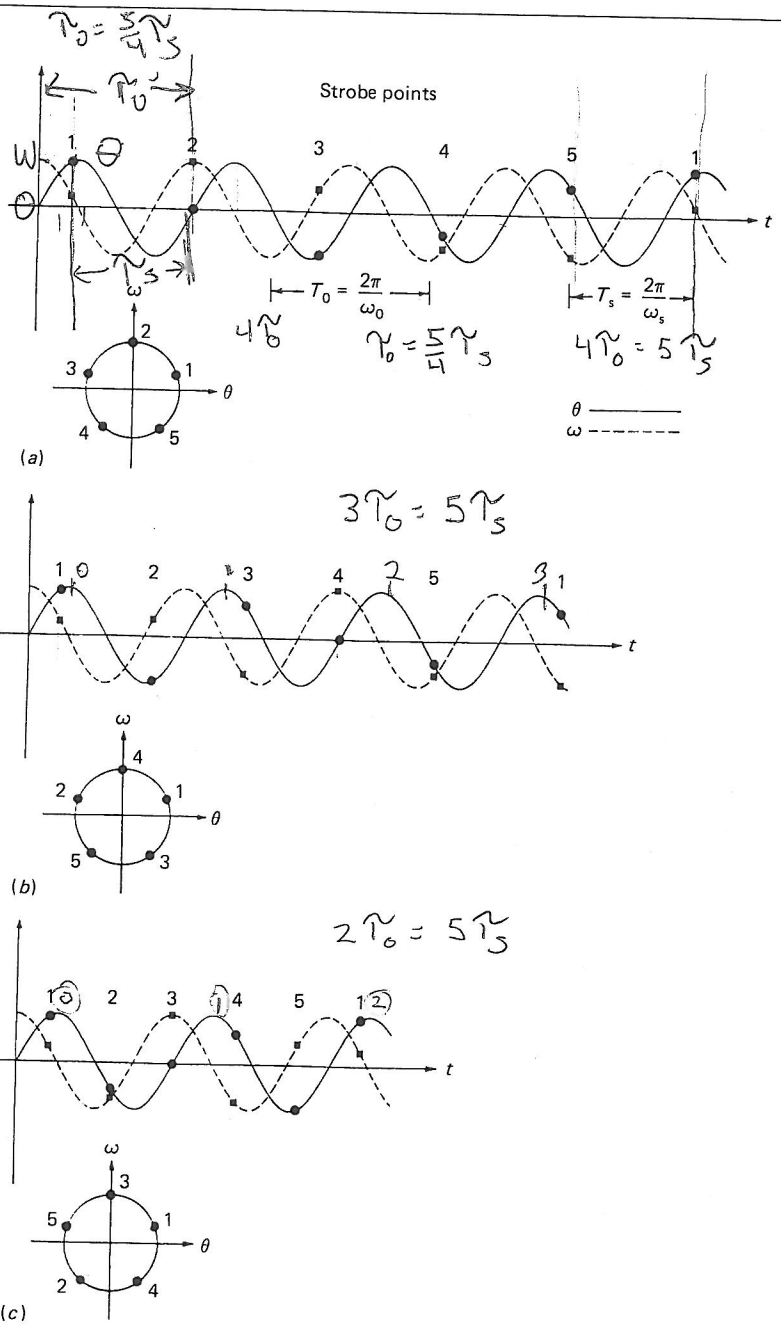

Fig. 2.17 Relationship of strobe frequency to dynamical motion frequency. The positioning and order of points on a Poincaré section is shown for different ratios of strobe (ω_s) and motion frequencies (ω_0). (*a*) $\omega_0 = \frac{4}{5}\omega_s$; (*b*) $\omega_0 = \frac{3}{5}\omega_s$; (*c*) $\omega_0 = \frac{2}{5}\omega_s$.

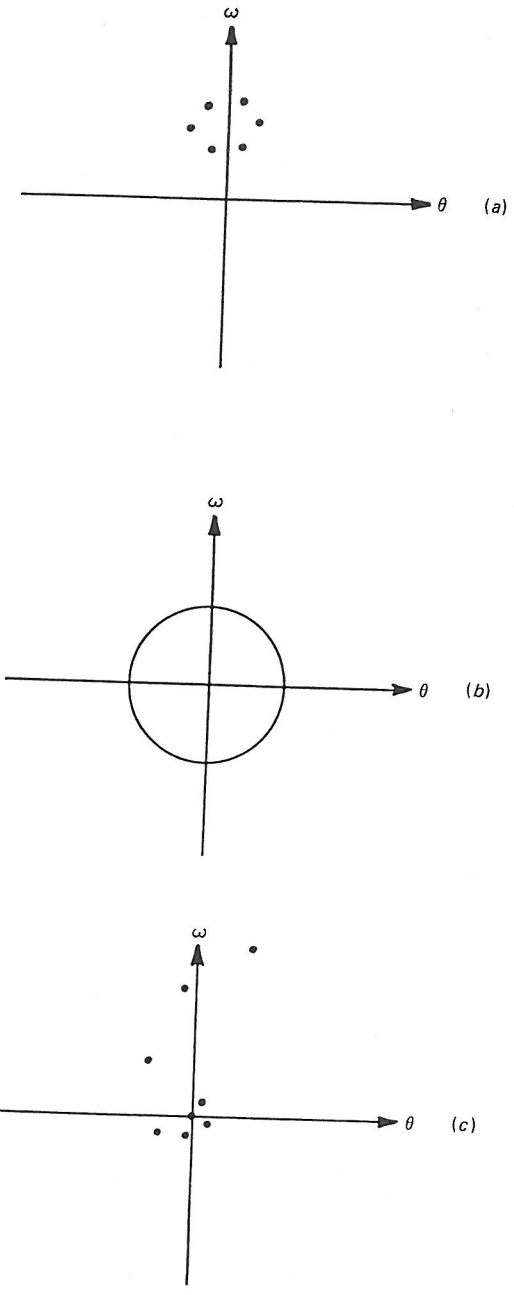

Fig. 2.18 Poincaré sections of different motions. (*a*) Combined oscillatory and rotational motion whose frequency is a rational fraction of the strobe frequency. (*b*) Oscillatory motion whose frequency is incommensurate with the strobe frequency. (*c*) Dissipative motion.

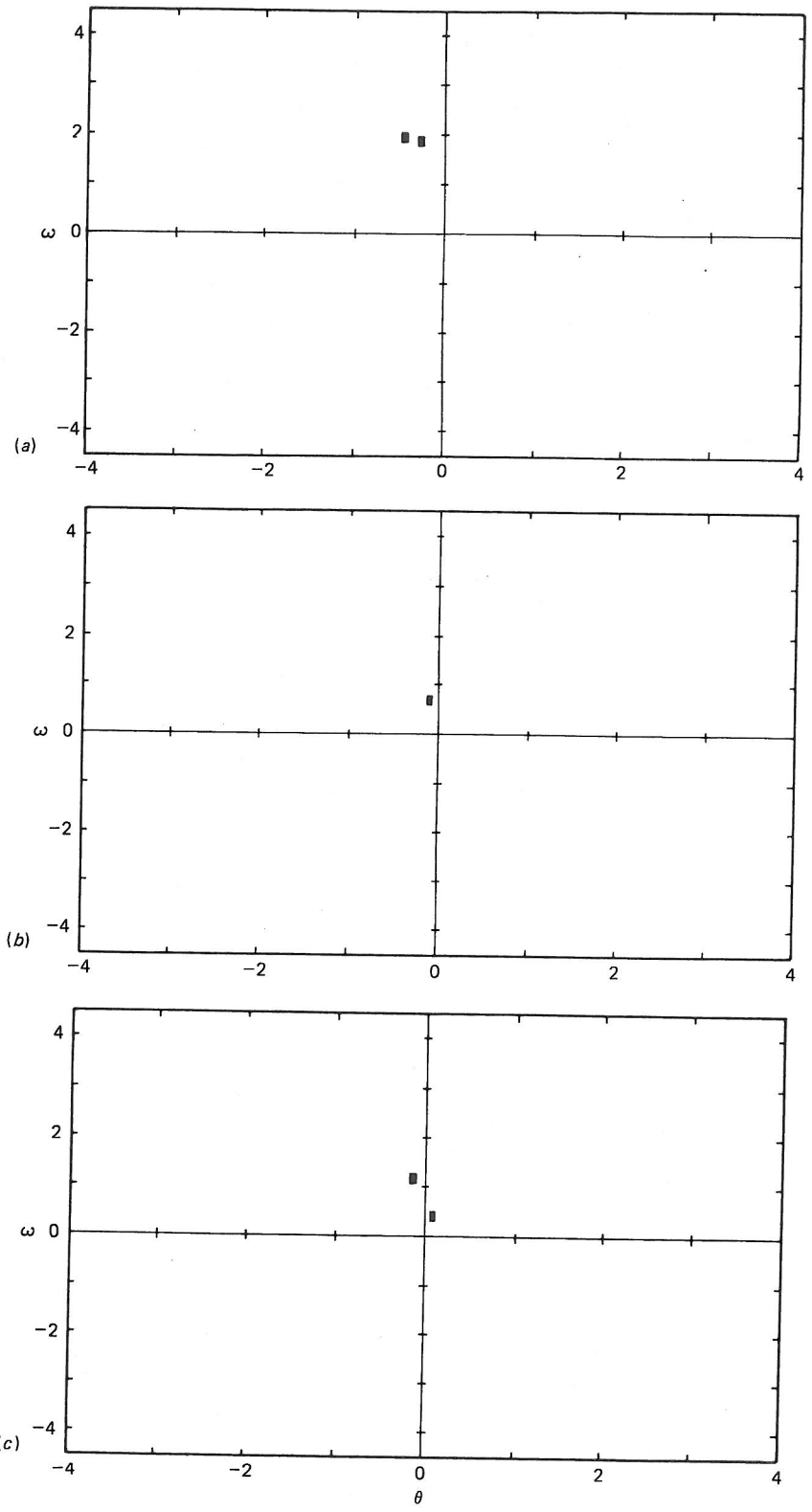

Fig. 2.19 Poincaré sections of motion illustrated in Figure 2.15. The section is taken at $\phi = 0$ ($q = 2$). (*a*) $g = 1.07$; (*b*) $g = 1.35$; (*c*) $g = 1.45$.

Spectral analysis of time series

The time evolution of a dynamical system is represented by the time variation $f(t)$ or (when sampled at regular intervals) *time series* of its dynamical variables. Any function $f(t)$ may be usefully represented as a superposition of periodic components. The determination of their relative strengths is called *spectral analysis*.

Depending upon the nature of the function, $f(t)$, we may represent it in two different but related ways. If $f(t)$ is periodic, then the spectrum may be expressed as a linear combination of oscillations whose frequencies are *integer multiples* of a basic frequency. This linear combination is called a *Fourier series*. However, it is more likely that $f(t)$ is not periodic, and the spectrum must then be expressed in terms of oscillations with a continuum of frequencies. Such a spectral representation is called the *Fourier transform* of $f(t)$. This representation is especially useful for chaotic dynamics. Because the Fourier transform is in general a complex-valued function, it is often preferable to define a real-valued function which is the modulus squared of the transform. This real function is called the *power spectrum* of $f(t)$. One familiar but crude example of the power spectrum is the LED display of an electronic graphics equalizer. The moving bars on the display indicate the instantaneous electronic power in each of the sections of the audio frequency spectrum.

In this section we review the main features of the Fourier series and then give the Fourier transform method as the limiting case of the Fourier series when the periodicity of $f(t)$ becomes infinitely large, that is, when $f(t)$ ceases to be periodic.

If the function is periodic such that $f(t)=f(t+nT)$ – with n being a positive or negative integer and T being the basic periodicity – then, as noted above, the frequencies of the various spectral components are all integer multiples of the basic frequency, $1/T=\omega_0/2\pi$. The *Fourier series* representation of $f(t)$ may be written compactly in complex notation:

$$f(t)=\sum_{n=-\infty}^{\infty} a_n e^{in\omega_0 t},$$

where the a_n are the amplitudes of the components of frequency $n\omega_0$. These amplitudes may be determined from the calculation:

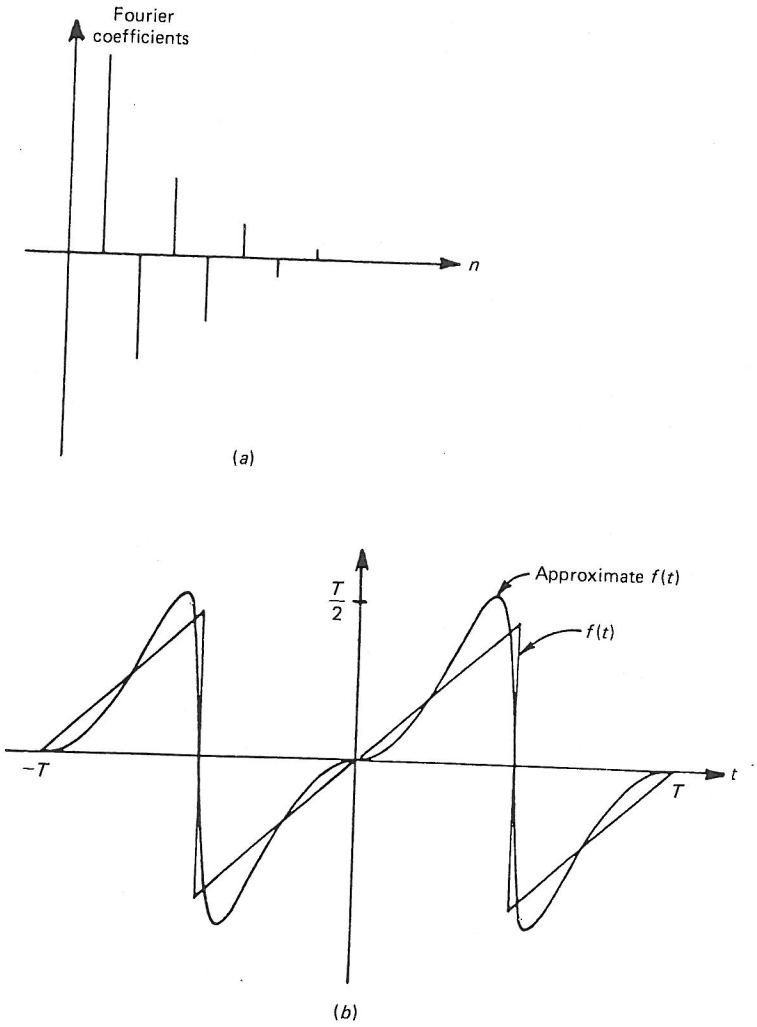

Fig. 2.20 Fourier spectrum of a sawtooth waveform. (*a*) Fourier coefficients. (*b*) Sawtooth, $f(t)$, together with an approximation of $f(t)$ using the two largest components of the Fourier spectrum.

$$a_n = \frac{\omega_0}{2\pi}\int_{-\pi/\omega_0}^{\pi/\omega_0} f(t)\mathrm{e}^{-\mathrm{i}n\omega_0 t}\mathrm{d}t.$$

(See, for example, Kaplan (1973).) An example of a periodic time series often found in electronics is the 'sawtooth' function, shown in Figure 2.20.

Example 2.4. The time series of the 'sawtooth' function is $f(t)=t:t\in(-T/2,T/2)$ where $T=2\pi/\omega_0$. (The pattern is repeated.)

It is left as an exercise to show that

$a_n=0$ for $n=0$;
$a_n=1/in\omega_0$ for $n=$odd integer; and
$a_n=-1/in\omega_0$ for $n=$even integer.

Substitution of these results back into the Fourier series expression and manipulation of the ensuing complex expressions leads to the result:

$$f(t)=\frac{2}{\omega_0}[\sin(\omega_0 t)-\tfrac{1}{2}\sin(2\omega_0 t)+\tfrac{1}{3}\sin(3\omega_0 t)-\cdots].$$

Note that the coefficients $1, -\frac{1}{2}, \frac{1}{3}$, and so forth are not the same as the a_n but are combinations of pairs of a_n. Figure 2.20(*a*) shows a bar chart of the coefficients. The original function $f(t)$, and the resultant of the first two frequency components are shown as an approximation to $f(t)$ in Figure 2.20(*b*).

The *Fourier transform* is an extension of the Fourier series in that the basic periodicity T of $f(t)$ is allowed to become infinitely large. This condition implies that $f(t)$ *need no longer be periodic.* In this circumstance the spacing between the frequency components becomes infinitesimal. The discrete spectrum of frequency components becomes a *continuum* of spectral densities as shown. Therefore, a given component a_n converts to $a(\omega)\delta\omega$ where $\delta\omega$ is a small interval of frequency and $a(\omega)$ is the frequency-dependent amplitude or *Fourier transform.* The practical advantage of the transform is that it can be used to analyze a function about whose properties we are totally ignorant. It often yields surprising and illuminating information.

One may think of the transition from the Fourier series to the Fourier transform in terms of the following set of transformations:

$T\to\infty$
$n\omega_0\to\omega$,

ω being a continuous variable, and

$a_n\to a(\omega)\mathrm{d}\omega$.

Taking the appropriate limits leads to the following conversions:

$$f(t)=\sum_{n=-\infty}^{\infty} a_n e^{in\omega_0 t} \text{ becomes } f(t)=\int_{-\infty}^{\infty} a(\omega)d\omega e^{i\omega t}$$

and

$$a_n=\frac{\omega_0}{2\pi}\int_{-\infty}^{\infty} f(t)e^{-in\omega_0 t}dt \text{ becomes } a(\omega)d\omega=\frac{d\omega}{2\pi}\int_{-\infty}^{\infty} f(t)e^{-i\omega t}dt.$$

The two right hand expressions lead to reciprocal expressions for the Fourier transform,

$$a(\omega)=\frac{1}{2\pi}\int_{-\infty}^{\infty} f(t)^{-i\omega t}dt,$$

and the original function,

$$f(t)=\int_{-\infty}^{\infty} a(\omega)e^{i\omega t}d\omega.$$

As noted earlier, the Fourier transform $a(\omega)$ often turns out to be complex, and it is useful to define a real-valued function, the *power spectrum*, as

$$S(\omega)=|a(\omega)|^2.$$

One might compare this definition with the relation between wave amplitude and wave energy. The power spectrum is the quantity typically calculated in experimental or numerical work.

Let us consider two examples that can be solved analytically.

Example 2.5. Let $f(t)$ be a decaying, oscillating function

$$f(t)=\begin{cases} e^{-\gamma t}e^{i\omega_0 t}, & t\in[0,\infty) \\ 0, & t\in(-\infty,0] \end{cases}$$

as shown in Figure 2.21(*a*). The function has a natural frequency ω_0. It could represent a dissipative tuned electrical circuit, for example. Calculation of the integral for $a(\omega)$ leads to

$$a(\omega)=\frac{1}{2\pi[\gamma+i(\omega-\omega_0)]}$$

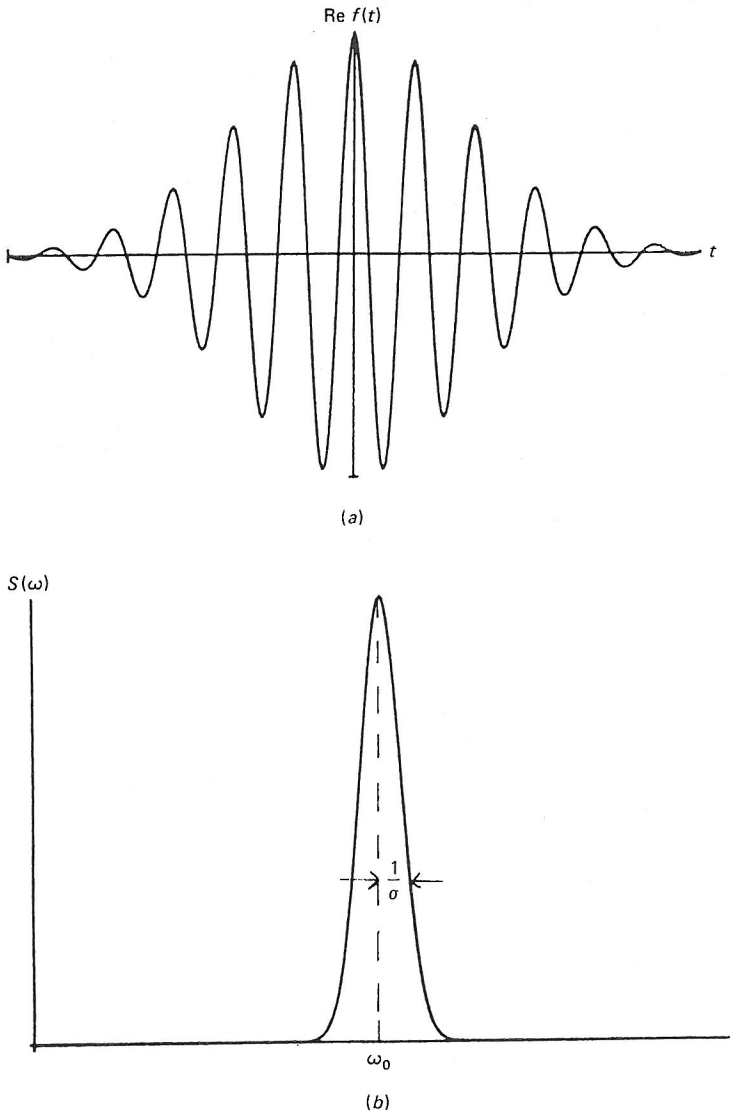

Fig. 2.22 (*a*) The real part of the Gaussian time series of Example 2.6. (*b*) Power spectrum.

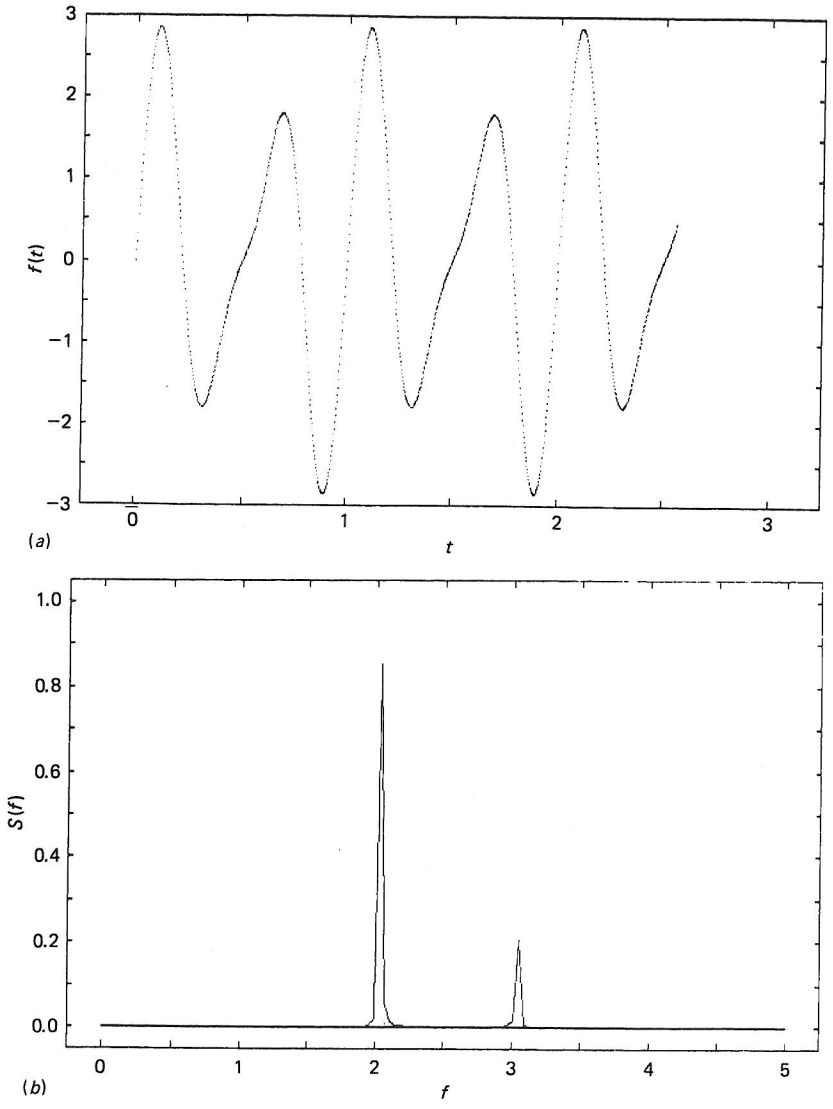

Fig. 2.23 (*a*) Two component times series. (*b*) Power spectrum.

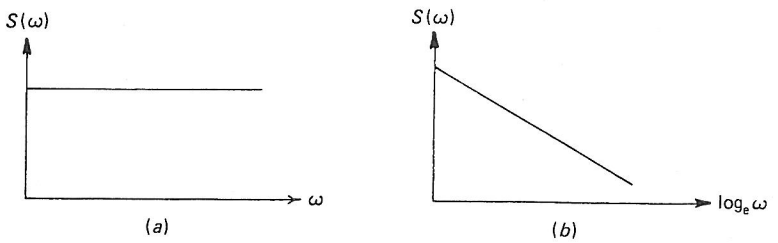

Fig. 2.24 Power spectra of noise time series. (*a*) White noise. (*b*) $1/f$ noise.

their power spectra. For example, Johnson noise which results from thermal agitation in electric circuits is frequency-independent or 'white' (in analogy with white light). On the other hand, '$1/f$' noise, which is common in resistors and solid state devices, has a spectrum varying as f^{-1} (or another power) at low frequencies (Malmstadt, Enke, and Crouch, 1981). These two types are illustrated in Figure 2.24.

Fourier analysis is an interesting subject and the reader who wishes to study it further may find helpful the treatment in Kaplan (1973). Occasionally a brief discussion in the context of quantum physics is provided in the modern physics sections of introductory physics texts. See, for example, Orear (1979).

Analytical calculation of the Fourier transform can become very difficult if the time variation is at all complicated, but numerical methods are straightforward. At first glance, it appears that the appropriate algorithms would involve numerical integration. However, a distinctly different and very efficient approach may be taken when the data are discrete or digitized. The algorithm is called the *fast Fourier transform* (FFT) and was reinvented by J.W. Cooley and J.W. Tukey in 1964. (The method had originally been discovered in 1942 and utilized with hand calculators.) It takes advantage of certain symmetry properties in the trigonometric functions at their points of evaluation, in order to achieve an increase in speed over more conventional methods. If N is the number of data points in the time variation of a signal, then conventional algorithms would require about N^2 computer operations, whereas the FFT requires about $N\log_2 N$ operations. For a 1000 point transform this means a reduction by a factor of about 100, and larger samples lead to even more significant gains. A short introduction is provided in Higgins (1976) and a listing in BASIC is given in Appendix B. (A more comprehensive treatment is available in Press *et al.* (1986), Chapter 12.)

With this background of mathematical tools now available, we may, in Chapter 3, concentrate more fully on the driven, damped pendulum.

Problems

1. For the linearized undamped pendulum show that the solutions, $\omega = A\sin t$ and $\theta = A\cos t$, lead to circular trajectories in the phase plane.
2. Show that one possible solution to the linearized damped pendulum:

   $$d^2\theta/dt^2 + d\theta/dt + \theta = 0$$

   is $\theta = Ae^{-\lambda t}\cos(\omega_0 t)$. Show that $\lambda = \frac{1}{2}$ and $\omega_0 = \sqrt{3}/2$.
3. A particle falls a distance $x(t)$ in a gravitational field, with velocity $v(t)$. The system of equations is

   $$dx/dt = v$$
   $$dv/dt = g$$

   Show that the phase area is conserved. If a friction force, $-kv$, is added to the acceleration equation show that the phase area shrinks.
4. Hénon and Heiles studied stellar orbits in a galaxy using a two-dimensional model with a potential $V(x,y) = \frac{1}{2}(x^2+y^2) + x^2y - \frac{1}{3}y^3$. This leads to a system of equations for the four-dimensional phase space of

   $$dp_x/dt = -x - 2xy$$
   $$dp_y/dt = -y - x^2 + y^2$$
   $$dx/dt = p_x$$
   $$dy/dt = p_y$$

   Is this system dissipative?
5. Lorenz developed the following system of equations to describe the interrelations of temperature variation and convective motion

   $$dx/dt = -\sigma x + \sigma y$$
   $$dy/dt = -xz + rx - y$$
   $$dz/dt = xy - bz$$

   where σ, r, b are constants. Prove that the system is dissipative.
6. Show that the system $d^2\theta/dt^2 + d\theta/dt + \sin\theta = 0$ linearizes to $d^2\theta/dt^2 + d\theta/dt + (\theta - n\pi) = 0$ near $\theta = n\pi$ when n is odd, and to

$d^2\theta/dt^2+d\theta/dt-(\theta-n\pi)=0$ near $\theta=n\pi$ when n is even. In general one would use a Taylor's series expansion – can this case be treated more intuitively?

7. Find the general solution to $d^2\theta/dt^2+d\theta/dt+(\theta-n\pi)=0$ when n is odd.
8. Following the rationale of Figure 2.17 develop the Poincaré plot for

   (i) $\omega=\frac{2}{3}\omega_s$ and (ii) $\omega=\frac{1}{3}\omega_s$.
9. (*a*) Find the power spectrum of the 'square' wave packet:

$$f(t)=\begin{cases}a & t\in[0,\pi/2]\\ 0 & \text{for all other values of } t.\end{cases}$$

   (*b*) Show that the average power is $f(t)^2=a^2$,
10. Prove the formula given in the text for the Fourier series amplitudes, a_n.
11. Develop the results for a_n in Example 2.4.
12. Do the calculation of $S(\omega)$ for the decaying exponential wave to obtain the Lorentzian curve.
13. Calculate the width of the Gaussian power spectrum.

The following problems require the use of a computer. Listings provided in Appendix B may be helpful, although they were primarily developed for the driven, damped pendulum, and therefore have to be modified for these exercises.

14. Write a program which will display trajectories in phase space for the undamped, linearized pendulum. The program should require a set of initial (θ,ω) coordinates as input. Remember to keep θ reasonably small so that $\sin\theta\approx\theta$.
15. Write a program which will display trajectories in phase space for the damped, linearized pendulum. Use the equation

    $d^2\theta/dt^2+\gamma d\theta/dt+\omega_0{}^2\theta=0.$
16. Modify the program described in Problem 15 so that the term in θ becomes $\omega_0{}^2\sin\theta$ and try various inputs. In this case you should modify the display of the θ coordinate so that its boundary conditions become periodic, as outlined in the chapter.
17. Modify the program described in Problem 14 so that the input

will be a set of initial coordinates which will form an initial area. The program should then demonstrate the motion of the given area in phase space.

18. Modify the program described in Problem 15 to follow the evolution of a block of initial coordinates. The development of this phase space should illustrate a dissipative system.
19. Develop a program to illustrate Poincaré sections similar to those shown in Figure 2.17. Use the linearized version of the pendulum.
20. In Appendix B the program called EXPFFT computes the power spectrum of a linear combination of periodic components. Use this program to look at $f(t)=\sin(2\pi f_0 t)$. Use a Nyquist frequency of 1 and sample 32 points for $f_0=\frac{1}{8}$. Try different numbers of points and different Nyquist frequencies. (The Nyquist frequency is the maximum frequency shown by the spectrum.) Try to determine the relationships which involve the number of points, the Nyquist frequency, and the resolution in frequency of the power spectrum.
21. Modify the above program to display the power spectrum of the function e^{-t} on $[0,\infty]$. Experiment with a variety of conditions (Nyquist frequency, number of points, etc.) in your program.

CHAPTER THREE

Visualization of the pendulum's dynamics

Using the tools described in Chapter 2, we are now in a position to discuss the main features of the motion of the driven pendulum. The equations of motion may be written as:

$$d\omega/dt = -\omega/q - \sin\theta + g\cos\phi$$
$$d\theta/dt = \omega$$
$$d\phi/dt = \omega_D$$

Since the system has three variables, its trajectory resides in a phase space of three dimensions, the minimum for chaotic behavior. In this chapter, we present and discuss a variety of computer simulations in order to characterize the dynamics of the pendulum. To allow compact illustration, values of θ and ϕ outside the range $(0,2\pi)$ are plotted at the equivalent point within that range.

The differential equations contain three adjustable parameters: the driving force amplitude g, the damping factor q, and the angular drive frequency ω_D. One could define a three-dimensional parameter space in which each point represents a particular choice of the parameters (g,q,ω_D). However a full exploration of the behavior as a function of all three parameters would be a forbidding task. Instead, we fix ω_D, choose a few values of q, and let g vary sufficiently to obtain a wide variety of dynamical behavior. As an aid to making appropriate parameter choices, we note that a constant torque of unity is just sufficient to keep the pendulum stationary at $\theta = \pi/2$. Therefore forcing amplitudes in the region $g \approx 1$ are used. Furthermore, the undamped pendulum of small amplitude has a 'natural' angular frequency equal to 1 in our units. Interesting dynamics occur when the forcing-term amplitude is of order unity and the drive frequency ω_D

is near (but not equal to) 1. Part of the rich variety of dynamical behavior comes from the interplay between the 'natural' frequency and the drive frequency. One set of parameters containing intervals of chaotic dynamics consists of $q=2$, $\omega_D=2/3$, and $0.5 \leq g \leq 1.5$ (Gwinn and Westervelt, 1985).

get programs

It is important that the reader develop an understanding of the physical content of the equations and diagrams. One way to accomplish this is to use a computer animation of the pendulum motion. The program in Appendix B entitled MOTION is one version of such a simulation. By running this program or a similar one, the reader can observe the pendulum's behavior for a variety of conditions (especially different values of g). Figure 3.1 shows a 'multiple exposure snapshot' of that animation. We encourage the reader to utilize the simulation frequently while reading this chapter. For some parameter values the motion appears to be periodic, while for others it is chaotic. In some cases the pendulum is nearly periodic for substantial intervals, with intervening irregular intervals; the net effect is that the motion is chaotic.

We are concerned here with the long-term behavior of the pendulum rather than the initial transients, which can be different. Therefore, the animation should be allowed to go through 20 or 30 drive cycles before one considers the motion to have converged to its long-term or statistically stationary state. We will sometimes refer to the long-term behavior as the 'steady state', though the motion need not be time-independent.

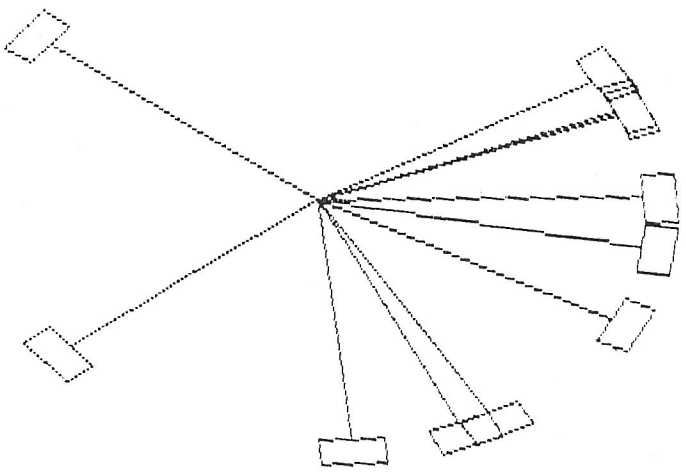

Fig. 3.1 A multiple exposure of the pendulum animation.

Sensitivity to initial conditions

The fundamental characteristic of a chaotic physical system is its sensitivity to the initial state. Sensitivity means that if two identical mechanical systems are started at initial conditions $\mathbf{x}$ and $\mathbf{x}+\boldsymbol{\varepsilon}$ respectively, where ε is a very small quantity, their dynamical states will diverge from each other very quickly in phase space, their separation increasing exponentially on the average. This phenomenon is illustrated for the pendulum in Figure 3.2(*a*). Phase trajectories of a chaotic pendulum, originating at two neighboring points, diverge markedly in less than one forcing period.

Sensitivity may also be illustrated by observing the phase space evolution of a block of pendulum states. (Figures 2.3 and 2.7 display unforced pendula in the undamped and damped cases, respectively.) Figure 3.2(*b*) shows the evolution of a block of initial phase points for the chaotic pendulum. After one half of a forcing period, the initial rectangular block has become long, thin, and curved. Because the system is dissipative, the area of the block shrinks with increasing time. Yet the set of phase points stretches along certain directions and contracts along other directions. The directions of divergence and shrinkage are different at different points in phase space. The net effect is that two closely spaced points are later found quite far apart.

The exponential divergence of adjacent phase points has a further consequence for the chaotic attractor. In order that the trajectories of two adjacent phase points remain bounded without intersecting, they must fold back on themselves, producing a three-dimensional chaotic attractor with many layers (actually an infinite number). A quantitative discussion of exponential divergence and the resulting geometrical complexity of the attractor is given in Chapters 4 and 5.

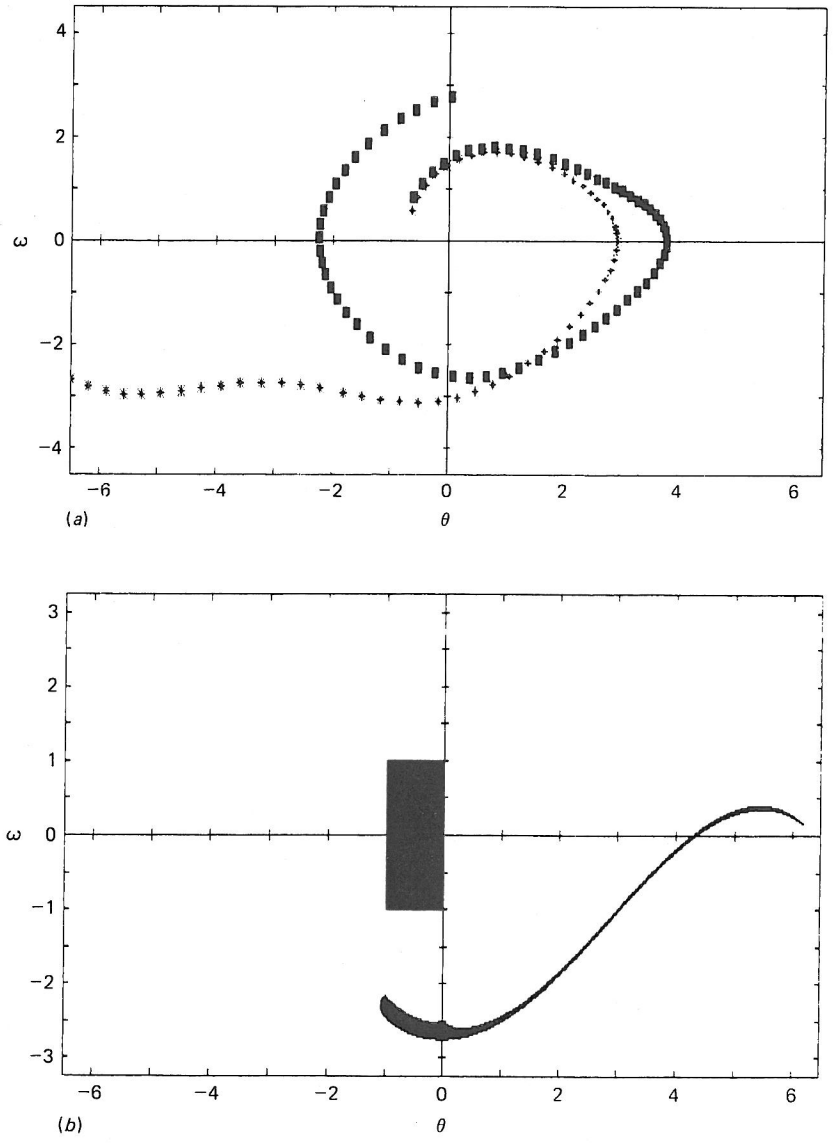

Fig. 3.2 Sensitivity to initial conditions. In (*a*) two phase trajectories, with neighboring initial points near the origin, evolve during one drive cycle ($g=1.5$, $q=4$). In (*b*) the phase points of trajectories from a block of initial points, $-0.5<\theta<0$ and $-0.5<\omega<0.5$, are shown after one half of a drive cycle. (The diagram may be regarded as a projection of the three-dimensional phase trajectories onto the (θ,ω) plane.)

Phase diagrams and Poincaré sections

We now use the geometrical tools of Chapter 2 to characterize the driven pendulum at a variety of driving force amplitudes g. The other parameters are held fixed at $\omega_D = 2/3$ and $q = 2$, though the effect of changing them is also interesting. (These parameters are pure numbers since the pendulum equation was made dimensionless.)

We begin by examining the trajectories in the three-dimensional space $(\theta, \omega, \varphi)$, as shown in Figure 3.3. The first case is periodic, since the trajectory retraces its path exactly. The situations in Figures 3.3 (b) and (c) are clearly more complicated, but it is difficult to tell exactly what has happened from this diagram. Finally, Figure 3.3 (d) is a chaotic state, and the diagram is so complex as to be nearly useless as a way of characterizing the dynamics.

Clearly, a better method of displaying the dynamics is needed. Two-dimensional phase projections and Poincaré sections turn out to be helpful, and these are shown in Figure 3.4. The value of g for each pair of diagrams is given in the caption. The upper parts of Figure 3.4 show projections of the trajectories onto the (θ,ω) phase plane. In this space, periodic motion appears as a closed orbit. Of course the projected orbits can appear to cross, and this occurs in the more complicated cases shown.

The lower parts of Figure 3.4 are the Poincaré sections, which are simply slices across the φ axis of the three-dimensional attractor. Periodic orbits ((a), (b), (d), (e), (f)) appear as a finite number of dots (enlarged for clarity), while chaotic orbits ((c), (g)) form complicated sets containing an infinite number of points. We shall return to an examination of their structure shortly.

The shape of the Poincaré sections varies with the phase at which they are taken. Sections for different values of φ are shown in Figure 3.5, and the aggregate of these shapes is similar to the full attractor of Figure 3.3 (d). As φ is increased, the attractors become stretched and folded repetitively, much like the kneading of dough. Evidence of this stretching and folding process may be seen in the fact that the sections contain a number of layers.

Actually, the structure of the attractors is much more complicated than is apparent from the sequence of Poincaré sections in Figure 3.5. This may be illustrated by looking at a small part of one of the sections, greatly magnified, as shown in Figure 3.6. The three parts of

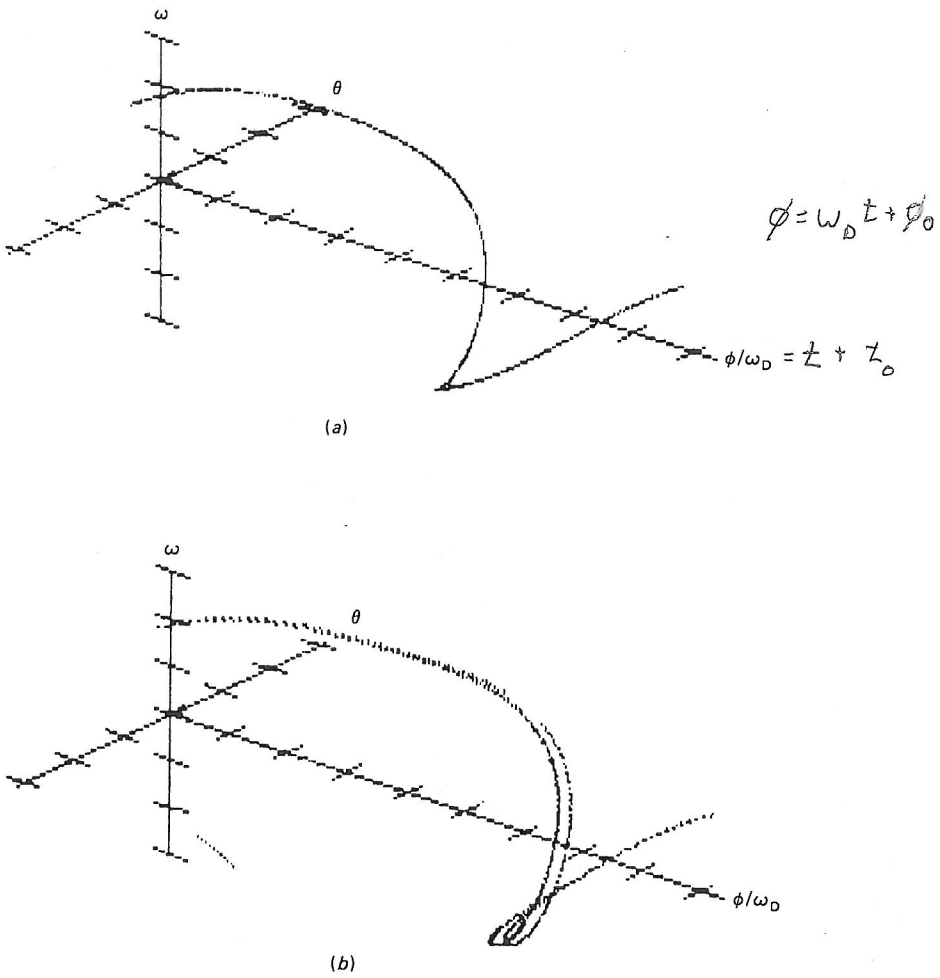

Fig. 3.3 Three-dimensional phase portraits for several values of driving force strength and $q=2$. (*a*) $g=0.9$; (*b*) $g=1.07$; (*c*) $g=1.47$; (*d*) $g=1.5$. This last case is chaotic.

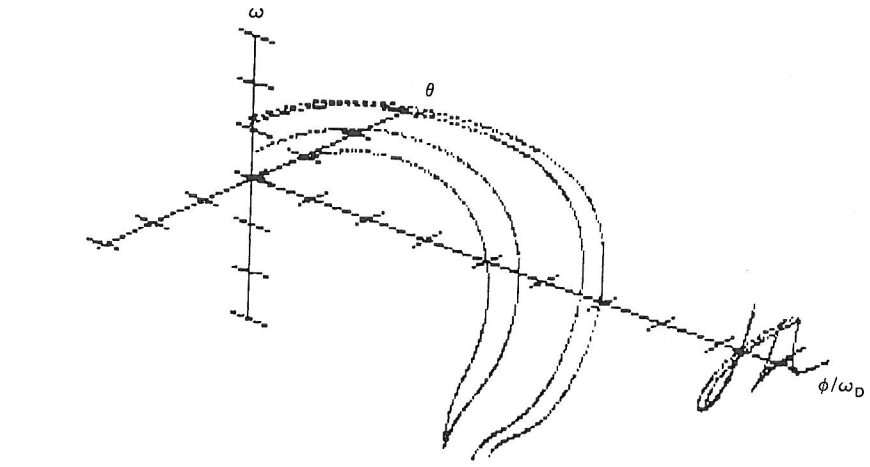

(c)

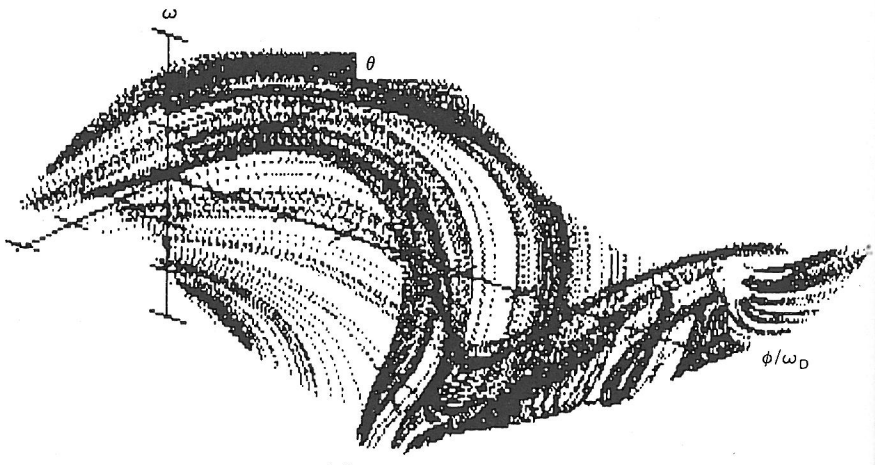

(d)

Fig. 3.3 (*cont.*)

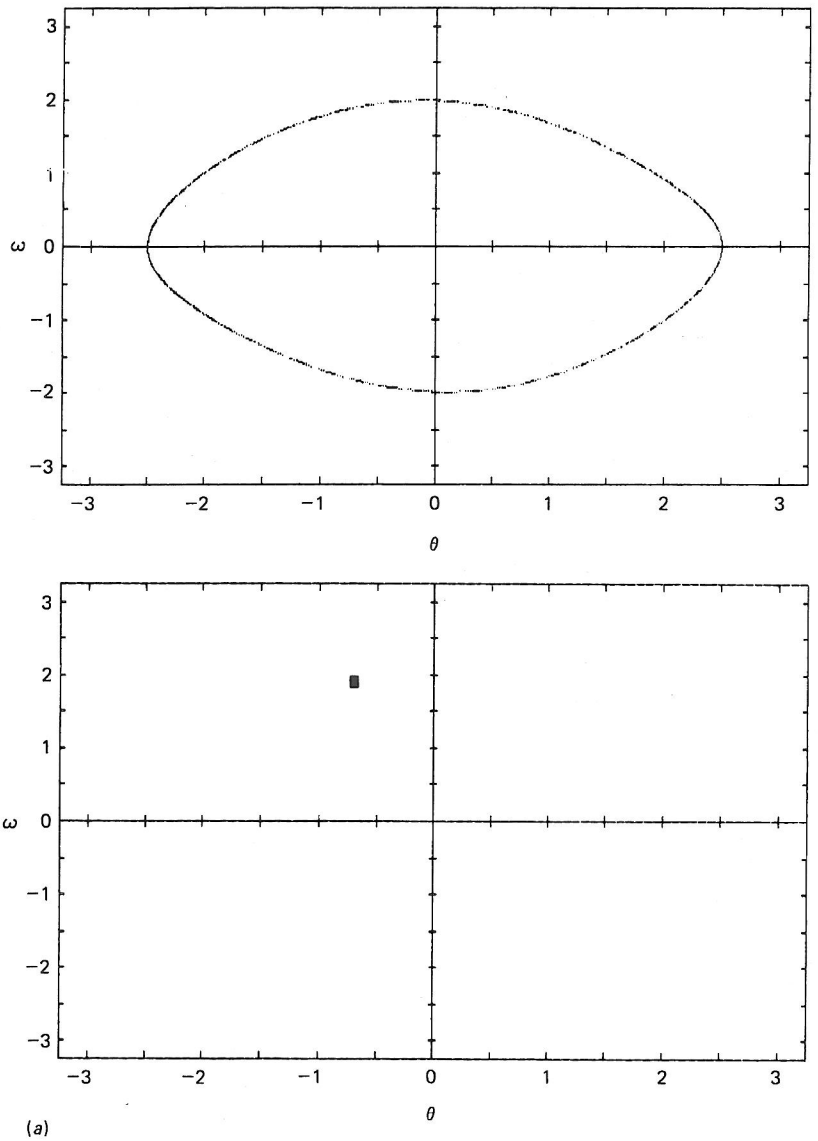

Fig. 3.4 Phase plane (above) and Poincaré sections (below) for several values of driving force amplitudes and $q=2$. In some cases the dots of the Poincaré sections have been enlarged for clarity. (*a*) $g=0.9$. (*b*) $g=1.07$, and a period doubling is apparent; (*c*) $g=1.15$, and the system is chaotic; (*d*) $g=1.35$, and the system is periodic again; (*e*) $g=1.45$, and another period doubling has occurred; (*f*) $g=1.47$, and a second period doubling is apparent; (*g*) $g=1.50$, another chaotic state.

$\omega_D = 2/3$

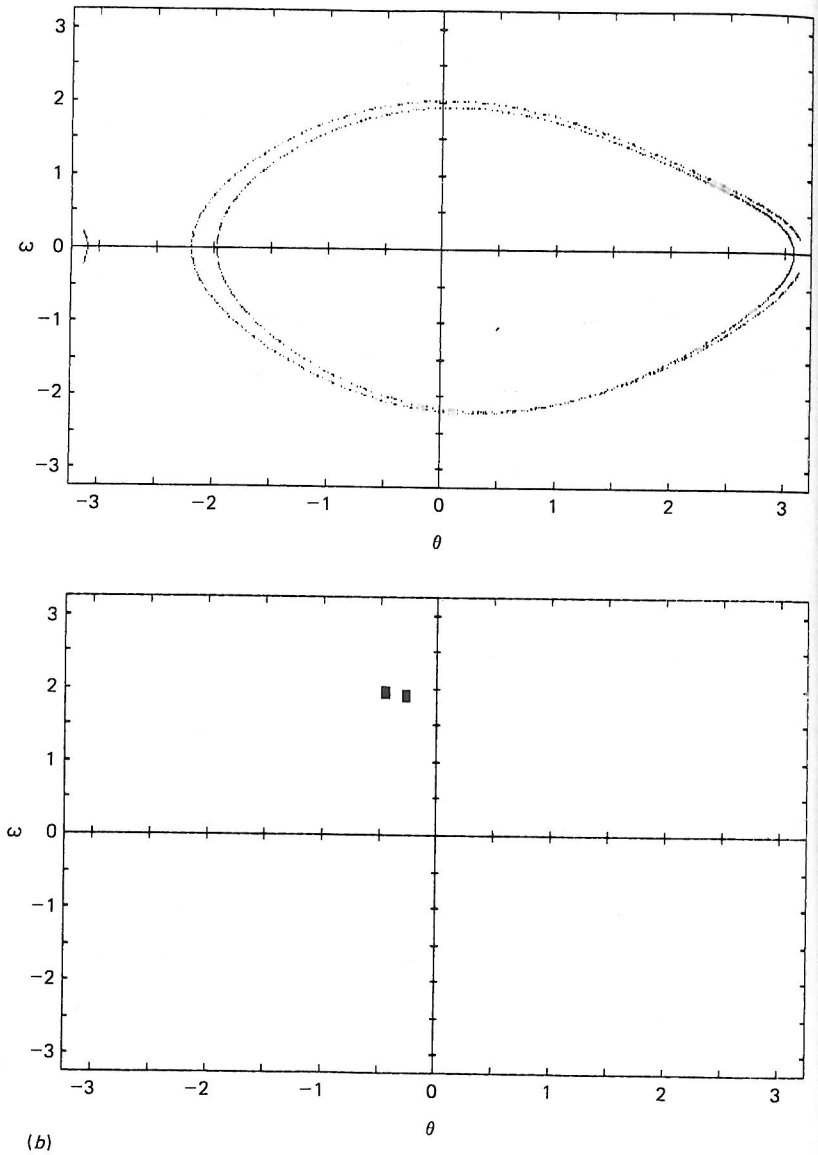

(*b*)

Fig. 3.4 (*cont.*)

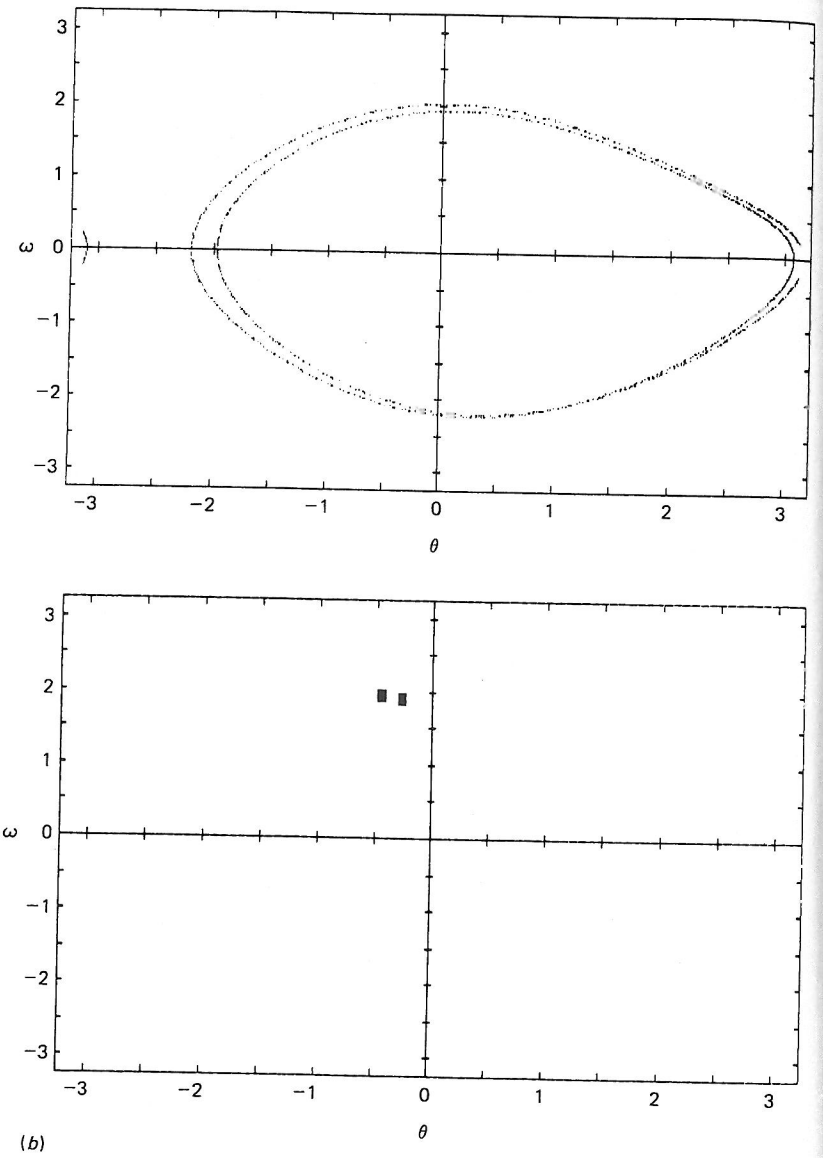

(*b*)

Fig. 3.4 (*cont.*)

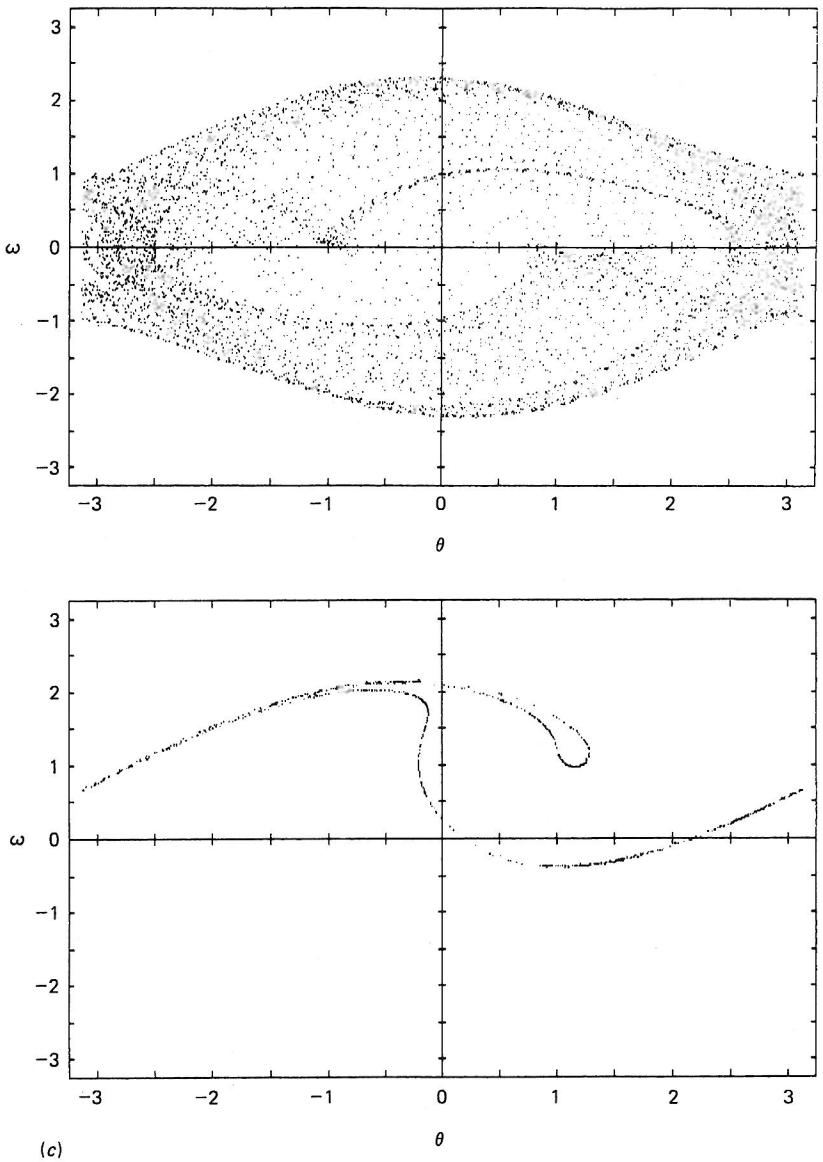

(*c*)

Fig. 3.4 (*cont.*)

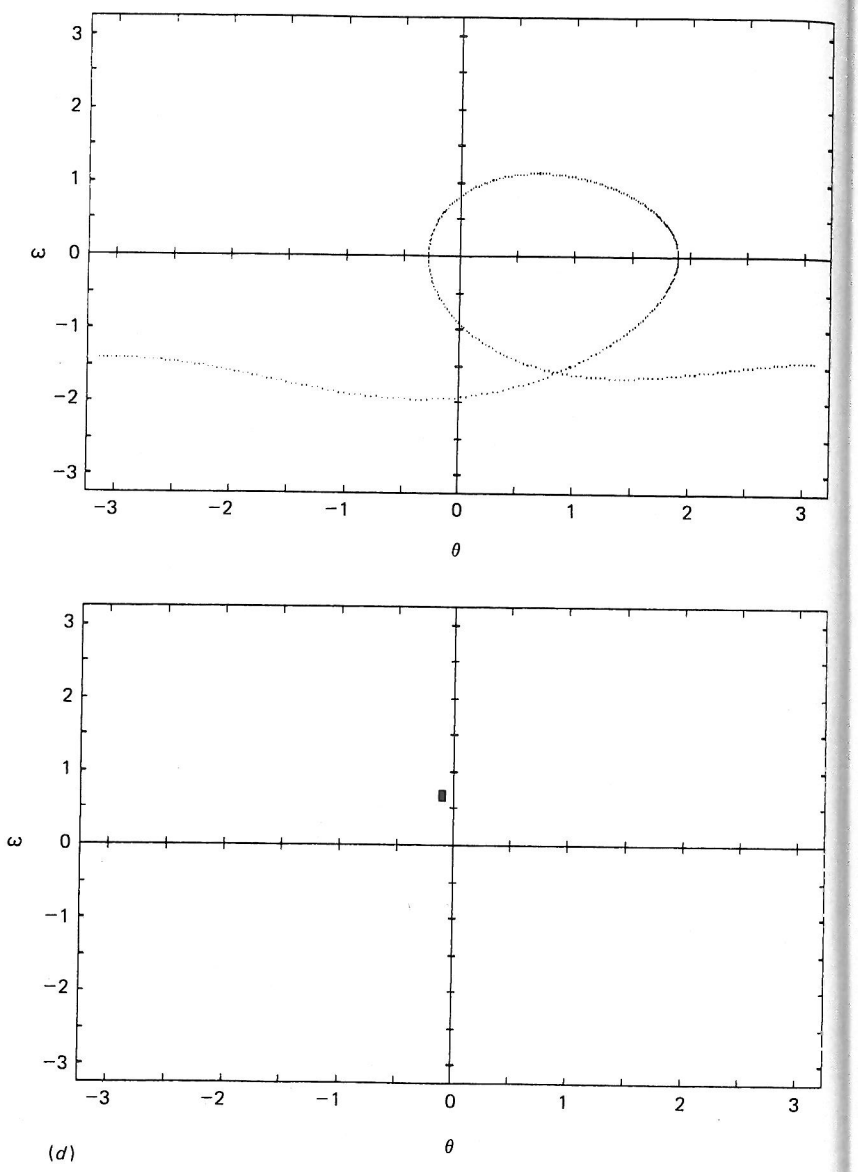

(*d*)

Fig. 3.4 (*cont.*)

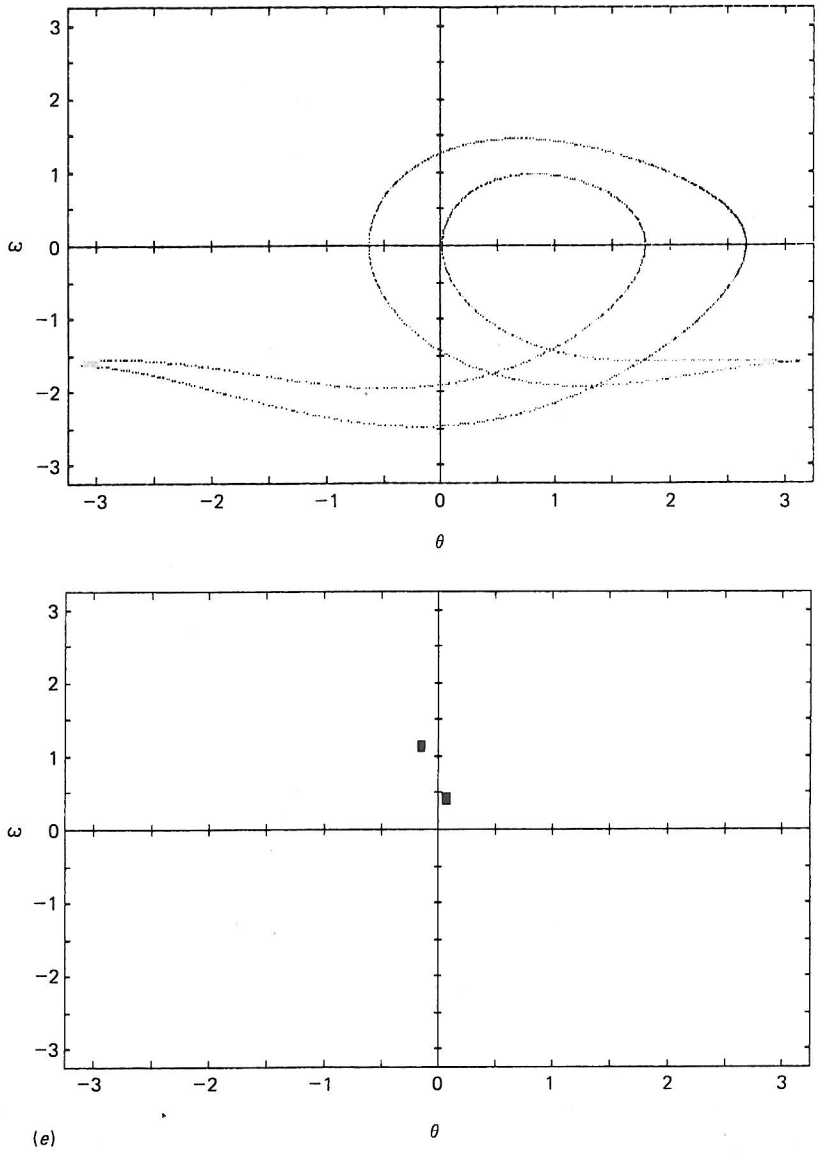

(*e*)

Fig. 3.4 (*cont.*)

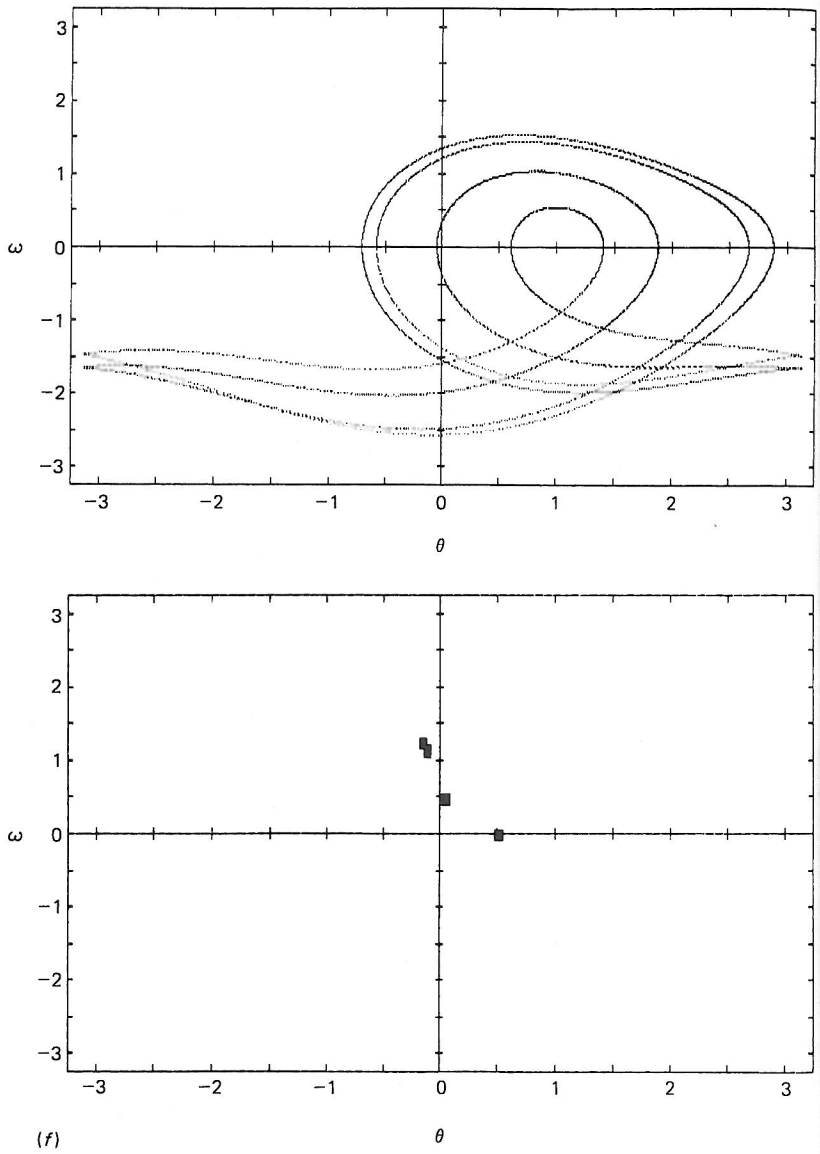

(*f*)

Fig. 3.4 (*cont.*)

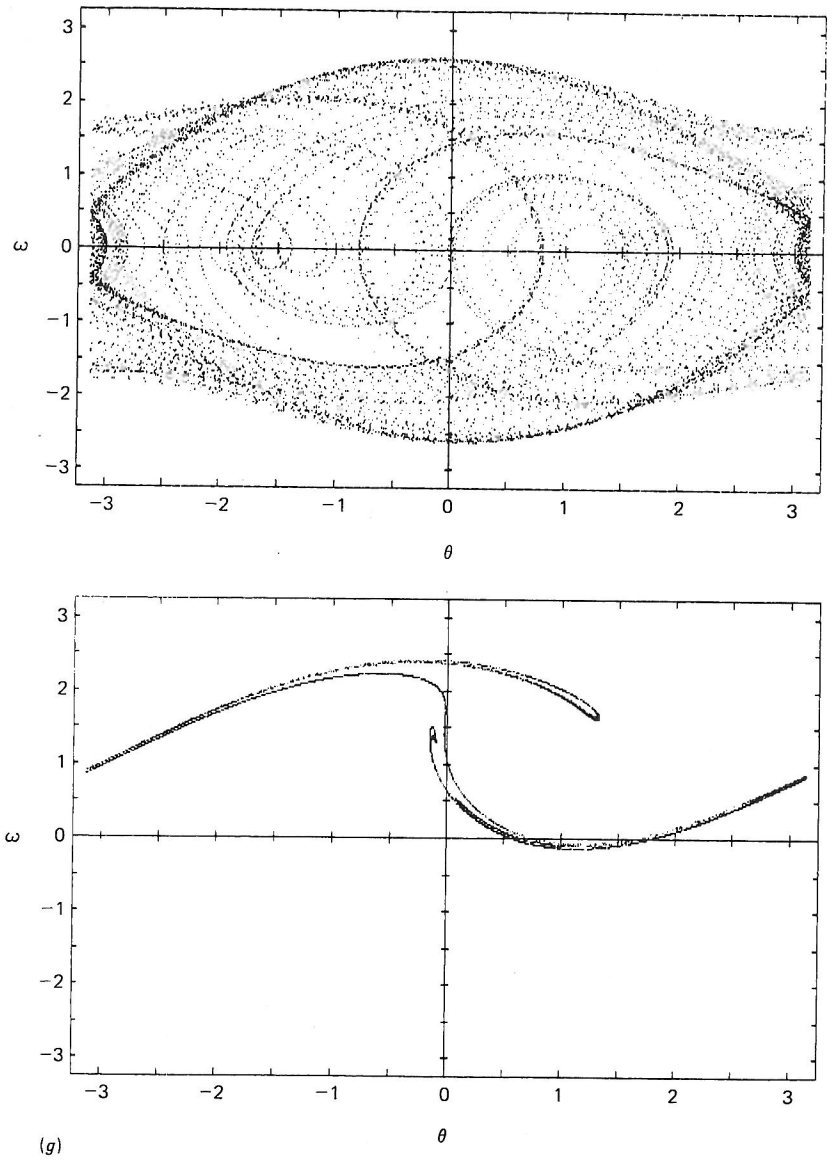

(*g*)

Fig. 3.4 (*cont.*)

this diagram show the attractor at different scales of magnification. (The different scales are obtained simply by changing the window for the graph. Each graph is abstracted from a set of about 10 000 points.) The stretching and folding processes lead to a cascade of scales: the attractor consists of an infinite number of layers. The fine structure, when magnified, resembles the gross structure. This property is called *self-similarity*.

These simulations of the chaotic attractor and its Poincaré sections reveal a hierarchical structure that is uncharacteristic of ordinary compact geometrical objects. In Chapter 5 the chaotic attractor and corresponding Poincaré sections are discussed as *fractals* – mathematical sets of noninteger dimension. While the periodic attractor is one-dimensional (Figures 3.3 (*a*), (*b*) and (*c*) and its Poincaré section is zero-dimensional (a few points), chaotic attractors are more complex, and their dimension is a fraction greater than two (see Chapter 5). Attractors having noninteger dimension are called *strange attractors*.

Finally, in Figure 3.7, we show several chaotic Poincaré sections corresponding to different values of the damping coefficient q. The layers of the attractor are more widely spaced as the damping decreases (or q increases).

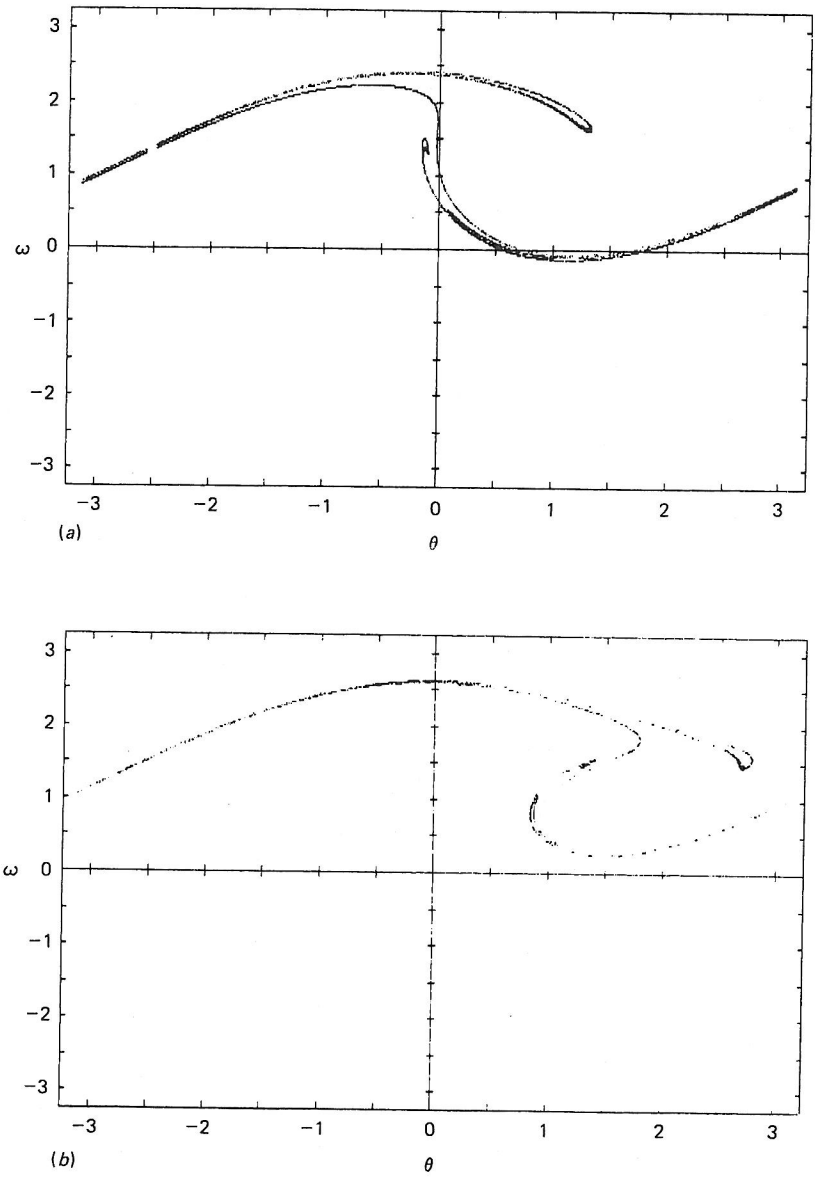

Fig. 3.5 Poincaré sections taken at incremented values of ϕ, the phase of the forcing term. $\Delta\phi = 2\pi/10$. At $\phi = \pi$ the section is anti-symmetric to the $\phi = 0$ case. $g = 1.5$, $q = 2$. (*a*) $\phi = 0.0$, (*b*) $\phi = 0.628319$, (*c*) $\phi = 1.25664$, (*d*) $\phi = 1.88496$, (*e*) $\phi = 2.51327$, (*f*) $\phi = 3.14159$.

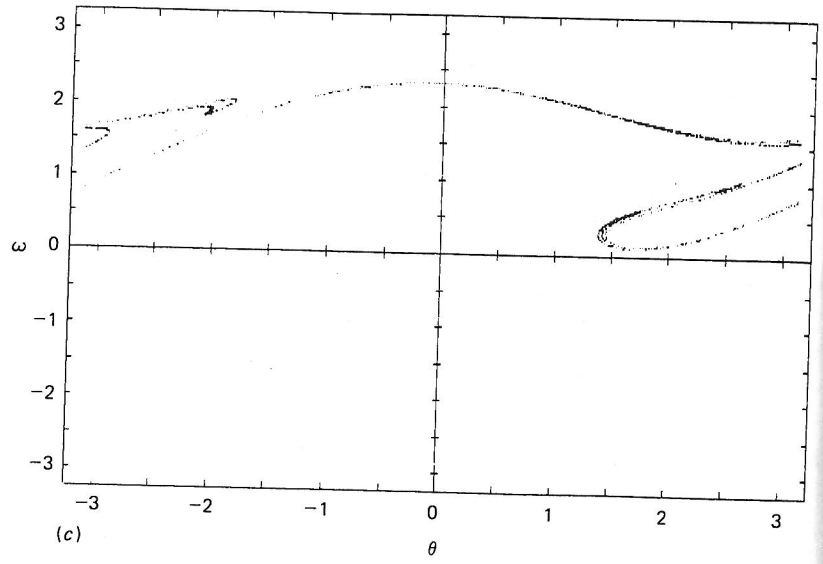

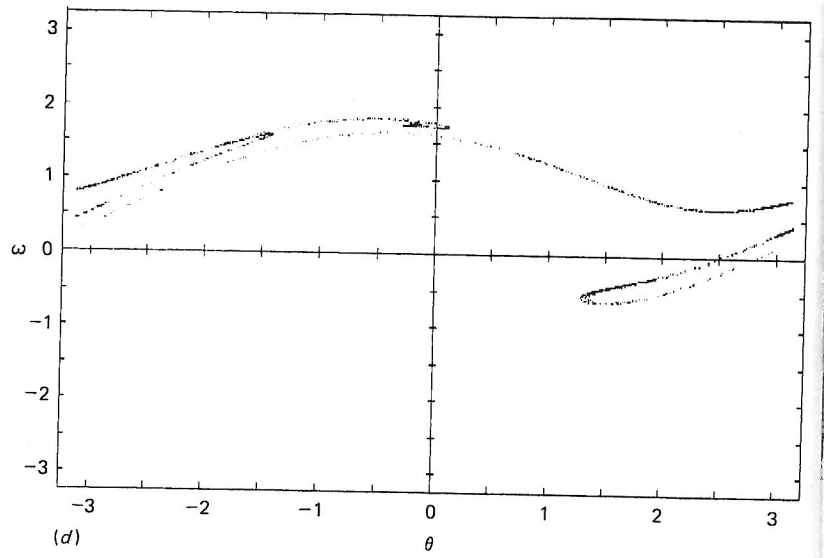

Fig. 3.5 (*cont.*)

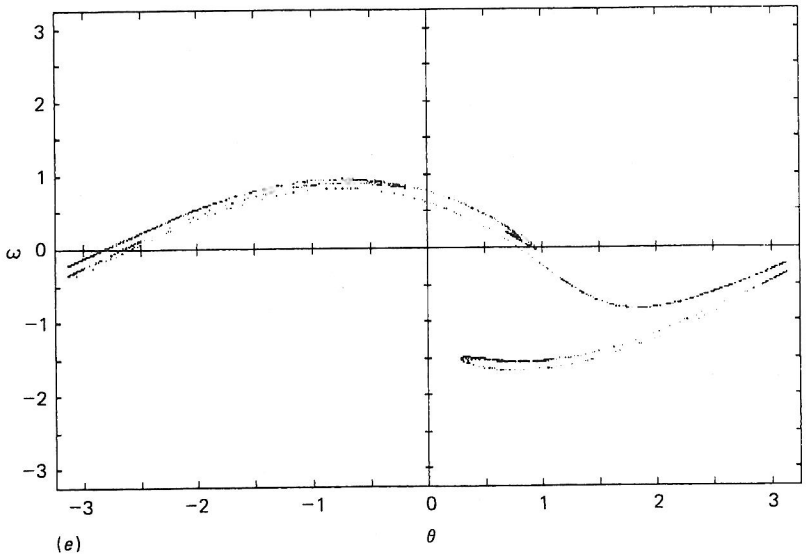

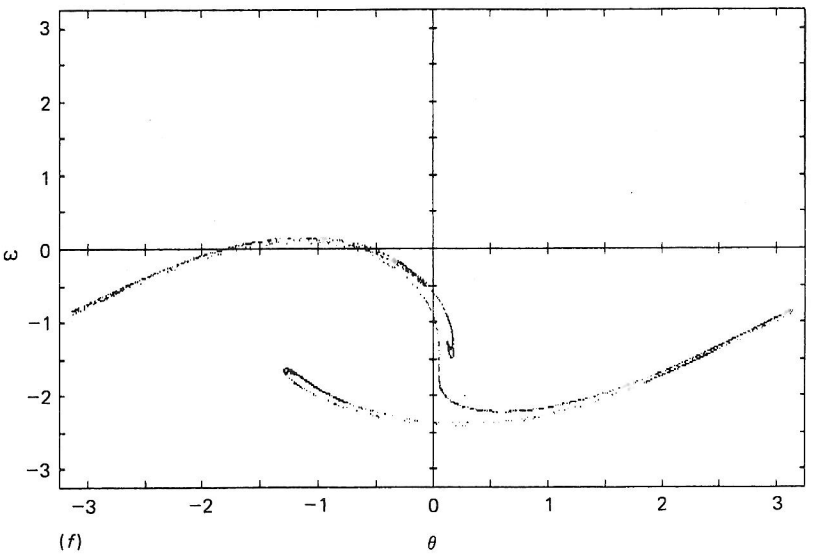

Fig. 3.5 (*cont.*)

$q = 4$
$g = 1.5$
$\omega_D = 2/3$

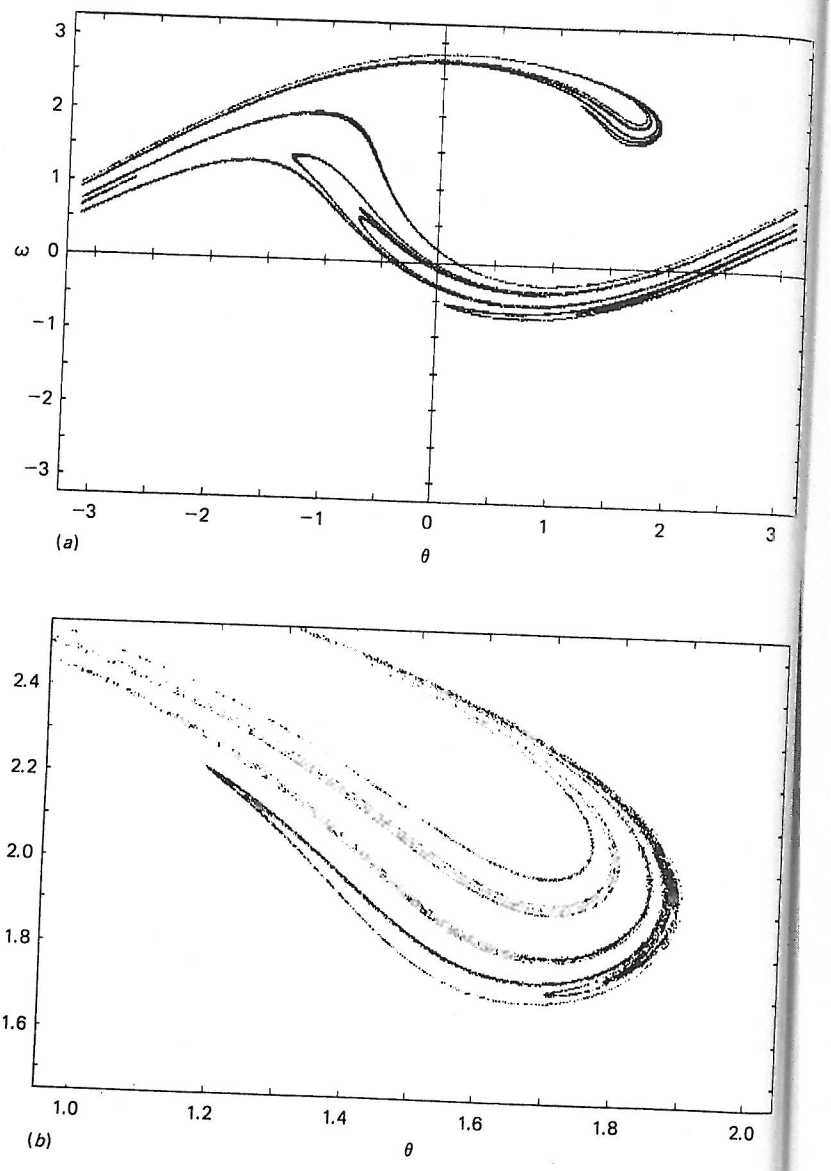

Fig. 3.6 (*a*, *b*, *c*) Attractor in the Poincaré section for $q=4$ and $g=1.5$ viewed at different magnifications, thus revealing the self-similar structure caused by the folding and stretching of phase volume.

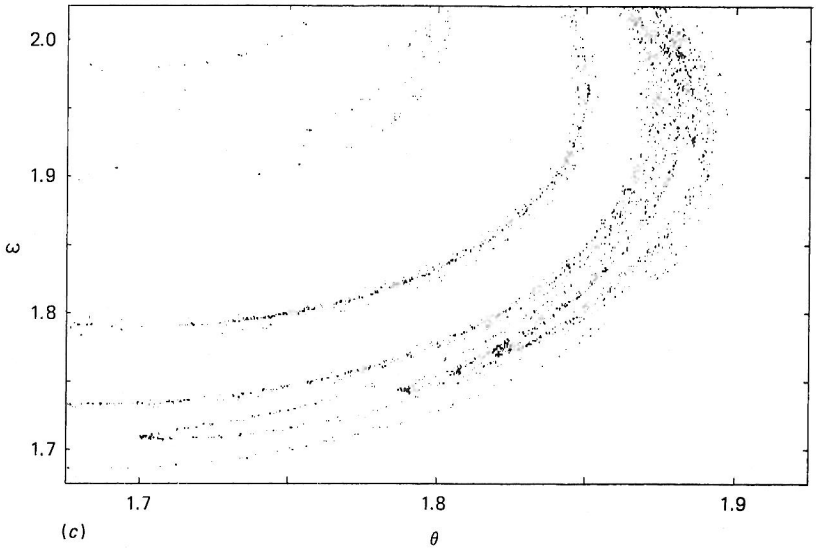

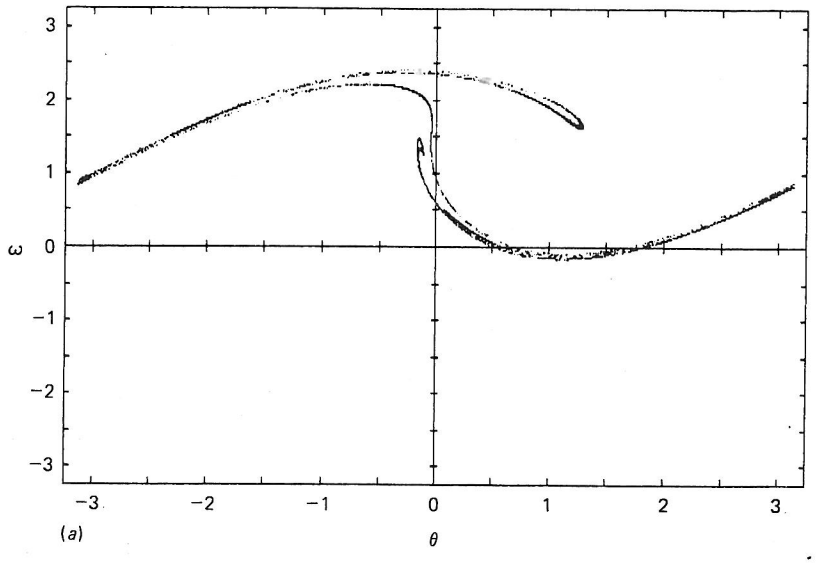

Fig. 3.7 Attractors in the Poincaré section for chaotic states of pendula with different amounts of damping ($g=1.5$): (*a*) $q=2$, (*b*) $q=2.8$, (*c*) $q=4$.

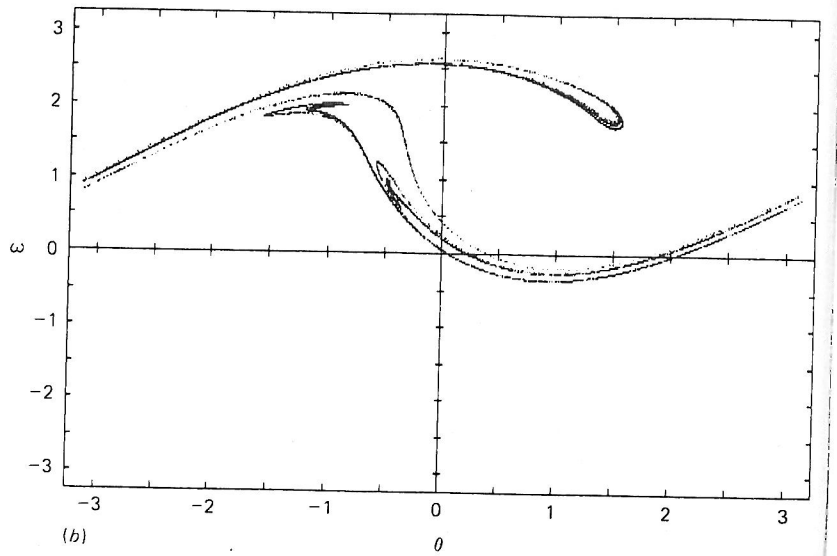

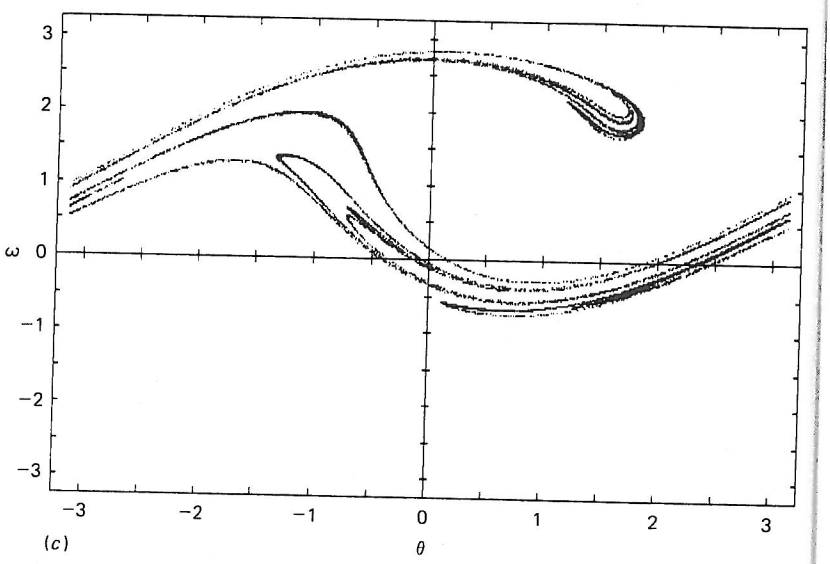

Fig. 3.7 (*cont.*)

Time series and power spectra

In Chapter 2 the power spectrum was introduced as a representation of the relative abundance of different frequencies in a given time series. Figure 3.8 shows a time series and power spectrum for the angular velocity ω at a drive amplitude of $g=0.95$. The time series in Figure 3.8(a) shows a periodic oscillation. The corresponding power spectrum (Figure 3.8 (b)) exhibits a strong peak at the drive frequency, $1/(3\pi)$ together with some higher frequency harmonics. The harmonics are not unexpected since the phase space pattern is asymmetric. Logarithmic plots are used to highlight components with low power levels – an important feature of chaotic spectra.

In Figure 3.9 a corresponding set of diagrams is given for a chaotic state at $g=1.5$. The time series is obviously irregular. The power spectrum is broadband, and contains substantial power at low frequencies. A sharp component at $\omega_D/2\pi$ is also present. Though a broad spectrum does not guarantee sensitivity to initial conditions, it is, in practice, a reliable indicator of chaos.

This book is primarily concerned with dynamical systems defined by sets of differential equations. However, it is worth noting that power spectra are also very useful for the analysis of experimental data. Measurements typically include time series of some dynamical variable, and the corresponding power spectrum can be readily analyzed to determine the state of the system. (See, for example, Gollub and Benson (1980) and Iansiti *et al.* (1985).)

Another useful technique for distinguishing chaotic and nonchaotic motions is the calculation of *Lyapunov exponents*, which are quantitative measures of the evolution of neighboring phase trajectories. As with Fourier analysis, the method is applicable to both numerical and experimental data; we describe it in Chapter 5.

Basins of attraction

Figure 2.13 showed the phase portrait of the damped *unforced* pendulum. Each of the point attractors at $\theta=2n\pi$ ($n=$integer) is encompassed by a region called a *basin of attraction.* All the points (θ,ω) in the basin converge on the enclosed point attractor. The boundary between two basins of attraction is called the *separatrix.*

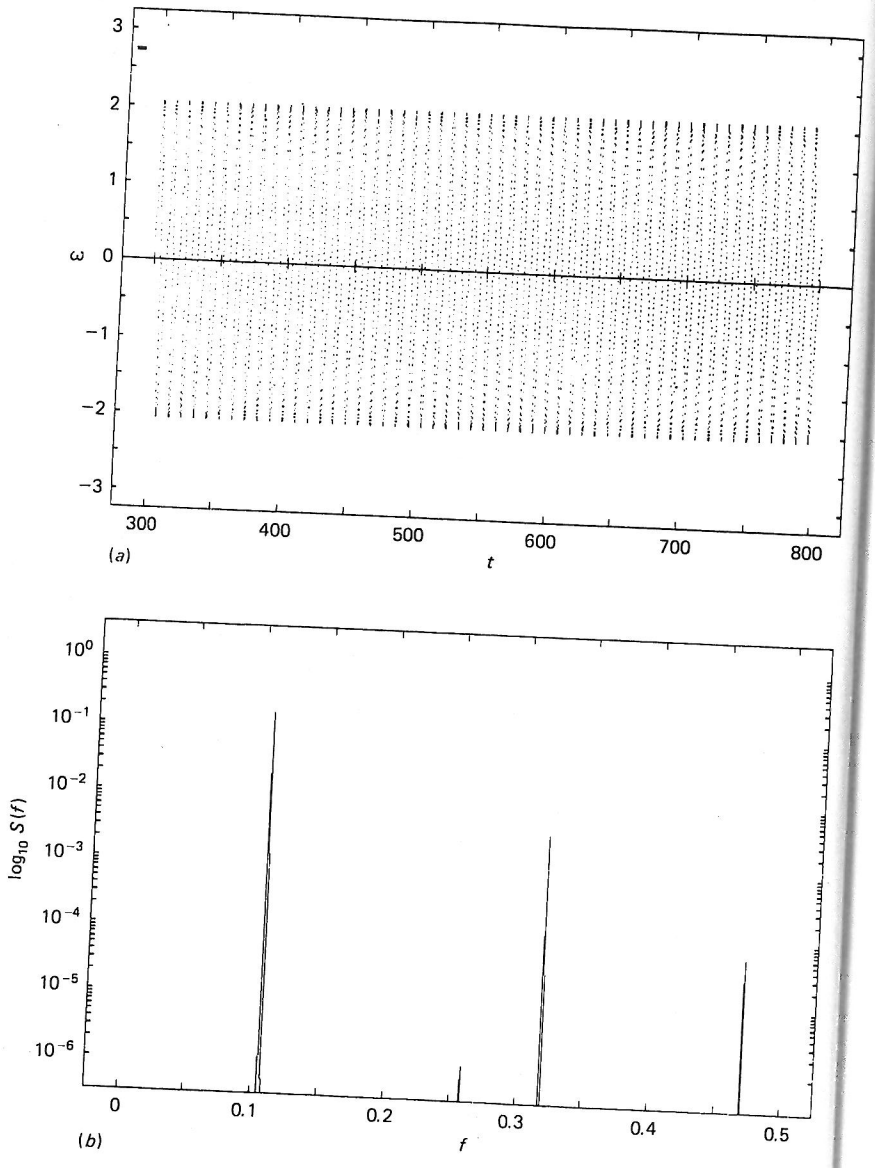

Fig. 3.8 (*a*) Time series and (*b*) power spectrum of angular velocity, ω, for periodic motion at $g=0.95$.

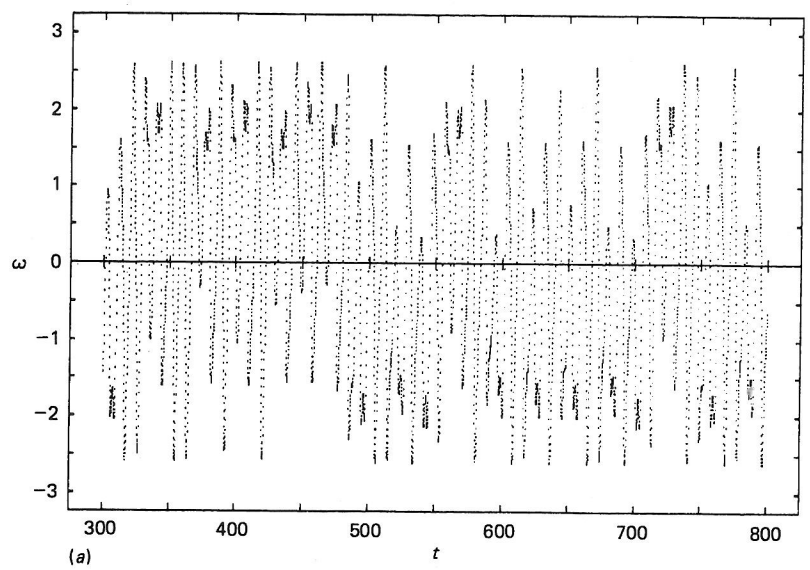

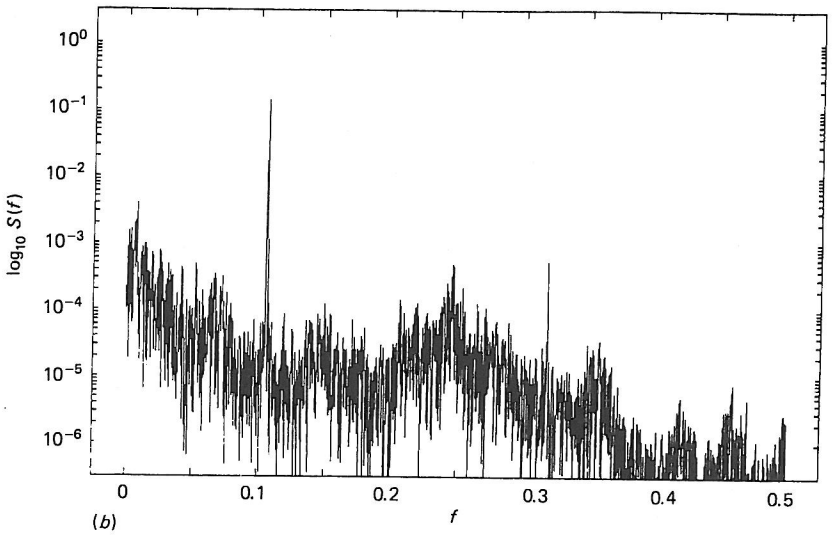

Fig. 3.9 (*a*) Time series and (*b*) power spectrum of angular velocity for chaotic motion at $g = 1.5$. The peak is located at the drive frequency.

For the case cited, the separatrix is a line defined by the stable phase trajectory going to the saddle point as shown in Figure 2.13.

In order to determine basins of attraction for the *forced* pendulum numerically, it is necessary to take advantage of some property that differs from one basin to another. For example (Gwinn and Westervelt, 1985), one can use the fact that, in the region $g > 1.3$, there are two stable rotary modes with average components of angular velocity close to $\pm\omega_D$ for the different basins. The phase portraits of these modes are shown in Figures 3.10(*a*) and (*b*).

The basins of attraction are obtained by taking each pair (θ,ω) of initial conditions on a grid, and calculating the trajectory of that pair over many cycles. To eliminate transient effects, the first 30 cycles are discarded; and the velocity is then averaged over the remaining cycles. The two basins of attraction are distinguished by the *sign* of $\langle\omega\rangle$ and, for positive $\langle\omega\rangle$ a circle is put at the corresponding location of the initial condition. Figure 3.11 shows the basins of attraction for $g=1.3$, a periodic state.

On a large scale the basins of attraction of Figure 3.11 bear some resemblance to those of the undriven pendulum, but the basin boundaries appear fuzzy. In fact, careful studies (Gwinn and Westerwelt, 1986) have shown the boundaries to be fractals (see Chapter 5); that is, the basins are interwoven near the boundaries. If the initial phase space coordinates of a trajectory near the boundary are not specified precisely, the basin of attraction for the trajectory is uncertain. This uncertainty is related to the fractal dimension of the boundary.

Further insight may be gained by looking at the basins of attraction with the Poincaré section superposed (Gwinn and Westervelt, 1985). This type of diagram may be generated by insertion of the Poincaré algorithm into the basin of attraction program. For a nonchaotic state one finds that each piece of the Poincaré section is unambiguously inside a single basin of attraction, as in the case $g=1.47$. (See Figure 3.12(*a*) where the Poincaré attractor consists of eight points, four from each of the two sets of initial conditions.) For $g=1.48$, Figure 3.12(*b*), the attractors spread out, reaching toward the basin boundaries. Finally, in the chaotic state for $g=1.5$, the basin structure breaks up, and the previously separate attractors corresponding to two different initial conditions join together to form a single attractor consisting of an infinite number of lines, as shown in Figure 3.12(*c*).

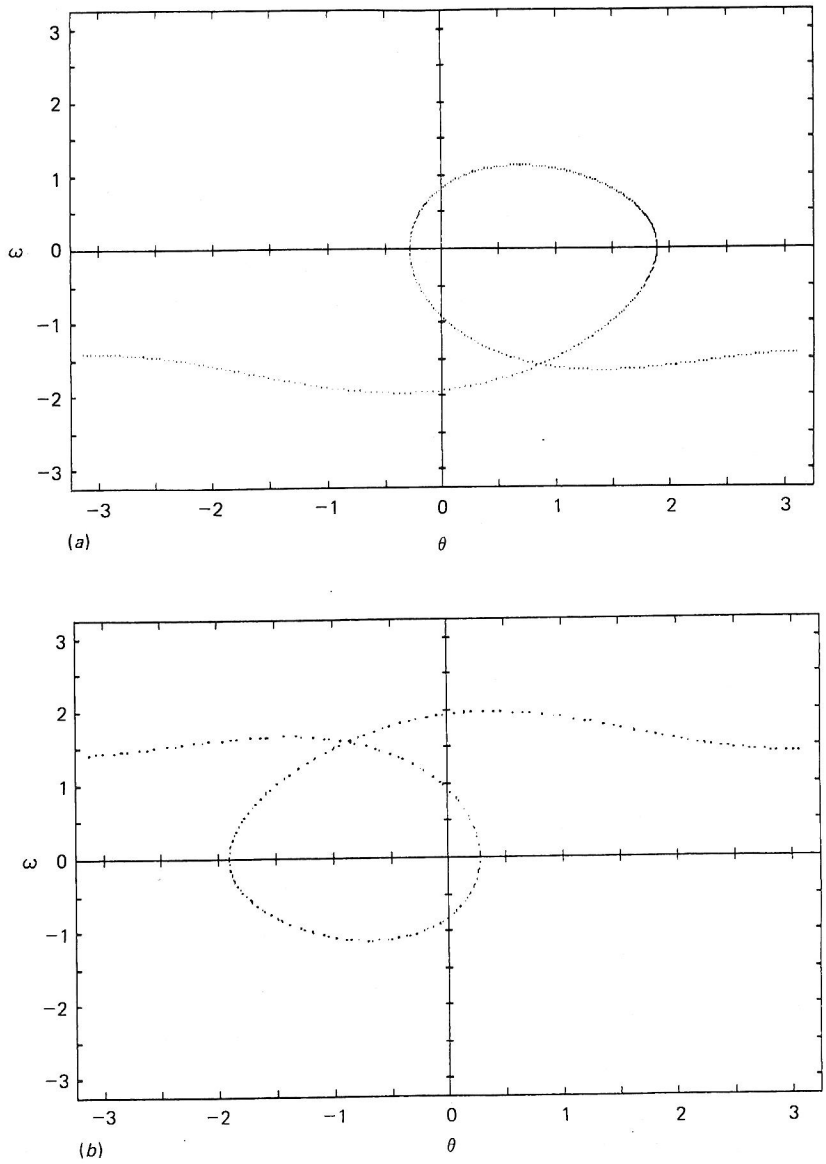

Fig. 3.10 Phase plane for $g=1.35$ and $q=2$ showing positive and negative drifting states for different initial conditions: (*a*) $\theta_0=0$, $\omega_0=0$; (*b*) $\theta_0=0$, $\omega_0=2.3$.

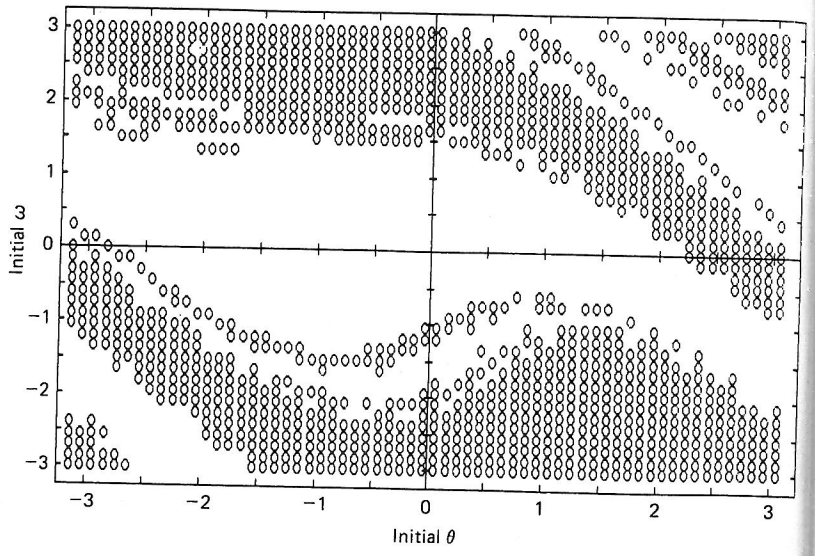

Fig. 3.11 Basin of attraction for $g=1.3$, a state of periodic motion. The circles indicate positive drift of the angular velocity. The blank regions correspond to negative average angular velocity. The basins are intertwined.

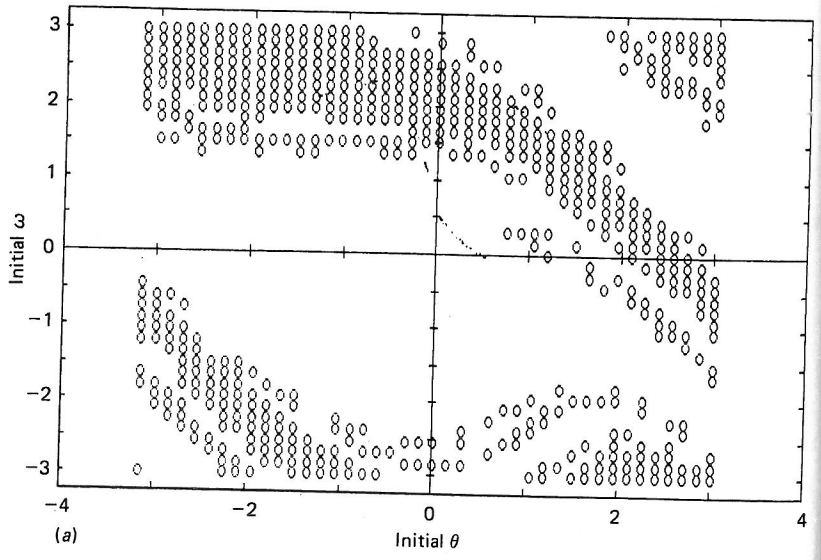

Fig. 3.12 Basins of attraction with the superposed Poincaré sections. The open circles indicate a positive average $\langle\omega\rangle$. (*a*) The Poincaré section consists of small clusters of points when $g=1.47$. (*b*) The attractors have spread toward the basin

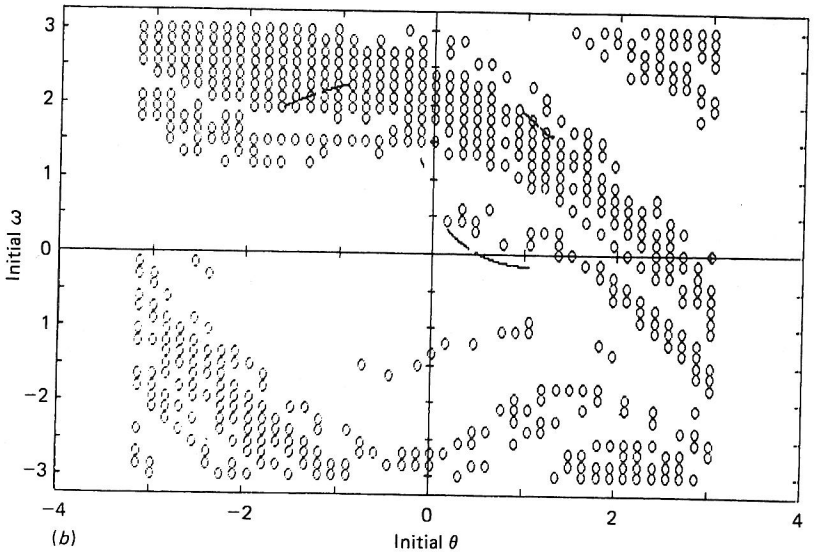

(*b*)

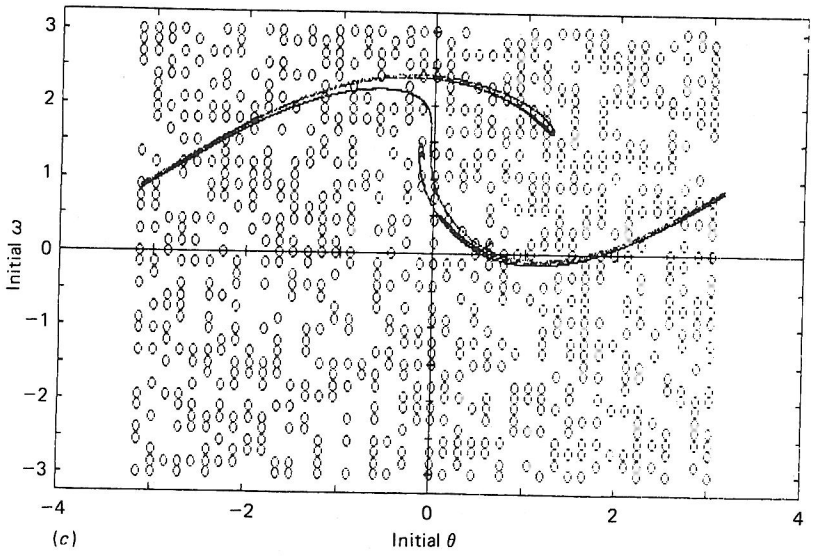

(*c*)

boundaries for $g = 1.48$. (*c*) The separate attractors corresponding to two different initial conditions merge and the basins lose their identities at the onset of chaos. Here, $g = 1.5$. In each case $q = 2$.

Bifurcation diagrams

Phase diagrams, Poincaré sections, time series, and power spectra provide information about the dynamics of the pendulum for specific values of the parameters g, q, and ω_D. The dynamics may also be viewed more globally over a range of parameter values, thereby allowing simultaneous comparison of periodic and chaotic behavior. The bifurcation diagram provides a summary of the essential dynamics and is therefore a useful method of acquiring this overview.

For some values of the parameters, a pendulum will have only one long-term motion, while for other slightly different choices, two or more motions may be possible. If several of them are stable, the actual behavior will depend on initial conditions. In dynamics a change in the number of solutions to a differential equation as a parameter is varied is called a *bifurcation.*

For the pendulum, bifurcations can be easily detected by examining a graph of ω (at a fixed phase in the drive cycle) versus the drive amplitude g. Several examples of these graphs, called *bifurcation diagrams*, are shown in Figure 3.13. The interpretation is relatively straightforward. If the pendulum is lightly driven and the motion is periodic with the same period as the drive frequency, ω_D, then the angular velocity ω has one value at a given time (point of constant phase) during the drive cycle. If the parameter g is increased sufficiently, further components of longer period are added to the motion, and one observes more than one value of ω at the given phase. The system has undergone a bifurcation.

For the diagrams shown in Figure 3.13, ω is taken at the *beginning* of the drive cycle ($\phi = 0$). The system is allowed to come to a steady state by omitting the first 30 drive cycles. The figure shows the next 30 drive cycles. Suppose first that the pendulum is lightly driven (say $g = 0.9$), as in Figure 3.13(a). Its motion is an oscillation at the forcing frequency. The phase trajectory is a limit cycle that is symmetric about the origin; the corresponding Poincaré section shows a fixed point. The angular velocity takes only a single value in the bifurcation diagram.

If the driving force is slightly increased to about 1.025, then the phase trajectory loses its symmetry about the origin and has two different shapes (Figure 3.14) depending on the choice of initial

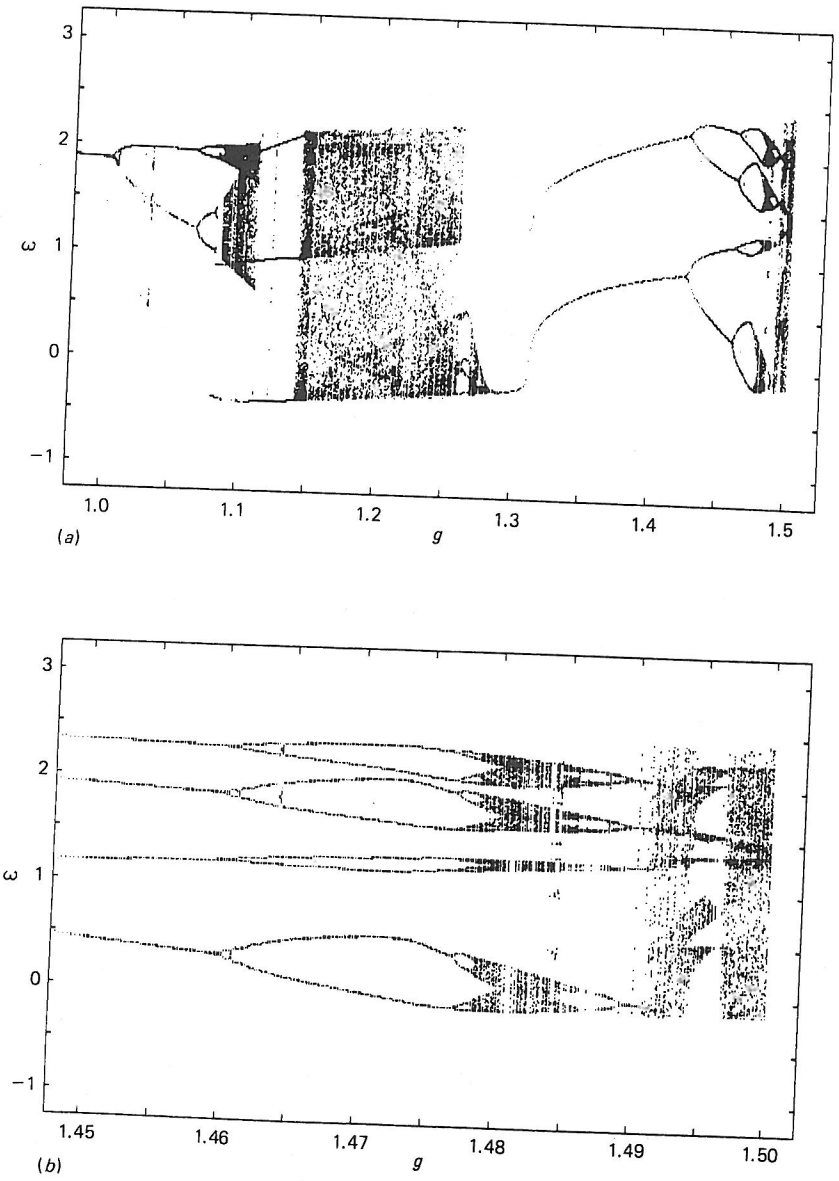

Fig. 3.13 (*a*) Bifurcation diagrams showing the long-term values of the angular velocity ω at the beginning of each drive cycle, plotted against the forcing amplitude g. (*b*) An expansion of one region of (*a*). The other parameters are $q=2$ and $\omega_D=2/3$.

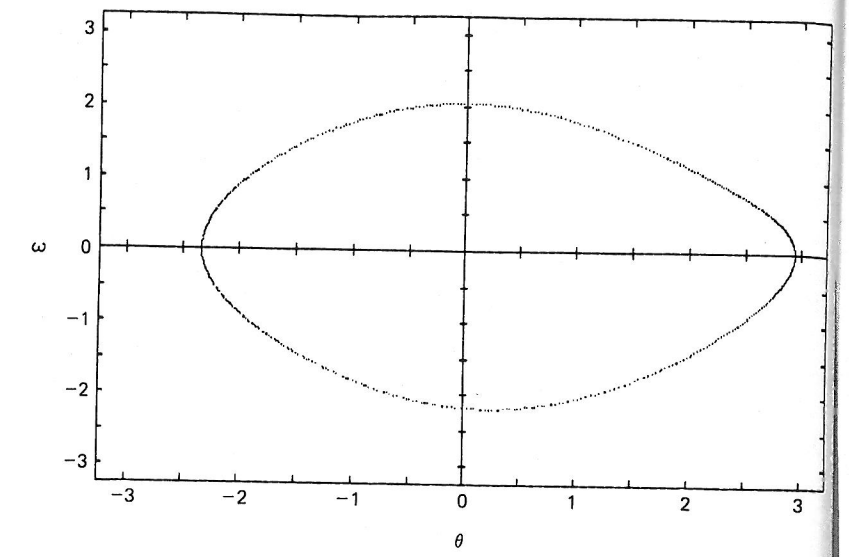

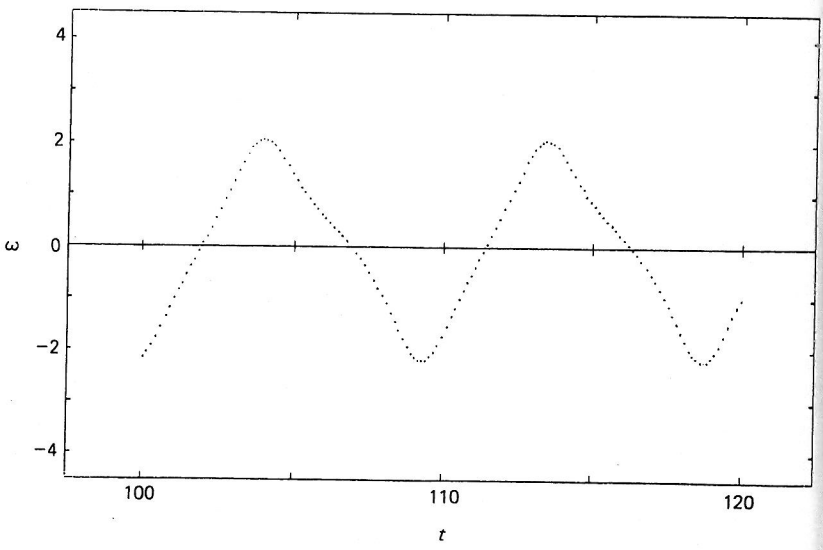

(*a*)

Fig. 3.14 Phase diagrams (above) and velocity time series (below) showing two periodic trajectories (*a*), (*b*), which develop from different sets of initial conditions. $g=1.025$, $q=2$, $\omega_D=\frac{2}{3}$.

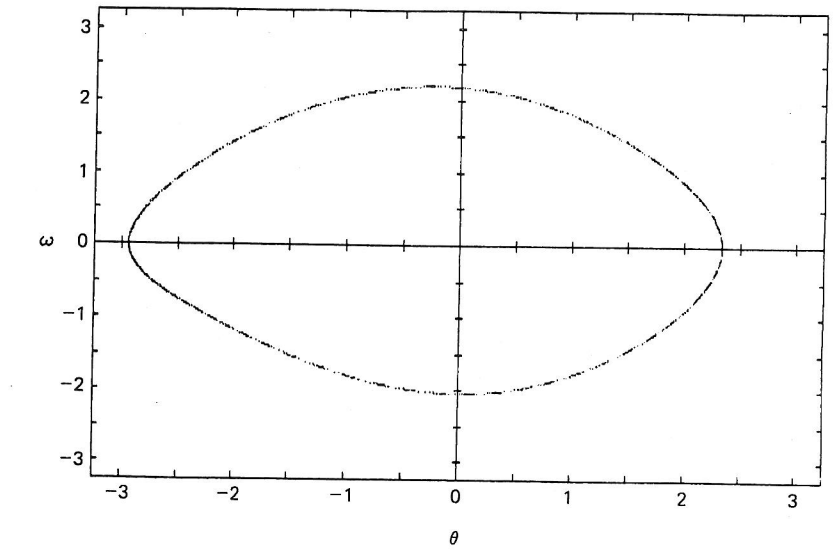

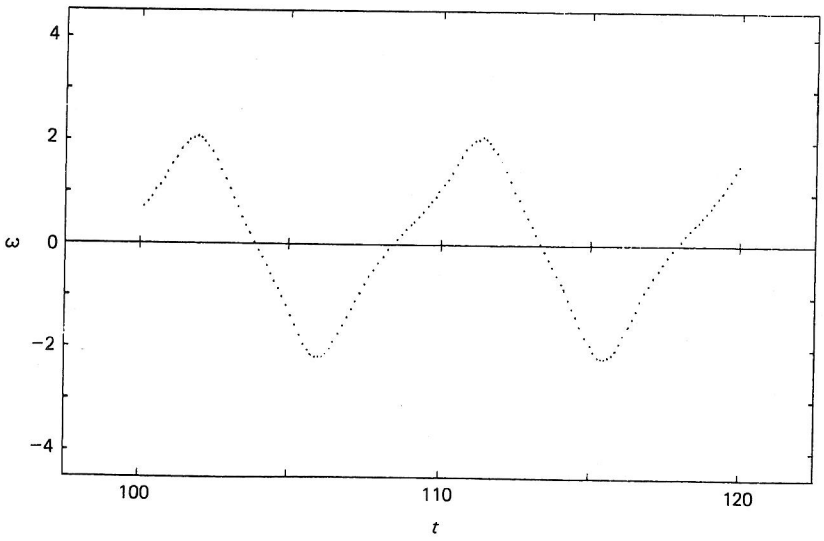

(*b*)

conditions. This two-valuedness appears in Figure 3.13(a) as a splitting. But note that the pendulum's motion still is oscillatory, with a main frequency ω_D and possibly some higher frequency harmonic content. Each set of initial conditions produces only one value of ω in the bifurcation diagram.

If the driving amplitude is increased to approximately 1.07, the periodicity of the pendulum doubles, and it now has frequency components at ω_D and $\omega_D/2$. Observation of the animation for a given set of initial conditions shows two slightly different oscillatory motions of frequency ω_D whose combination has a frequency of $\omega_D/2$. The motion is sketched in Figure 2.15(a). This effect is called *period doubling*. It causes the system to cycle between two values of ω (at the beginning of the drive cycle) for each set of initial conditions. This change is evident in the bifurcation diagram of Figure 3.13(a). Given the two-valuedness resulting from the two asymmetric attractors, a total of four values of ω may occur at $\phi = 0$.

The bifurcation diagram is very complex. For certain ranges of the parameter g, the angular velocity takes on an infinite number of values, though there are also many holes; these states are chaotic. It is also interesting to see that within the chaotic regions there are small intervals in which the motion abruptly becomes periodic again (for example, $g \sim 1.12$). Beyond the large chaotic region occupying much of the interval $1.08 < g < 1.28$, a wide interval of periodic motion appears again, centered at $g = 1.35$. Study of the animation in this region shows a rotary motion with a small, superposed oscillation. Depending upon the initial conditions, the rotary motion has either a positive or negative average angular velocity. (See Figure 3.3(e).) This two-valuedness is evident in the bifurcation diagram.

Beyond $g = 1.43$, a new *subharmonic cascade* occurs. At $g = 1.45$ (see Figure 3.13(b)) the Poincaré section consists of two points, and at $g = 1.47$ four points (for a given set of initial conditions). In the region around $g = 1.48$ there are four densely occupied bands of ω. The motion is chaotic and ω takes different values in a regular cycling around the bands. A narrow periodic interval occurs for $1.487 < g < 1.493$, followed by chaotic motion for higher g.

The bifurcation sequences observed as a function of g change dramatically if the parameters q and ω_D are changed. One example of a different sequence is given in Figure 3.15, where the damping factor is reduced by a factor of 2 so that $q = 4$. The regions of chaotic

behavior are much broader, and there is a prominent window of periodic behavior around $g = 1.25$.

The bifurcation diagram is an important tool for discovering interesting parameter regimes for a dynamical system. While our discussion focused upon variation of the forcing g, bifurcation diagrams utilizing q and ω_D as the independent variable also yield similar displays of varied dynamical behavior.

The numerical computations discussed in this chapter illustrate the complexity and variety of motions of the pendulum. Experiments illustrating some of these phenomena have been performed (Blackburn *et al.*, 1989). Analytic solution of the pendulum equations is apparently not feasible except for special cases. Therefore, in order to understand the development of chaos we consider in Chapter 4 several nonlinear mappings, which are more tractable than differential equations. Despite their simplicity, these maps exhibit many of the phenomena illustrated by the pendulum.

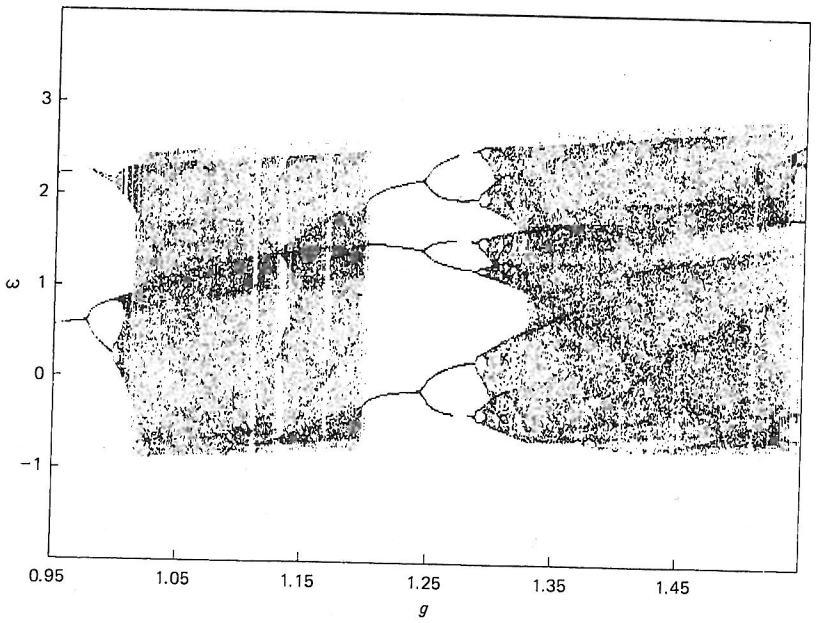

Fig. 3.15 A bifurcation diagram for $q = 4$; this corresponds to lighter damping than in Figure 3.13.

Simulations

1. Use the program MOTION listed in Appendix B or the MOTION option in the menu of the program CHAOS to study the motion of the driven pendulum. Try different values of the parameter set (ω,g,q). Let the motion run for many cycles in order to observe the long term behavior.
2. Use the program PENDULUM listed in Appendix B or the 2D-PHASE DIAGRAM option in the menu of CHAOS to study the two-dimensional projection of the phase space for the pendulum. Try different values of (ω_D,g,q) and different sets of initial conditions (θ_0,ω_0). Discard the first ten cycles to allow the pendulum to reach a steady state.
3. Use the INIT. BLOCK FLO option in the menu of CHAOS (or modify PENDULUM) to study the motion of a block of initial conditions in (θ,ω) space. Note the change in shape and area of the block.
4. Use the program POINCARE listed in Appendix B or the POINCARE SECTION option in the menu of CHAOS to study the Poincaré section of the pendulum. Try different values of (ω,g,q) and phase angle. Discard the first ten cycles to allow the pendulum to reach a steady state.
5. An electrical circuit with resistance, inductance, and nonlinear capacitance may be driven sinusoidally into chaotic states. The differential equation for the circuit is

   $$d^2x/dt^2 + A dx/dt + x^3 = B\cos t$$

   where A and B are adjustable parameters. It has been suggested that the transition to chaos may be observed for parameter values $A=0.1$ and $9.8<B<13.4$ (Moon, 1987, p. 272). Modify the programs PENDULUM and POINCARE (listed in Appendix B) or the source code on the diskette for the libraries LPHASE2D and LPOINCAR in order to develop programs to study the behaviour of this dynamical system. Note that the drive angular frequency is 1. Eliminate the periodic boundary conditions on the position coordinate and put larger boundaries on the axes.
6. Use the listing BIFURCATION in Appendix B or the BIFURCATION DIAG option in the menu of CHAOS to generate a

bifurcation diagram for the pendulum. Since the process is equivalent to the computation of many Poincaré sections, the program takes a lot of processing time and you may wish to save the computed data on a separate diskette.

7. Modify the bifurcation program to develop a bifurcation diagram for the equation of Problem 5. Use the range of B values suggested in that problem.
8. Use the FFT listing in Appendix B or the FFT option from the CHAOS menu to generate a power spectrum for the pendulum for $g=1.5$ and $q=4$.
9. Modify the Runge–Kutta procedure in the FFT program for the equation of Problem 5 and run the program for a value of B which gives a chaotic behavior. (Use your bifurcation diagram from Problem 7 to find an appropriate value of B.)
10. Use the BASINS listing in Appendix B or the BASINS OF ATTRA option from the CHAOS menu to generate a diagram of the basins of attraction. Try $g=1.3$ and $q=2$.

CHAPTER FOUR

Toward an understanding of chaos

The driven pendulum, our primary example in this work, may seem to be one of the simplest physical systems to exhibit chaotic behavior. Mathematically and computationally, however, nonlinear differential equations are difficult to solve. Even more elementary model systems can give insight into the mechanisms leading to chaotic behavior. These are stated in the form of *difference equations*, rather than *differential equations*. A typical difference equation is of the form

$$x_{n+1} = f(\mu, x_n),$$

where x_n refers to the nth value of x, a real number on the unit interval (0,1), and μ is a parameter. One may think of nT as a time, where T is a basic time interval. The parameter μ may vary with the particular model and, in the examples we will discuss, varying μ leads to the onset of chaotic behavior. The function, f, is said to be a *map* of the interval (0,1) onto itself, since it generates x_{n+1} from x_n. The function $f(\mu, x_n)$ may be nonlinear in the argument x_n, just as the differential equations for the pendulum are nonlinear in θ.

Difference equations may be solved quite readily by iteration, and their numerical solution is much less time consuming than is the case for differential equations. A dynamical system whose phase space is three-dimensional (such as the pendulum) may be converted to a mapping through the Poincaré section. These sections are 'snapshots' of the phase plane taken at each drive period. Because the differential equation is deterministic a definite relation exists between the coordinates (θ_n, ω_n) at the end of the nth drive period and the coordinates $(\theta_{n+1}, \omega_{n+1})$ at the end of the $(n+1)$th period. This relation can, in principle, be written as a mapping in two dimensions:

$$\theta_{n+1} = G_1(\theta_n, \omega_n)$$
$$\omega_{n+1} = G_2(\theta_n, \omega_n).$$

Sometimes (but not generally) such mappings may be further simplified to one dimension. While a particular analytic form of the pendulum mapping has not been found, simple maps may be used to illustrate some aspects of the pendulum's behavior.

Because of their relative simplicity, one-dimensional maps provide several advantages over the differential equations. They allow for simple, clear statements of many characteristics of chaotic behavior, such as sensitivity to initial conditions and the evolution of information. Maps also illustrate clearly the mechanisms of bifurcation of solutions, and the folding and stretching required for chaos in a finite phase space. In this chapter several maps and their properties are explored to aid in further understanding chaotic behavior.

The logistic map

This simple map, given by the difference equation

$$x_{n+1} = \mu x_n(1 - x_n), \qquad x_n \in [0,1]$$

takes its name from the corresponding differential equation

$$dx/dt = \mu x(1 - x)$$

originally used by P.F. Verhulst in 1845 to model population development in a limited environment (May, 1976). The logistic map is one-dimensional and nonlinear, and may be visualized as indicated in Figure 4.1. The diagram has three parts: the parabolic curve $y = \mu x(1 - x)$, the diagonal line $x_{n+1} = x_n$, and a set of lines connecting the successive iterations of the map. The time sequence produced by the mapping is obtained by choosing a value of μ (in this case $\mu = 2$), plotting the corresponding quadratic curve, and repetitively generating subsequent points starting with some initial value (in this case, $x_0 = 0.2$). The first point, x_1, is found where the line $x_0 = 0.2$ meets the quadratic curve. The next step is easily determined by moving laterally to the $x_{n+1} = x_n$ diagonal. From the diagonal x_2 can be found by again going vertically to the quadratic curve. The process is repeated until x settles (in this case) to a steady state where $x_{n+1} = x_n$.

Such a 'fixed' point is obtained whenever the *magnitude of the slope* of the map where it intersects the diagonal is less than unity.

In Figure 4.1 the sequence $\{x_n\}$ reaches a fixed point. A little experimentation shows that this is apparently the case for all initial conditions x_0 when $\mu = 2$. If μ is increased to approximately 3.3 as in Figure 4.2 the situation changes. The quadratic curve is steeper and the magnitude of its slope $|f'(x)|$ is greater than 1 at the intersection. Therefore, the fixed point is unstable and, after an initial transient, x_n oscillates between two values so that $x_{n+2} = x_n$. This effect is reminiscent of the Poincaré map of the pendulum for values of the driving force around $g = 1.07$. Higher values of μ lead to further bifurcations and even to chaotic behavior. Figure 4.3 shows the situation for $\mu = 3.9$. The long-term behavior is such that the x_n are not limited to a few points but rather fill much of the original quadratic curve, and the behavior is chaotic. This behavior is reminiscent of the Poincaré sections for the pendulum in the chaotic region.

Rather than continuing to describe the behavior of the logistic map for individual values of μ, we present a more global view of the model through a bifurcation diagram, as shown in Figure 4.4, where μ varies smoothly from 2.9 to 4.0. In this diagram the map is iterated several hundred times at each of many intervening values of μ, with the first 100 values discarded to ensure that only the long-term behavior is

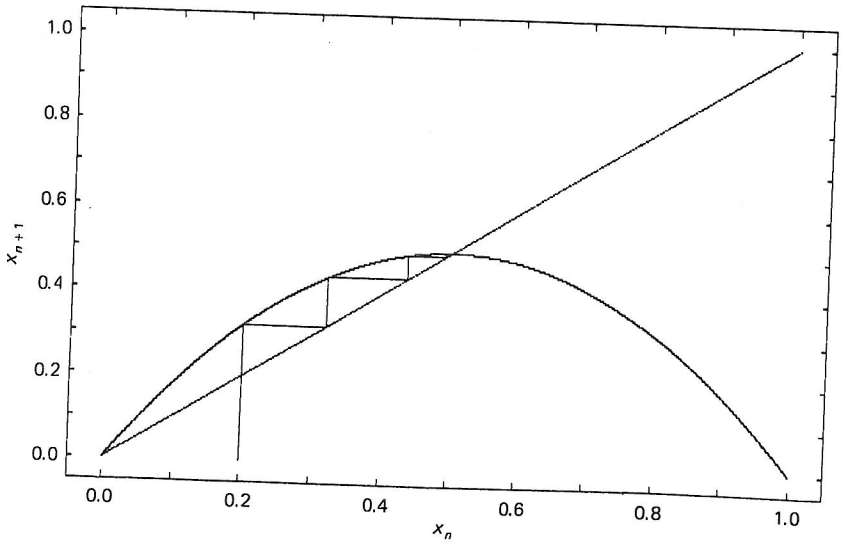

Fig. 4.1 Evolution of the logistic map for $\mu = 2$. The equilibrium value is $x = 0.5$.

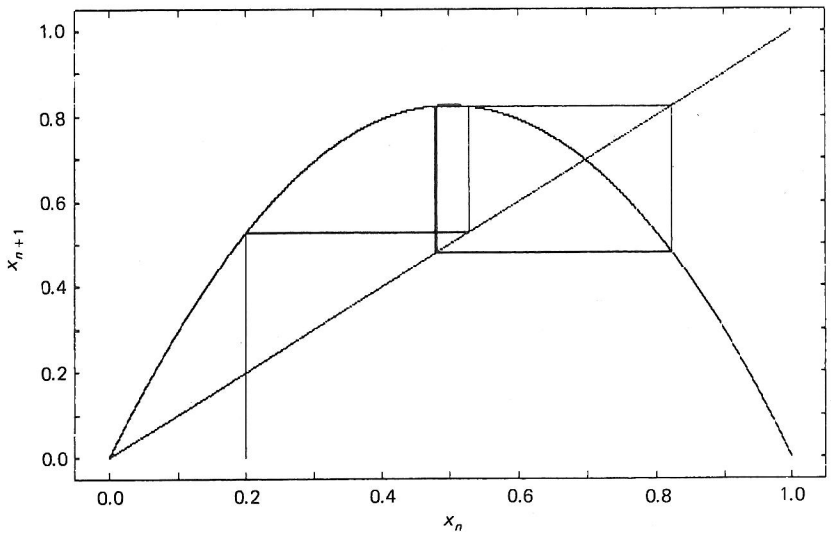

Fig. 4.2 The logistic map for $\mu = 3.3$ showing an oscillation between $x = 0.48$ and $x = 0.83$.

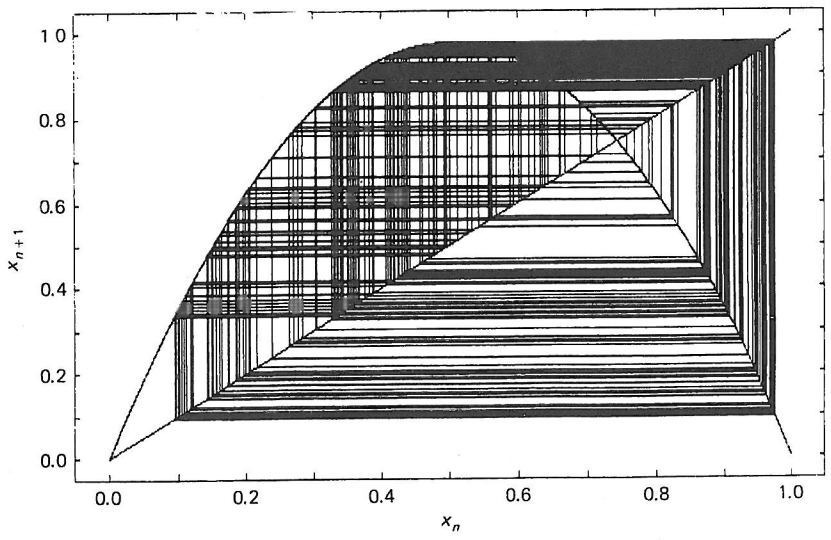

Fig. 4.3 Iteration of the logistic map for a chaotic state at $\mu = 3.9$.

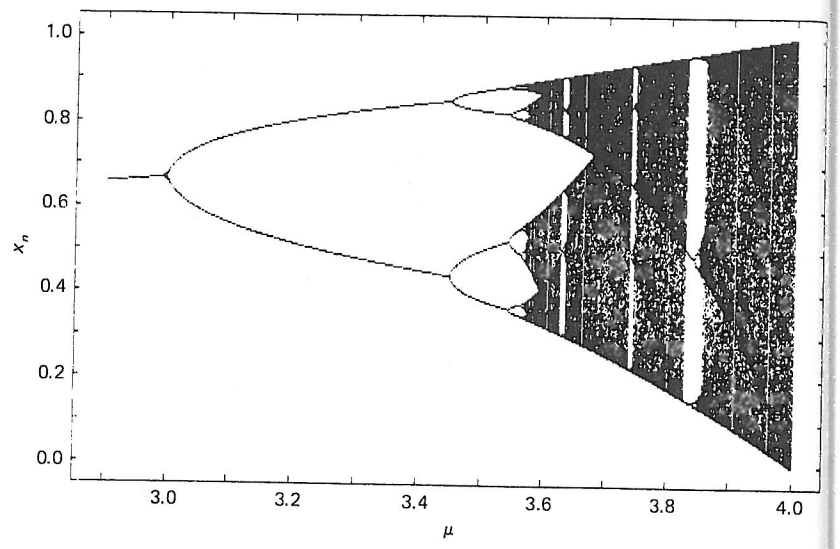

Fig. 4.4 Bifurcation diagram of the logistic map. Long-term values of x_n are plotted for $2.9 < \mu < 4$.

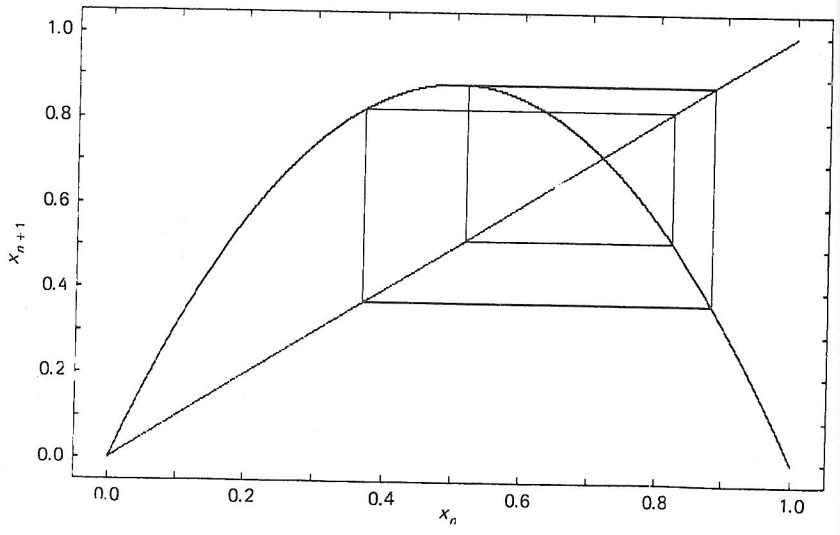

Fig. 4.5 A period-4 logistic map cycling between four values: $x = 0.37$, 0.52, 0.83, and 0.88.

plotted. The appearance of this diagram is similar to that of the pendulum bifurcation diagram (Figure 3.13), including regions where the behavior is chaotic and regions or *windows* of periodicity. We now focus on some general features of chaotic maps that are illustrated by the logistic map.

Period doubling

One important feature of the logistic map is the passage to chaos through a sequence of period doublings; the bifurcation where this doubling occurs is called a *pitchfork* bifurcation, because the local shape of the bifurcation diagram resembles a pitchfork. This *period doubling* effect is illustrated in Figure 4.5, which shows the long-term behavior of the map at $\mu = 3.53$. Two such bifurcations have occurred and $x_{n+4} = x_n$.

The period-doubling mechanism is one *route to chaos* that has been much studied as it is common in many dynamical systems, including the pendulum for g slightly greater than 1. The period-doubling route is particularly interesting because it may be characterized by certain universal numbers that do not depend (within certain limits) on the nature of the map (or ordinary differential equation). For example, the ratio of the spacings between consecutive values of μ at the bifurcations approaches a universal constant, called the Feigenbaum number after its discoverer. If the first bifurcation occurs at μ_1, the second at μ_2, and so forth, then this universal number is defined as (Feigenbaum, 1978)

$$\lim_{k\to\infty} \frac{\mu_k - \mu_{k-1}}{\mu_{k+1} - \mu_k} = \delta = 4.669\,201\,609\,102\,990\,9\ldots.$$

This number can be roughly checked by careful scrutiny of the bifurcation diagram. Furthermore, it can be used to generate the sequence $\{\mu_k\}$, using the bifurcation diagram to select the first few values. Finally, it can be shown that an infinite number of bifurcations occur as $\mu = 3.569\,944\ldots$ is approached.

The Feigenbaum number is a universal property of the period-doubling route to chaos for maps that have a quadratic maximum. *Universality* expresses the notion that certain properties of nonlinear maps are independent of the specific form of the map.

The periodic windows

The regions of chaotic behavior are interrupted by intervals of periodic behavior for $\mu > \mu_\infty = 3.569$. One of the largest of these *windows* occurs near $\mu = 3.83$, where a periodic orbit (a 3-cycle) occurs, as shown in Figure 4.6. The existence of this periodic behavior is evident from the shape of the third return map, for which

$$x_{n+3} = f(f(f(x_n))).$$

In Figure 4.7 two such maps are shown for two values of μ; (*a*) at the start of the window where $\mu = 3.8282$, and (*b*) inside the window before the period doubling cascade begins, where $\mu \approx 3.84$. Although these diagrams have very similar appearances there are some important differences.

At the left boundary of this window, the third order return map (Figure. 4.7(*a*)) shows three values of x where the curve is tangent to the diagonal line, $x_{n+3} = x_n$. These points are the cyclic steady state values of x which appear at the beginning of the window. Other initial values of x will be drawn to these fixed points since the shallow slopes of the curve near the fixed points lead to stability. This particular type of transition is called a *tangent bifurcation*.

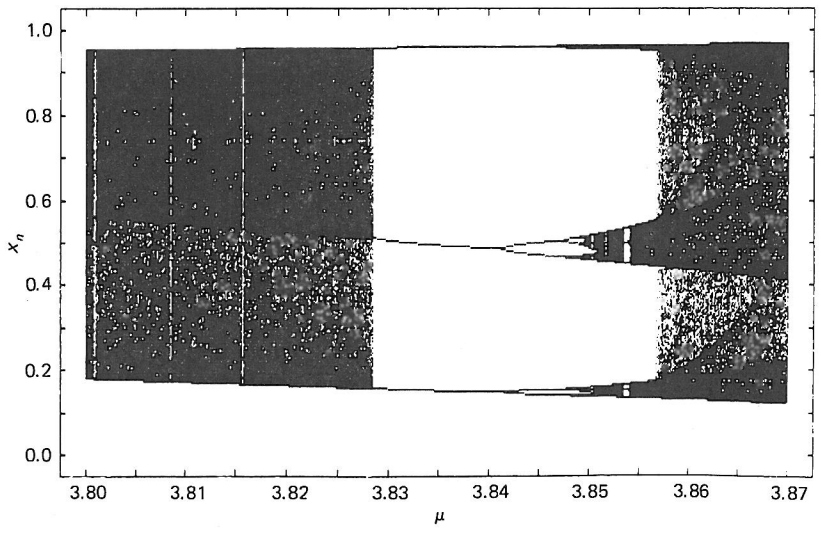

Fig. 4.6 Magnification of the bifurcation diagram in the region of the period-3 window.

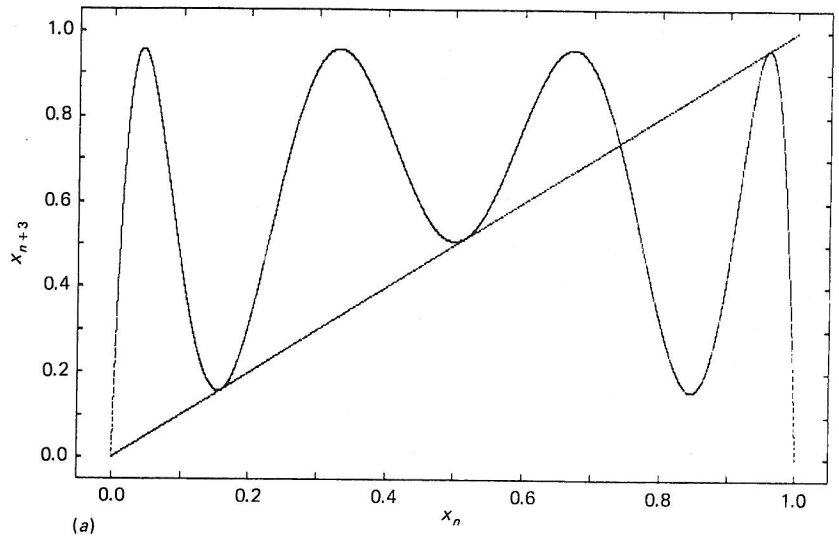

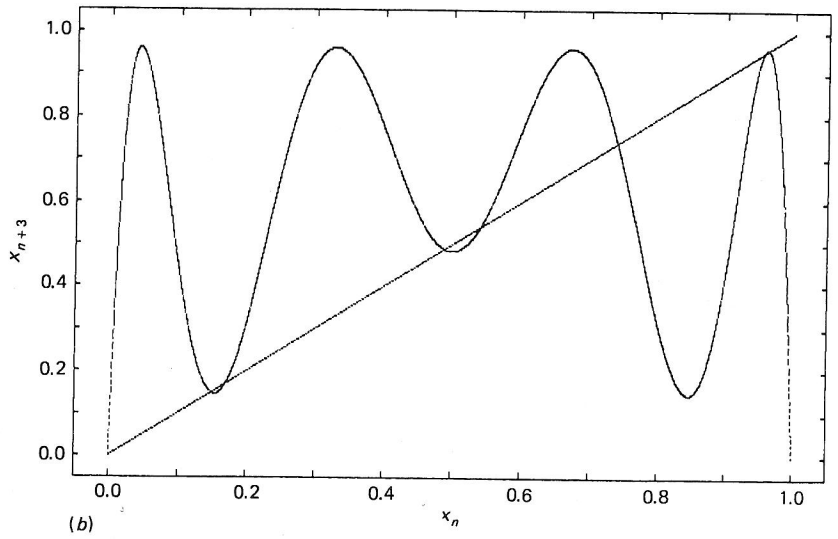

Fig. 4.7 (*a*) The map $x_{n+3}=f^3(x_n)$ at the onset of the period-3 window ($\mu=3.8282$) showing three stable values of x_n at about 0.16, 0.51, and 0.95. An unstable point where $x_{n+3}=x_n$ appears at about $x_n\approx 0.76$. The origin of the term 'tangent bifurcation' is apparent. (*b*) The map $x_{n+3}=f^3(x_n)$ just inside the window at $\mu=3.84$.

For slightly larger μ the bifurcation diagram continues to show the period-3 behavior. Figure 4.7(*b*) shows the behavior of the corresponding third order return map. The curve now crosses the diagonal at three pairs of values of x. (The isolated crossing is unstable.) The slopes of the curve in the neighborhood of three of the points (one from each close pair) are sufficiently steep that the map wanders away from these fixed points. On the other hand, the magnitudes of the slopes at the other three points are less than 1 so these points are attractors. Therefore the cyclic behavior, initiated by the tangent bifurcation, continues to be stable.

At $\mu = 3.842$ a subharmonic cascade to chaos occurs. The slopes of the third order maps near the previously stable values of x now become too steep for stability. For the first period doubling the sixth order map has six attractors; this process continues until chaotic bands form at $\mu \approx 3.85$. The resulting bands merge near $\mu \approx 3.857$ to form a continuum of values of x. This expansion of the chaotic regime and similar discrete changes in a chaotic attractor are sometimes called *crises* (Grebogi, Ott, and Yorke, 1987).

For values of μ just below the onset of the period-3 window, the third order return map is not quite tangent to the diagonal line. Therefore x_n can pass through the resulting narrow gaps and then go freely around the plane until it again becomes temporarily trapped in

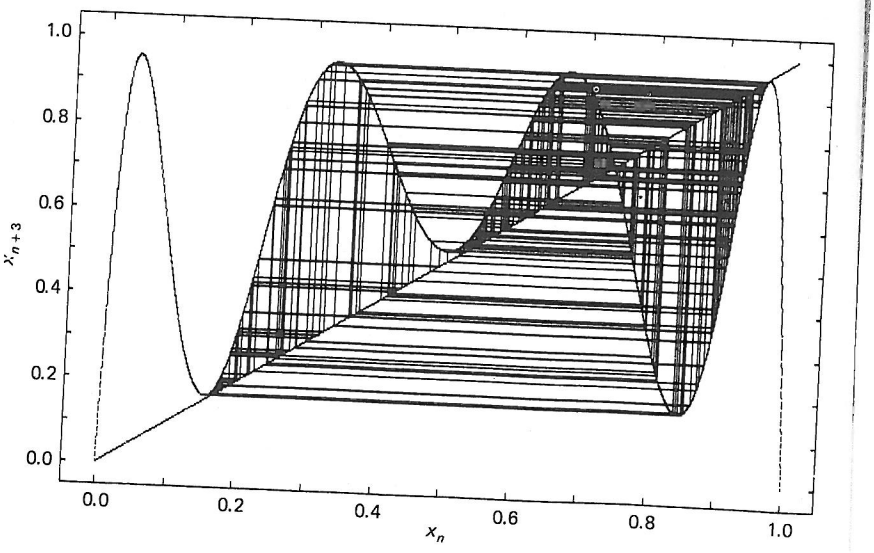

Fig. 4.8 An illustration of 'type I' intermittency as the trajectory squeezes through the gap between the map and the tangent line. During the passage through the gap, x changes very slowly.

a narrow gap as shown in Figure 4.8. While it is in the gap, x_n is nearly fixed. If we think of the map as a Poincaré section for a differential equation representing a physical system such as the pendulum, the physical variable would show nearly periodic motion with occasionally irregular bursts. This common type of chaotic motion is called *type I intermittency* and occurs when a dynamical system is close to a tangent bifurcation if there is a mechanism for intermittent return to the narrow gap.

Lyapunov exponent

The Lyapunov exponent of a map (named after A.M. Lyapunov, 1857–1918, a Russian mathematician) may be used to obtain a measure of the sensitive dependence upon initial conditions that is characteristic of chaotic behavior. This exponent (often written as λ) may be readily computed for a one-dimensional map such as the logistic map. If a system is allowed to evolve from two slightly differing initial states, x and $x+\varepsilon$, then after n iterations their divergence may be characterized approximately as

$$\varepsilon(n) \approx \varepsilon e^{\lambda n},$$

where the Lyapunov exponent λ gives the average rate of divergence. (The average must be taken over many 'initial conditions' spread over the trajectory.) If λ is negative, slightly separated trajectories converge and the evolution is not chaotic. If λ is positive, nearby trajectories diverge; the evolution is sensitive to initial conditions and therefore chaotic.

Consider a specific one-dimensional map given by $x_{n+1} = f(x_n)$. The difference between two initially nearby states after the nth step is written as

$$f^n(x+\varepsilon) - f^n(x) \approx \varepsilon e^{n\lambda},$$

or

$$\log_e \left[\frac{f^n(x+\varepsilon) - f^n(x)}{\varepsilon} \right] \approx n\lambda.$$

For small ε, this expression becomes

$$\lambda \approx \frac{1}{n} \log_e \left| \frac{df^n}{dx} \right|.$$

of phase space develops on average as

$$V = V_0 e^{(\lambda_1 + \lambda_2 + \cdots + \lambda_n)t}.$$

For the driven pendulum there are three Lyapunov exponents corresponding to the three dimensions of the phase space (θ,ω,ϕ). Since the orbits are solutions to a set of ordinary differential equations, the calculation of Lyapunov exponents is less straightforward than for maps. On a chaotic attractor such as that of the pendulum at $g = 1.5$, the directions of divergence and contraction are locally defined, and the calculation must constantly adjust for this condition. Despite this difficulty, computer algorithms have been developed for calculating Lyapunov exponents both from differential equations and from experimental data; the Lyapunov exponents of the pendulum are discussed further in Chapter 5.

Entropy

The complex appearance of the various graphical representations of chaotic behavior naturally leads to the question of the relationship between statistical mechanics and chaos. One way to connect these phenomena is to apply the concept of *entropy* to a chaotic system, comparing the result to an associated statistical system. This comparison is readily done with the logistic map.

Consider a hypothetical statistical system for which the outcome of a certain measurement must be located on the unit interval. If the line is subdivided into N subintervals, we can associate a probability p_i with the ith subinterval containing a particular range of possible outcomes. The entropy of the system is then defined as

$$S = -\sum_{i=1}^{N} p_i \log_e p_i.$$

This quantity may be interpreted as a measure of the amount of disorder in the system or as the information necessary to specify the state of the system. If the subintervals are equally probable so that $p_i = 1/N$ for all i, then the entropy reduces to $S = \log_e N$, which can be shown to be its maximum value. (See Problem 5.) Conversely, if the outcome is known to be in a particular subinterval, then $S = 0$, the minimum value. When $S = \log_e N$, the amount of further information needed to specify the result of a measurement is at a maximum. On the

Finally, we use the chain rule for the derivative of the nth iterate and take the limit as n tends to infinity to obtain

$$\lambda = \lim_{n\to\infty} \frac{1}{n} \sum_{i=0}^{n-1} \log_e |f'(x_i)|.$$

Therefore the Lyapunov exponent gives the stretching rate per iteration, averaged over the trajectory. In Figure 4.9, the Lyapunov exponent is plotted as a function of the parameter μ. The sign of λ correlates very well with the behavior of the system as shown in the bifurcation diagram, Figure 4.4. Beyond $\mu_\infty = 3.56$, the regions of periodic behavior correspond to the intervals in which $\lambda < 0$.

For n-dimensional maps there are n Lyapunov exponents, since stretching can occur for each axis. An n-dimensional initial volume develops, on average, as

$$V = V_0 e^{(\lambda_1 + \lambda_2 + \cdots + \lambda_n)n}.$$

For a dissipative system the sum of the exponents must be negative. If the system is chaotic then at least one of the exponents is positive. (See Problem 14 for a soluble two-dimensional map.)

Lyapunov exponents are also defined for continuous time dynamical systems such as the pendulum. An initial n-dimensional volume

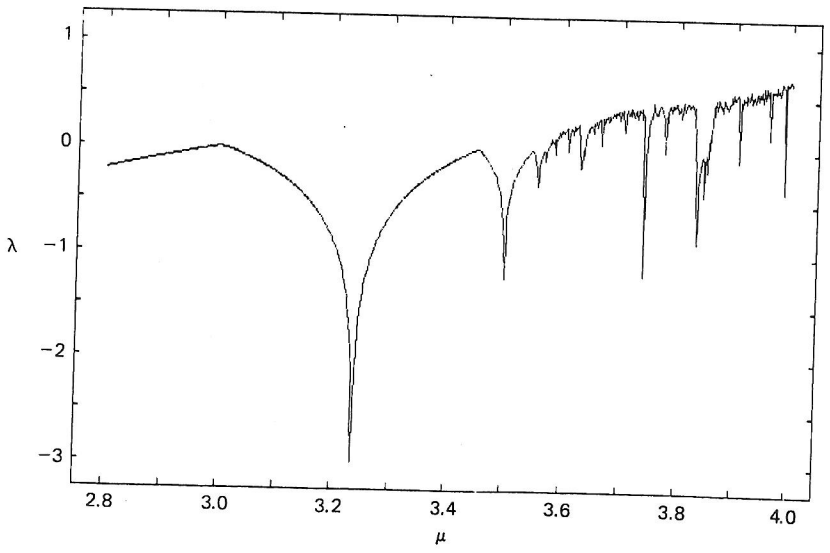

Fig. 4.9 Lyapunov exponent λ versus μ for the logistic map. Sensitivity to initial conditions occurs where the exponent is positive.

other hand when $S=0$ no further information is required. (See, for example, Baierlein (1971), for a discussion of the interpretation of entropy as 'missing' information.)

We now apply this formulation to the logistic map by establishing N 'bins' or subintervals of the unit interval into which the values of x_n may fall. In the nonchaotic state the x_n will fall in relatively few of the bins, and the entropy is low. But in the chaotic state, the entropy is higher, and if the frequencies of occurrence are equal, then it approaches $\log_e N$. Figure 4.10 shows the results of applying the entropy concept to the logistic map. As expected, the entropy generally increases with μ, except for the downward spikes in the windows of periodic behavior. The entropy does not quite get to $\log_e N$ until $\mu=4$, since the distribution of x_n does not span the whole unit interval evenly for $\mu<4$. This feature may be observed in the bifurcation diagram. For $\mu=4$, the entropy is similar to that of a random process with a uniform probability distribution. Nevertheless, short-term correlations *do* exist for chaotic motion, but not for the idealized random system.

For dynamical systems such as the pendulum, information changes in time. It turns out that the average temporal rate of information change can be related both to the Lyapunov exponents and to the

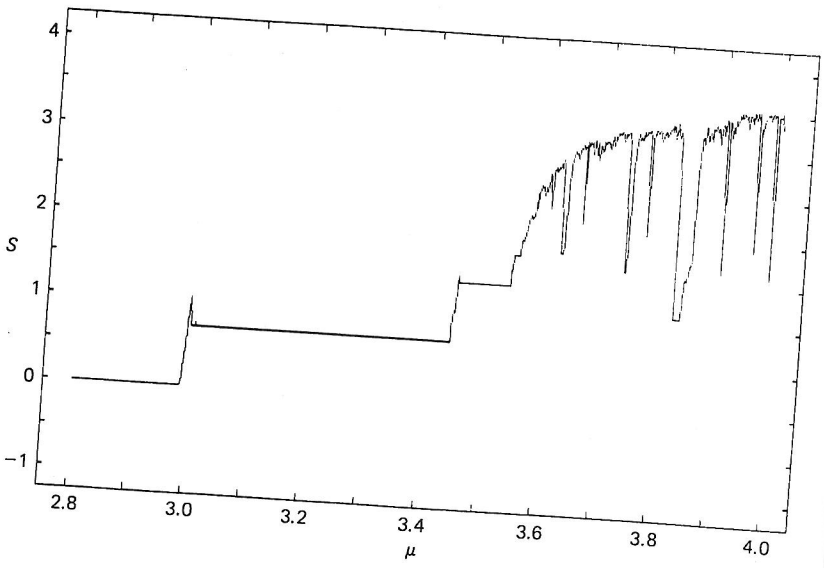

Fig. 4.10 Entropy S as a function of μ for the logistic map. The maximum entropy corresponding to equal probability for each of the 40 cells is 3.6888.

fractal dimension of the attractor. These subjects and their relationships are discussed in Chapter 5.

Stretching and folding

The logistic map also provides some insight into the stretching and folding mechanism that is necessary to keep chaotic trajectories within a finite volume of phase space, despite the exponential divergence of neighboring states. For the logistic map the stretching (divergence of neighboring trajectories) and folding (confinement to the bounded space) can be demonstrated fairly easily, by reference to Figure 4.11.

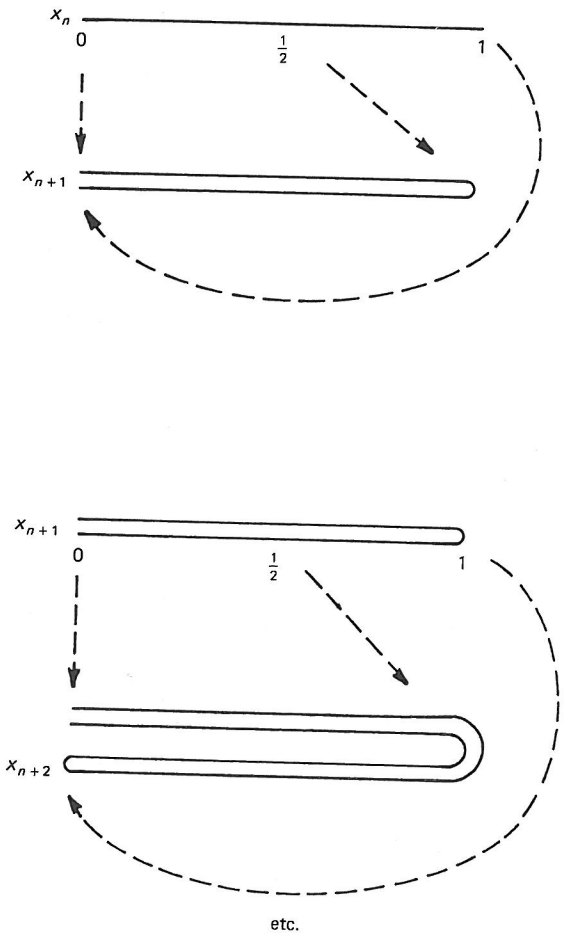

4.11 The stretching folding property of ogistic map for $\mu=4$.

For $\mu = 4$ the logistic map has a maximum value of 1 at $x_n = \frac{1}{2}$ and the values of $x_n \in (0,\frac{1}{2})$ map to $x_{n+1} \in (0,1)$. Similarly the values of $x_n \in (\frac{1}{2},1)$ map to $x_{n+1} \in (0,1)$, but in the reverse order. Therefore both intervals of x_n are stretched by a factor of 2, but because the order of the mappings is opposite, the second stretched interval is folded onto the first stretched interval. The figure illustrates a few cycles of the mechanism. The process resembles the one used to make taffy candy or knead dough for bread.

The stretching and folding process illustrates another important feature of chaotic systems that was implied in our discussion of entropy, namely the loss of information about the initial conditions of a system as time or iteration number increases. Mathematically this arises from the *noninvertibility* of the map $f(x_n,\mu)$. That is, it is always possible to predict x_{n+1} from x_n but there is ambiguity in trying to retrodict x_n from x_{n+1}. (One finds the same noninvertibility with elementary functions such as $y = \sin x$, $y = x^2$, and so forth. The inverse functions can be defined only by limiting the original domains.) It turns out that a necessary condition for any one-dimensional map to exhibit chaotic behavior is that it be noninvertible.

The circle map

The logistic model illustrates many characteristics of chaotic dynamics, such as bifurcations, period doubling, intermittency, sensitivity to initial conditions, and the stretching and folding process. However, some important features of the pendulum, especially the phenomenon of 'phase locking', require a two-parameter map for their explanation. Phase locking is said to occur when the ratio of the frequency of the pendulum to that of the forcing becomes locked at the ratio p/q of two integers, over some finite domain of parameter values (D'Humieres *et al.*, 1982). A similar phenomenon was observed by Christian Huygens in the seventeenth century: the synchronization of two clocks on the same wall. The common attachment to the same wall must have provided a coupling of the clocks to each other. (This phenomenon is mentioned in Bak (1986).)

The pendulum's Poincaré section may be modeled as a two-dimensional (but unknown) map:

$$\theta_{n+1} = G_1(\theta_n, \omega_n)$$
$$\omega_{n+1} = G_2(\theta_n, \omega_n).$$

If ω_n is a function only of θ_n after the initial transients have died away, then $\omega_n = f(\theta_n)$, and the two-dimensional Poincaré map reduces to a one-dimensional map:

$$\theta_{n+1} = G_1(\theta_n, f(\theta_n))$$

or

$$\theta_{n+1} = F(\theta_n).$$

This map may be regarded as a mapping of the circle to itself. It is one-dimensional, with an angular coordinate $\theta_n \in [0,1]$ and periodic boundary conditions (corresponding to the pendulum angular coordinate, $\theta \in [0, 2\pi]$).

For a certain range of forcing amplitudes and frequencies, a circle map may be a reasonable approximation to the driven pendulum. The difference equation of a particularly useful circle map known as the *standard map* is

$$\theta_{n+1} = \theta_n + \Omega - (K/2\pi)\sin(2\pi\theta_n) \qquad \text{mod } 1.$$

There are two parameters (Ω, K) for the standard map, in contrast to the single parameter μ for the logistic map. The parameter Ω is the rotation frequency ('winding number') in the absence of nonlinearity, whereas K gives the strength of the nonlinear coupling of the oscillator to the forcing. This nonlinear coupling can modify the angular change per iteration. (A numerical justification of the connection between the standard map and the pendulum over a range of parameters is given in Jensen, Bak, and Bohr (1984).)

To obtain a sense of the behavior of the standard map, we first omit the nonlinear term by setting $K = 0$. Then the map reduces to

$$\theta_{n+1} = \theta_n + \Omega,$$

which is illustrated in Figure 4.12 for the case $\Omega = 0.4$. After five iterations θ returns to its initial value $\theta_0 = 0.3$, having made two revolutions. The *winding number*, W, is $\frac{2}{5}$, and it is just equal to Ω. If the winding number is a rational number, p/q, then the map is cyclic or *periodic*. If the winding number is irrational then θ does not return exactly to its initial value and the motion is termed *quasiperiodic*.

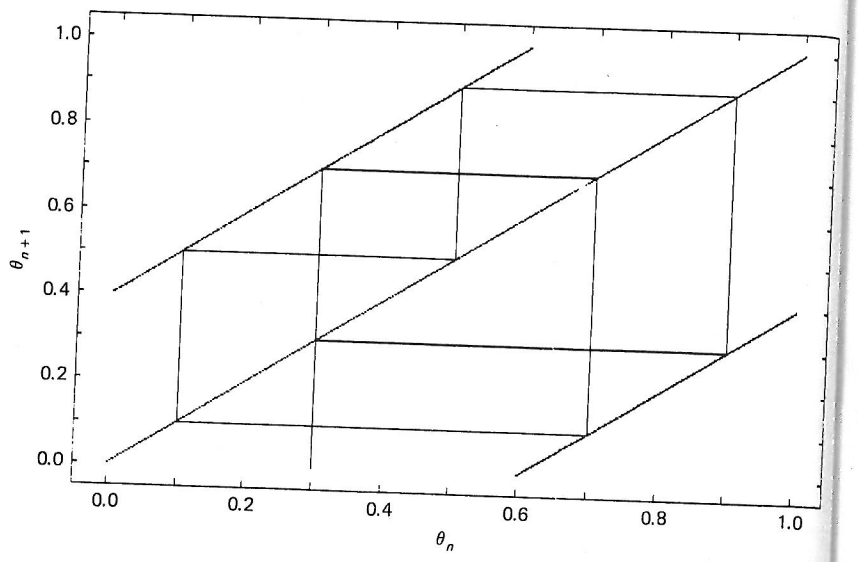

Fig. 4.12 The linearized circle map for a rational winding number of 0.4, using periodic boundary conditions on θ. The diagonal line represents $\theta_{n+1}=\theta_n$.

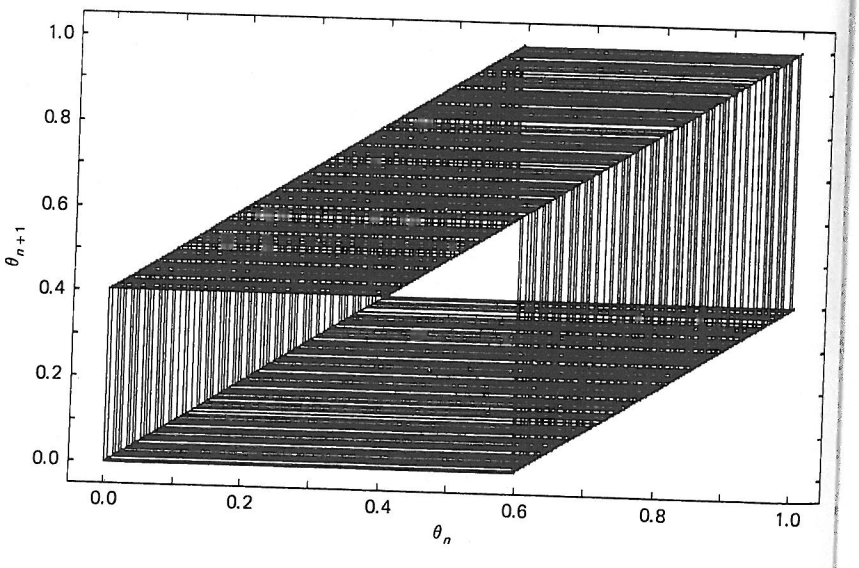

Fig. 4.13 The linearized circle map for an irrational winding number, 0.404 004 . . . .

Figure 4.13 illustrates quasiperiodic motion with $\Omega = 0.404\,004\ldots$ (irrational) for 200 iterations. The angle comes arbitrarily close to any particular value if n is sufficiently large. Mode locking occurs when the nonlinear term is added; this keeps the motion periodic even when Ω is irrational. In Figure 4.14, for example, $K = 0.95$ and $\Omega = 0.404\,004\ldots$ as before. However, the motion repeats every five iterations. The winding number measures the average phase change per iteration. For $K \neq 0$, it is not equal to Ω and is defined generally as

$$W = \lim_{n\to\infty}\left(\frac{\theta_n - \theta_0}{n}\right).$$

The nonlinear term obviously changes the shape of the function representing the map. Note that at $K = 0.95$ the map is still invertible. The widths in Ω of the various mode-locked regions where the winding number is fixed increase with K, as shown in Figure 4.15. The resulting 'Arnold tongues' are named after the Russian mathematician who discovered this structure (Arnold, 1965).

There are an infinite number of phase-locked intervals. There are also an infinite number of irrational winding numbers. As Ω varies at fixed K, the map displays both periodic and quasiperiodic motion. But as K approaches 1, the rational intervals increase in size. At $K = 1$ the set of rational intervals is a fractal. Figure 4.16(*a*) shows the rational winding numbers as plateaus in a plot of W versus Ω. If the figure is magnified (Figure 4.16(*b*)), more plateaus become evident, and the curve shows repetition of the same patterns at the new magnification. Such a curve is said to be *self-similar*. This structure is called the *Devil's staircase*. (For a discussion of the Devil's staircase and some applications, see Bak (1986).)

Beyond the $K = 1$ critical value, the phase-locked motions overlap; this implies that several different periodic oscillations can occur for given (K,Ω) depending on initial conditions. The graph of W versus Ω ceases to be monotonic. The map develops local maxima and minima and therefore becomes noninvertible for $K > 1$, a necessary condition for chaotic behavior, as we also noted for the logistic map. A noninvertible case of the standard map is shown in Figure 4.17. Chaos is, in fact, observed for some values of Ω.

Several routes to chaos occur for the standard map. In Figure 4.18 we illustrate three representative paths through the Arnold tongues of the (Ω,K) parameter space. Path (*a*) shows the system in a state where

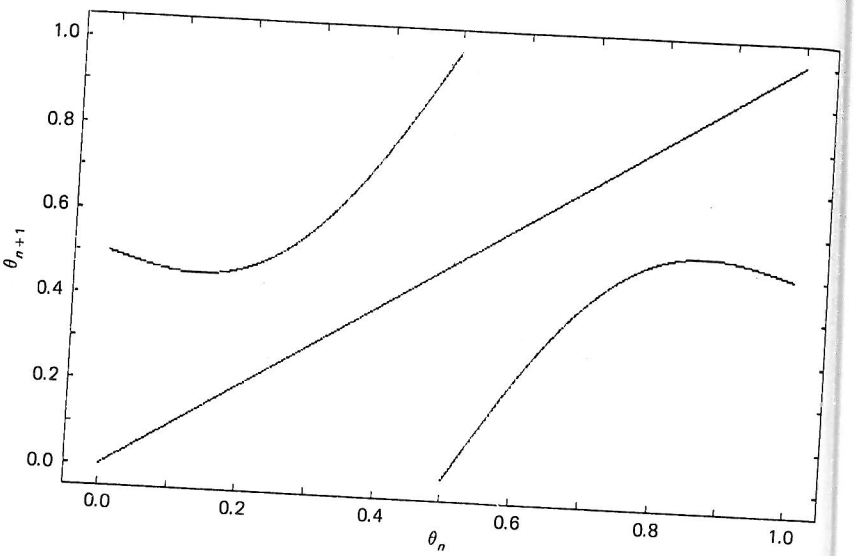

Fig. 4.17 The standard map becomes noninvertible for $K>1$ (here $\Omega=0.5$ and $K=1$).

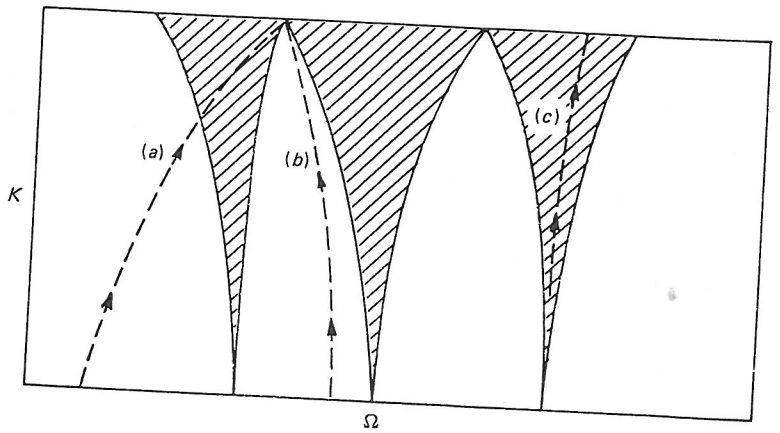

Fig. 4.18 Various possible routes to chaos: (*a*) quasiperiodic→phase locking→chaos; (*b*) quasiperiodic→chaos; (*c*) periodic→chaos.

the winding number is irrational and the behavior is quasiperiodic. The system continues in the quasiperiodic state until it reaches the junction of two phase-locking modes at $K=1$ and becomes chaotic. Path (*b*) shows the system as initially quasiperiodic but then passing into a mode-locking regime and eventually becoming chaotic. Path (*c*) shows the system starting in a mode-locked state, traveling toward the critical line, $K=1$, but then continuing to a larger value of K, beyond which a period-doubling cascade to chaos begins. The prominence of the period-doubling route to chaos is consistent with the existence of a quadratic maximum (Figure 4.17). This aspect of the circle map is similar to the logistic map.

The logistic and circle maps provide many valuable insights into chaotic dynamics. As we discuss in the final section of this chapter, many of the concepts developed from these one-dimensional maps apply to the driven pendulum. As a final model for chaotic behavior we consider a two-dimensional map.

The horseshoe map

In our discussion of the logistic map we saw that the interval (0,1) is stretched and then folded back upon itself. The stretching and folding phenomenon is a primary mechanism for allowing sensitivity to initial conditions in a finite-sized phase space. The horseshoe map introduced by Smale (1963) is a two-dimensional mapping that illustrates the stretching and folding action. It has been shown to be embedded in the dynamics of the pendulum for some parameter choices (Gwinn and Westervelt, 1986).

The horseshoe map consists of the sequence of operations shown in Figure 4.19. First consider a map f which acts upon the unit square, and consists of (*a*) an expansion in the y direction by a factor $\mu > 2$, (*b*) a contraction in the x direction by a factor $\lambda \in (0,\frac{1}{2})$, and (*c*) a folding, as illustrated in Figure 4.19. The transformed set $f(S)$ is then intersected with the original set S so that the map is now confined to a subset of the original unit square. If the entire sequence of operations is repeated, then four stripes appear from the original two, and so on. Repetition of the process n times leads to 2^n stripes, and a cut across the stripes would, in the limit of large n, lead to a fractal (see Chapter 5).

Horseshoe configurations occur in the phase space of dynamical systems where there are regions of strong contraction and expansion. For example, we recall from the initial discussion (Chapter 2) of the pendulum phase plane that there are saddle points at $\theta = \pm\pi$ and $\omega = 0$. Near these saddle points, trajectories approach most rapidly along certain 'stable' directions, and depart most rapidly along other 'unstable' directions, as shown in Figure 2.13. Along these directions, the Lyapunov exponents are negative and positive, respectively. Alternatively stated, tangent vectors along the stable directions are contracting, and tangent vectors along the unstable directions are expanding. Any region of phase space where these two types of

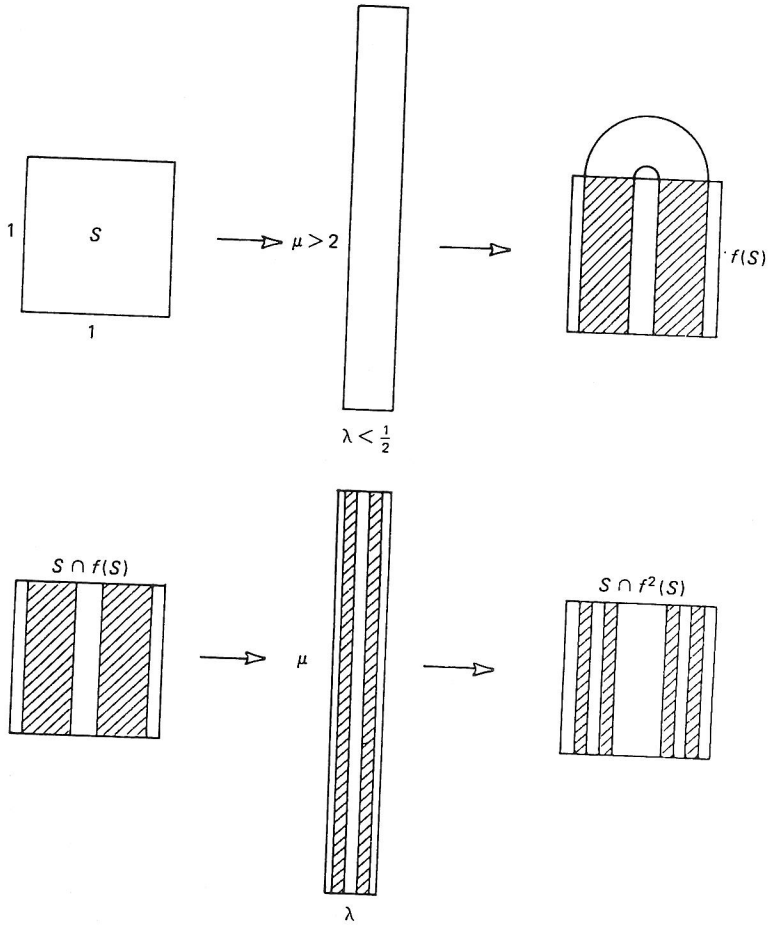

Fig. 4.19 The construction of the horseshoe map for two iterations.

behavior are in close proximity may exhibit stretching and folding.

Trajectories containing both types of behavior develop in a complex way. For example, see Moon (1987), Chapter 5. This may be explained with reference to Figure 4.20, which shows the phase plane for the damped, undriven pendulum as in Figure 2.13, but with the *stable and unstable manifolds* W^s and W^u of the saddle points labeled, and the two basins of attractions shaded differently. The manifolds W^s and W^u are simply the trajectories that approach and depart most quickly from the unstable equilibrium. If the pendulum is now *driven periodically* but weakly, the same diagram may be regarded as a Poincaré section of the three-dimensional phase space, except that the lines should be regarded as a sequence of dots corresponding to successive passages of the trajectories through the Poincaré plane.

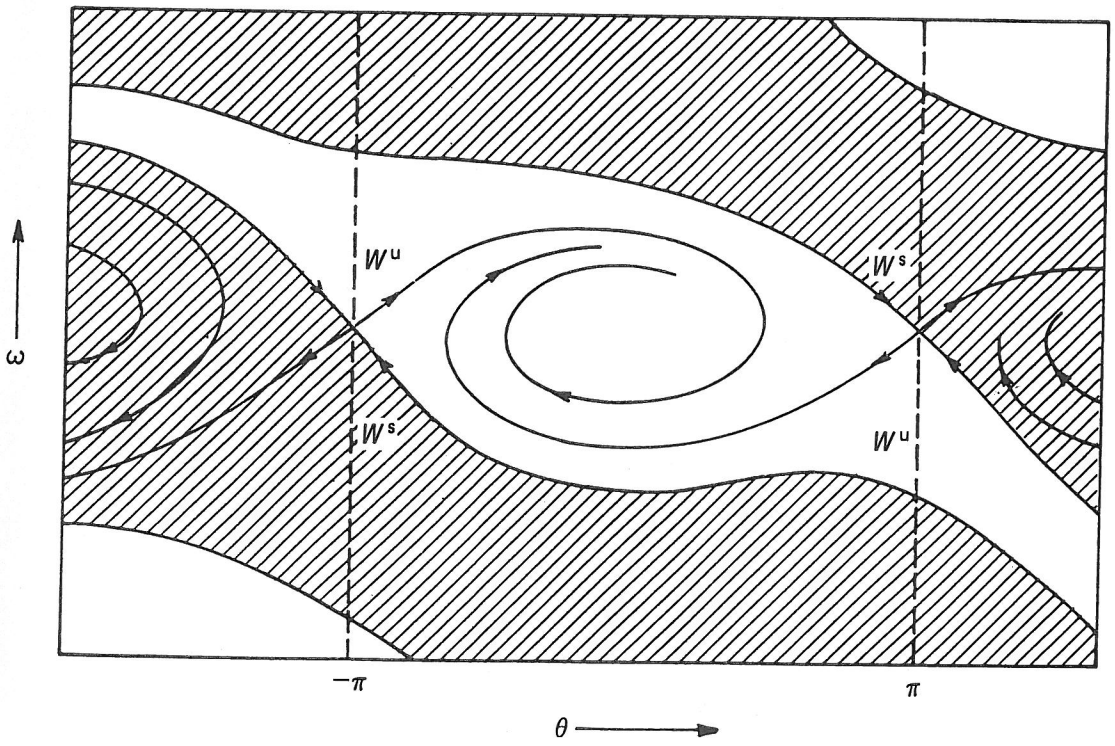

Fig. 4.20 Sketch of the phase plane of the damped, but undriven pendulum, showing the stable and unstable manifolds of the saddle points. Shaded and unshaded regions correspond to distinct basins of attraction.

If the pendulum is driven more strongly, the unstable manifold from the saddle at π and the stable manifold from the saddle at $-\pi$ may approach each other and touch as shown in Figure 4.21(*a*), or even cross at the point I_1 in Figure 4.21(*b*). (The actual trajectories do not cross of course, but the stable and unstable manifolds in the Poincaré section can cross.) Now comes the surprise. Each crossing is mapped into another one closer to the saddle point, leading to an infinite number of intersections I_2, I_3, and so forth. The resulting

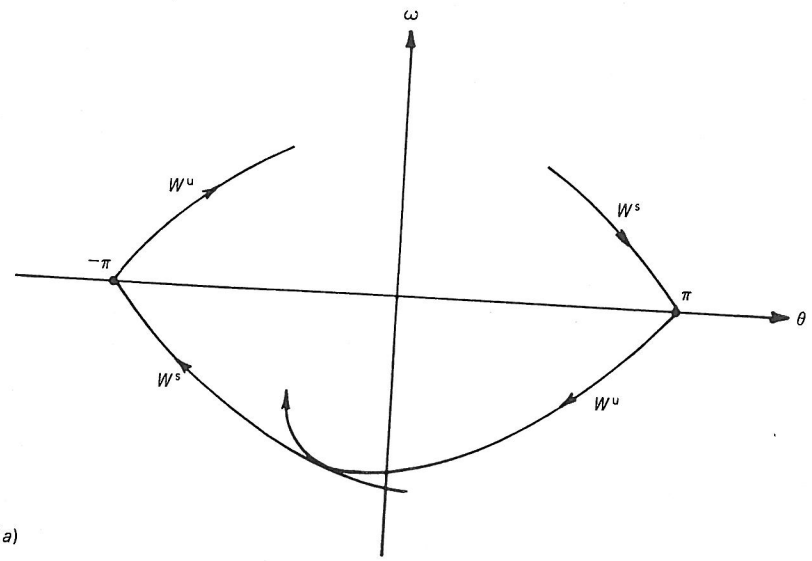

(*a*)

Fig. 4.21 The formation of a heteroclinic tangle in the Poincaré map of the pendulum. (*a*) The unstable and stable orbits barely touch, signaling the beginning of chaos. (*b*) The tangle forms with an infinite number of intersections $I_1, I_2, \ldots$. Two nearby points may be mapped far apart, yielding chaos. (*c*) Additional detail (see text).

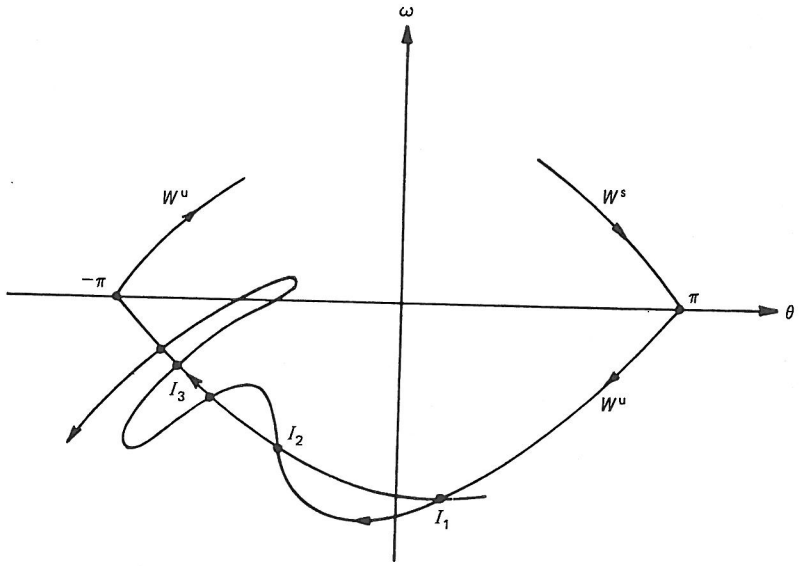

(*b*)

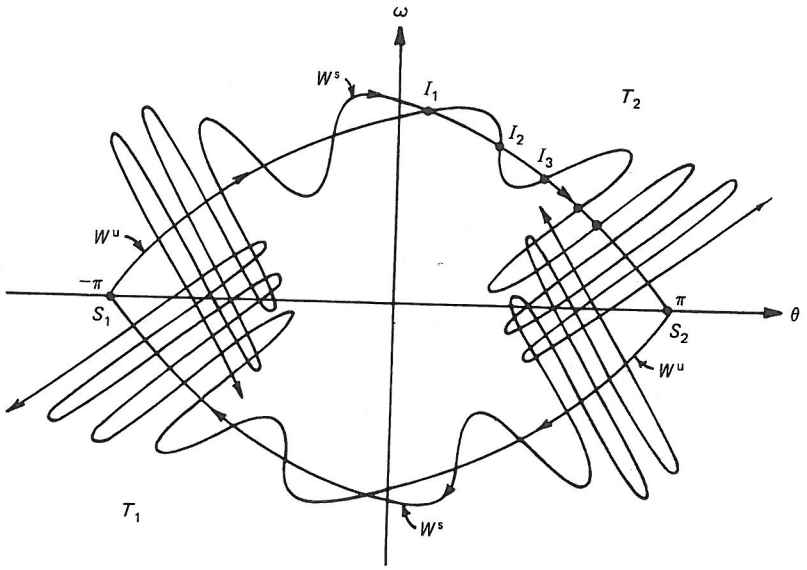

(*c*)

configuration is called a *heteroclinic tangle.* (If W^s and W^u come from the same fixed point, the configuration is known as *homoclinic.*)

Because of the strong bending of the manifolds near the saddle point, a small rectangular section of the plane near I_1 will suffer stretching and folding much like that of the horseshoe map. In fact, that distorted rectangle is topologically equivalent to (can be smoothly deformed into) the iterated Smale horseshoe (Abraham and Shaw, 1984). As a result, two points that are initially close together will be found far apart after a few iterations. Therefore, chaos is a natural consequence of a heteroclinic tangle.

The actual situation is even more complicated than Figure 4.21(*b*) suggests. Let us label the first tangle near saddle S_1 as T_1 (see Figure 4.21(*c*)). Clearly there must be a second tangle T_2 near the saddle S_2 at π, since the geometry there is the same as that near S_1. But where did the first intersection I_1 in that tangle come from? It must have resulted from an earlier iteration. Going *backward* in time takes I_1 back through an infinite sequence of intersections to the neighborhood of S_1. This implies that the stable and unstable manifolds from S_2 must cross each other an infinite number of times near S_1. Thus, the geometry of the pendulum (as visualized in the Poincaré plane) is infinitely complex, and the essential character of that complexity is contained in the horseshoe map.

Applications to simulations of the pendulum

The logistic map, the standard map, and the horseshoe map illustrate the kinds of phenomena that are important aspects of the motion of the driven pendulum. Though we have alluded briefly to connections between the driven pendulum and the maps, we now discuss several of these connections in greater detail.

(*i*) *Period doubling.* The logistic map illustrates the period-doubling route to chaos. Reference to the bifurcation diagram of Figure 4.22 provides evidence of similar behavior for the pendulum. A pair of period-doubling cascades begins at $g \approx 1.07$ (preceded by symmetry breaking at $g = 1.0$, where the angle exceeds π). An examination of the data of Figure 4.22 (*b*) at greater magnification of g and ω than in Figure 4.22 (*a*) – shows period doubling at $g = 1.066$, $g = 1.077$, and

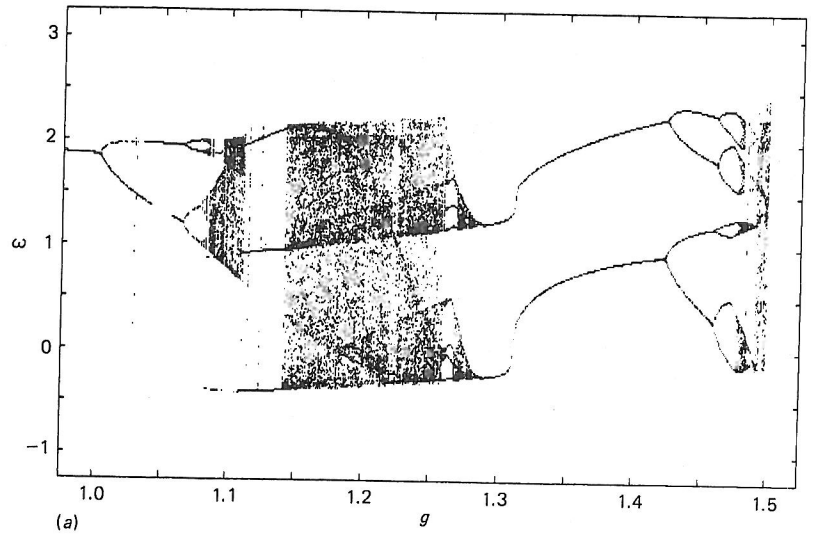

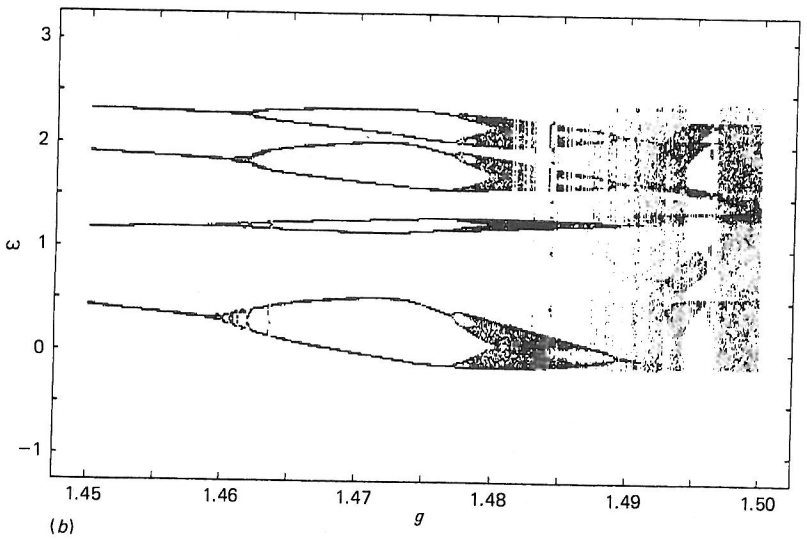

Fig. 4.22 Bifurcation diagrams for the pendulum, indicating various dynamical regimes. The diagrams are generated by following the long-term behavior of two initial points (θ_0,ω_0), one each from the positive $\langle\omega\rangle$ and negative $\langle\omega\rangle$ basins of attraction. (*b*) Magnification of part of (*a*).

$g \approx 1.080$, with further bifurcations unresolved. Using these data the ratios of the changes in g can be estimated and compared with the Feigenbaum number, 4.669 . . . . For this sequence the result is 4 ± 1. It is remarkable that the behavior of the logistic map is manifested (to within the computational accuracy) in the more complex pendulum.

(*ii*) *Phase locking.* Phase locking of the pendulum is evident when the average angular velocity is some rational multiple (usually low order) of the angular forcing frequency ω_D. This condition may be specified in the following way. If the pendulum is phase locked at a ratio p/q, then for q drive periods the angle difference is $\theta(t+qT)-\theta(t)=2\pi p$, where T is the drive period, $2\pi/\omega_D$. Then the average value of $\omega = \mathrm{d}\theta/\mathrm{d}t$ over q periods is

$$\langle\omega\rangle = (1/qT)\int_t^{t+qT} \omega \mathrm{d}t = (p/q)\omega_D.$$

Measurement or computation of the average angular velocity is a useful tool for analysis of the pendulum motion. A graph of $\langle\omega\rangle$ versus g as shown in Figure 4.23 should reveal phase-locked motion. This figure complements the bifurcation diagrams of Figure 4.22. Two sets of initial conditions were chosen, one from each basin of attraction at $g = 1.45$, to illustrate positive and negative rotary modes. The plateaus of $\langle\omega\rangle$ are indicative of phase locking; they correspond to the periodic intervals of the bifurcation diagram. The regions in which $\langle\omega\rangle$ varies erratically correspond to the chaotic state (Gwinn and Westervelt, 1986).

Another approach to the study of phase locking is direct examination of the winding number for a range of forcing amplitudes, g. In the diagrams of Figure 4.24 the winding number is shown for two ranges of g. It is defined for the pendulum as

$$W = \lim_{n\to\infty}\left(\frac{\theta_n - \theta_0}{2\pi n}\right),$$

where n is the number of drive cycles. As in the previous diagrams initial values were chosen from the two basins of attraction to show positive and negative angular velocities. For each value of g an initial motion corresponding to 50 drive cycles is discarded, and the next 30 cycles ($n=30$) of angular displacement are used to obtain W. The features of these diagrams are essentially the same as those of the

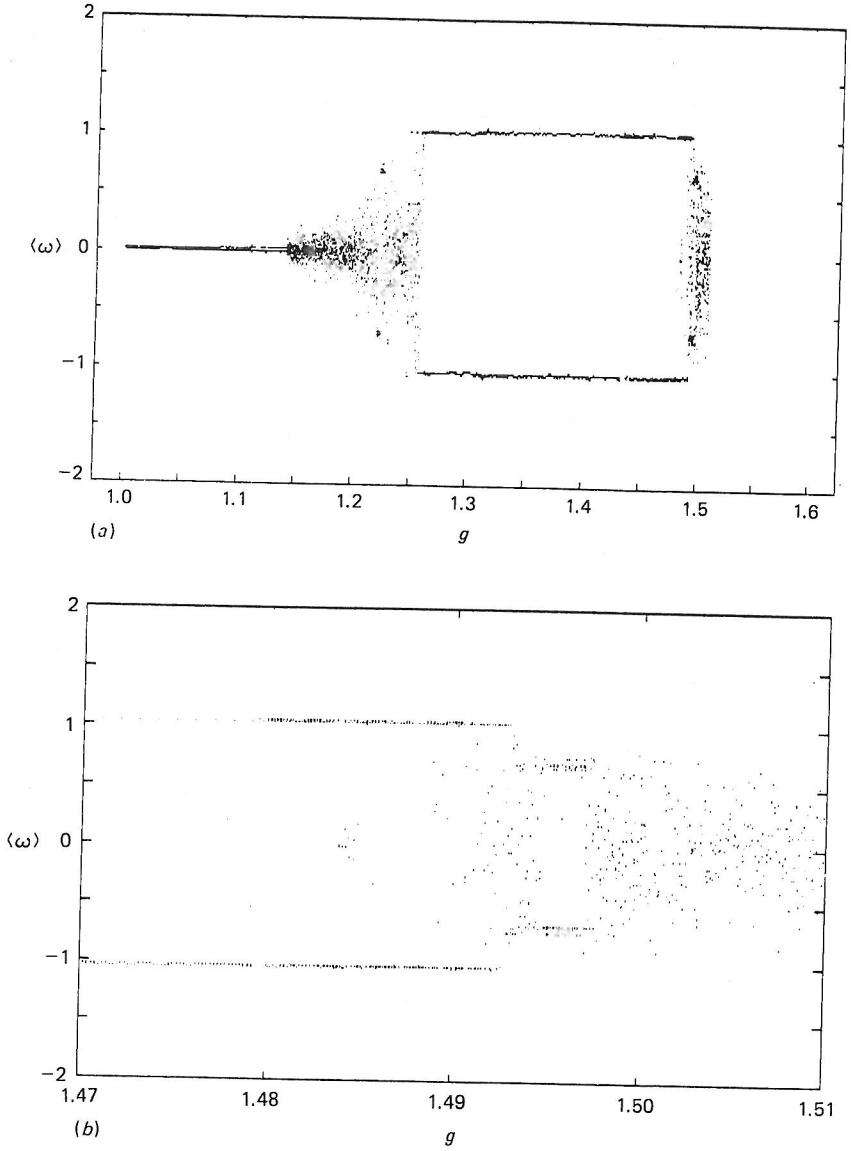

Fig. 4.23 Phase locking of the pendulum as revealed by the average angular velocity $\langle\omega\rangle$ (in units of ω_D) as a function of the driving force amplitude g. Sets of initial coordinates (θ_0,ω_0) were chosen from the two basins of attraction. (*b*) Magnification of part of (*a*).

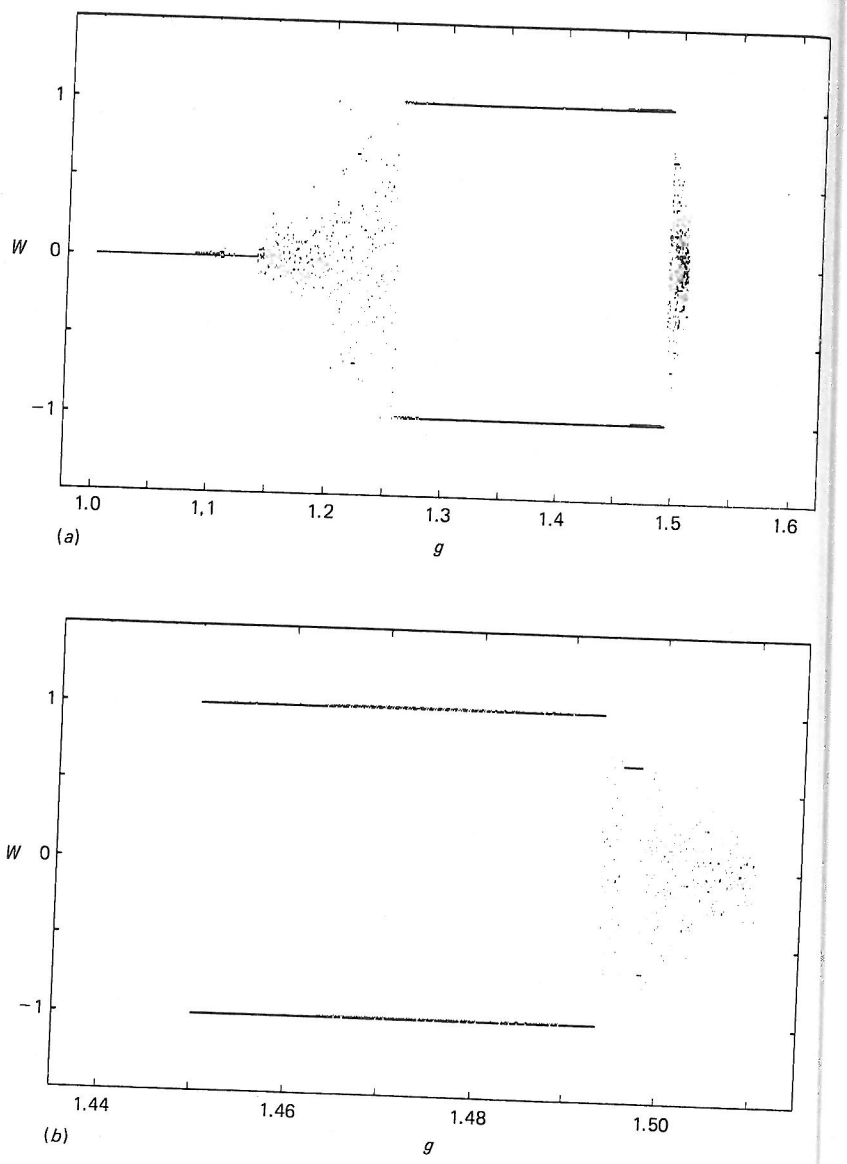

Fig. 4.24 Phase locking of the pendulum as revealed by the winding number W as a function of driving amplitude g. Sets of initial coordinates were chosen from the two basins of attraction. (*b*) Magnification of part of (*a*).

Table 4.1. *Correlation of dynamical behavior with winding number. Behavior designated 'chaotic(ma)' indicates multiple chaotic attractors.* $q=2$ *and* $\omega_D=\frac{2}{3}$

Range	Type of behavior	Winding number
$g<1.085$	periodic	0
$1.085<g<1.11$	chaotic(ma)	~ 0
$1.11<g<1.14$	periodic	0
$1.14<g1.22$	chaotic	scattered
$g\sim 1.22$	periodic	$\pm\frac{2}{3}$
$1.22<g<1.26$	chaotic	scattered
$1.26<g<1.28$	chaotic(ma)	$\sim \pm 1$
$1.28<g<1.475$	periodic	± 1
$1.475<g<1.485$	chaotic(ma)	$\sim \pm 1$
$1.485<g<1.493$	periodic	± 1
$1.493<g<1.495$	chaotic	scattered
$1.495<g<1.497$	periodic	$\pm\frac{2}{3}$
$g>1.497$	chaotic	scattered

graphs of $\langle\omega\rangle$ versus g, since both measure the average rotation rate, using different computational schemes.

The graph of W versus g shows two types of behavior; (*a*) phase locking with constant W for periodic pendulum states, and (*b*) scattered values of W for chaotic states. The various types of behavior detected as g increases, and the corresponding values of W, are shown in Table 4.1.

In this chapter we have demonstrated that discrete mappings can give insight into the complex behavior of the driven pendulum. In the next chapter we examine various aspects of the fractal geometry associated with chaotic motion.

Problems

1. Use the listing LOGISTIC MAP in Appendix B or the option LOGISTIC MAP from the CHAOS menu to study the logistic return map. Try different values of the parameter μ and different initial values x_0.
2. Use one of the programs suggested in Problem 1 to study regions where period doubling occurs. First look at the appropriate first order return map and then generate higher order return maps that correspond to the degree of period doubling.
3. Using one of the programs suggested in Problem 1, generate a bifurcation diagram for the logistic map. Expand the scale of μ in order to magnify certain regions of the diagram. In particular, expand the scale in a chaotic region and note that windows of periodic behavior are more evident at the higher magnifications.
4. Expand the scale of μ for a bifurcation diagram in the region of period doubling. Try to observe many bifurcations and thereby approximately verify the Feigenbaum number.
5. For the second bifurcation of the logistic map, the entropy, as defined in the text, is constant over that region of μ. What does this fact imply about the distribution of points over the four possible values of x_n for that range of μ? Now assume that the values of x_n are tossed with equal probability into each of four bins (out of a total of 40 bins). What is the entropy of this situation? Compare your answer with that of Figure 4.10, and suggest an interpretation of the diagram in that particular region. Using the method of Lagrange multipliers or otherwise, prove that the entropy function is a maximum when $p_i = 1/N$ for all values of i.
6. Another map which shares many properties of the logistic map is the *tent* map:

$$x_{n+1} = 2\beta x_n \quad \text{for } 0 < x < \tfrac{1}{2}: 0 < \beta < 1$$
$$x_{n+1} = 2\beta(1 - x_n) \quad \text{for } \tfrac{1}{2} < x < 1$$

Use either the TENT MAP option from the CHAOS menu or your own modification of the listing LOGISTIC MAP in Appendix B to generate some mappings and bifurcation diagrams of the tent map.

7. Use one of the programs suggested in Problem 6 to generate a plot of the Lyapunov exponent versus β for the tent map. Prove analytically that the Lyapunov exponent is $\log_e(2\beta)$. Note that the exponent becomes positive as β passes through 0.5, the initial point of chaotic behavior.
8. In the chaotic region of the tent map it is possible to estimate how many iterations are necessary before knowledge of the x coordinate (with an initial uncertainty) is lost. If the uncertainty in the coordinate after the nth iteration is ε_n then the uncertainty after the $n+1$ iteration is

   $$\varepsilon_{n+1} = \varepsilon_n e^{\log_e 2\beta}$$

   (This expression uses the Lyapunov exponent from Problem 7.) If the initial uncertainty is ε how many steps does it require to have an uncertainty equal to 1? (Answer: $n = \log_2(1/\varepsilon)$)
9. Show that the logistic map (with $\mu = 4$) with the variable x_n may be transformed to the tent map with the variable y_n by the coordinate transformation: $y_n = (2/\pi)\sin^{-1}(x_n^{\frac{1}{2}})$.
10. Using either the listing CIRCLE MAP in Appendix B or the option CIRCLE MAP from the CHAOS menu generate the standard map using various values of K and Ω. Determine the differing effects of each of these parameters on the shape of the map. For what value of K does the map become noninvertible?
11. Using one of the programs suggested in Problem 10 generate several versions of the Devil's staircase. By appropriate scaling of the coordinates examine the staircase at various magnifications.
12. The phenomenon of mode locking in the driven pendulum can be examined by considering a modified version of the bifurcation diagram. Instead of keeping ω_D constant and varying g, reverse the operation and let ω_D be the independent variable, for constant g. (This requires the appropriate modification of the bifurcation program.) Try $g = 1.46$ for example and let ω_D vary from 0 to 1. You should observe that in the region where $\omega_D \approx p/q$ for small integer values of p and q, the pendulum locks onto a periodic motion.
13. Horseshoes can be generated in a variety of ways. One example is the baker's transformation:

    $$x_{n+1} = 2x_n, \text{ mod } 1$$